STUDYING IDEAL TEMPERATURE FOR FASTER CARBONATION IN WASTE SLAG: EXAMINING THERMAL EFFECTS ON CO2 UPTAKE AND REACTION EFFICIENCY

LEE JIA JUN

UNIVERSITI TUNKU ABDUL RAHMAN

**STUDYING IDEAL TEMPERATURE FOR FASTER CARBONATION
IN WASTE SLAG: EXAMINING THERMAL EFFECTS ON CO2
UPTAKE AND REACTION EFFICIENCY**

LEE JIA JUN

**A project report submitted in partial fulfilment of the
requirements for the award of Bachelor of Civil Engineering
Engineering with Honours**

**Lee Kong Chian Faculty of Engineering and Science
Universiti Tunku Abdul Rahman**

September 2024

DECLARATION

I hereby declare that this project report is based on my original work except for citations and quotations which have been duly acknowledged. I also declare that it has not been previously and concurrently submitted for any other degree or award at UTAR or other institutions.

Signature :

Name : Lee Jia Jun

ID No. : 21UEB00560

Date : 17 September 2024

APPROVAL FOR SUBMISSION

I certify that this project report entitled **"STUDYING IDEAL TEMPERATURE FOR FASTER CARBONATION IN WASTE SLAG: EXAMINING THERMAL EFFECTS ON CO2 UPTAKE AND REACTION EFFICIENCY"** was prepared by **LEE JIA JUN** has met the required standard for submission in partial fulfilment of the requirements for the award of Bachelor of Civil Engineering with Honours at Universiti Tunku Abdul Rahman.

Approved by,

Signature   :

Supervisor   :   Ir Ts Dr Lee Foo Wei

Date   :   17/09/2024

Signature   :

Co-Supervisor :

Date   :

ACKNOWLEDGEMENTS

I want thank everyone who contributed to the successful completion of this project. First and foremost, I am deeply thankful to my research supervisor, Dr. Lee Foo Wei, for his invaluable advice, insightful guidance, and unwavering patience throughout the research process.

I want to thank my parents for their endless love and encouragement, which have been a great source of strength throughout this journey. Their constant support has been invaluable. I also want to thank my friends for their ongoing motivation, help, and reassurance during tough times. This project would not have been possible without their collective support.

ABSTRACT

This study explores the potential of Electric Arc Furnace slag for CO_2 sequestration by investigating its carbonation behaviour under varying temperatures, humidity levels, and CO_2 concentrations. The research aims to optimize CO_2 conversion efficiency and assess the stability of the resulting carbonate minerals. Utilizing techniques like X-ray Diffraction, Energy-Dispersive X-ray Spectroscopy, Scanning Electron Microscopy, and Thermogravimetric Analysis, the study reveals that carbonation significantly influences the microstructure and mechanical properties of slag-based mortar. Higher temperatures are shown to enhance CO_2 uptake and promote the formation of carbonate crystals. The findings highlight EAF slag's potential as a sustainable construction material capable of contributing to CO_2 mitigation efforts. The maximum compressive strength recorded was 28.94 kN for concrete made with EAF slag, under conditions of 30°C, 80% humidity, and 20% CO_2 concentration. This research highlights the effectiveness of carbonated steel slag as a sustainable material for concrete production, offering both improved mechanical performance and enhanced carbon sequestration, making it a promising solution for greener construction practices.

TABLE OF CONTENTS

LIST OF TABLES

LIST OF FIGURES

LIST OF SYMBOLS / ABBREVIATIONS

θ	incidence angle
n	variables
d	beam wavelength
λ	spacing between diffracting planes
GHGs	Greenhouse gases
CO_2	Carbon dioxide
CO	Carbon monoxide
Mt	Million metric tonnes
Ca	Calcium
CaCO3	Calcium carbonate
Mg	Magnesium
Si	Silicate
CH4	Methane
XCO3	Carbonate of any metal
SiO2	Silicon dioxide
MgO	Magnesium oxide
AL2O3	Aluminium oxide
N2O	Nitrous oxide
MO	M oxide
SS	Steelmaking slags
LD	Ladle slags
BFS	Blast furnace slag
BOF	Basic oxygen furnace
EAF	Electric-Arc Furnace
CCU	Carbon capture and utilisation
NC-1	Normal concrete 1
LWC-1	Lightweight concrete 1
CSSC-1	Coarse steel slag concrete 1
SSGC-1	Steel slag and glass concrete 1
NC-2	Normal concrete 2
LWC-2	Lightweight concrete 2
CSSC-2	Coarse steel slag concrete 2

SSGC-2	Steel slag and glass concrete 2
FSSC-2	Fine steel slag concrete 2
XRD	X-Ray Diffraction Analysis
TGA	Thermogravimetric Analysis
SEM	Scanning Electron Microscopy
EDS	Energy Dispersive X-ray Spectroscopy
ASTM	American Society for Testing and Materials
Cu	Coefficient of Uniformity
Cc	Curvature Coefficient

CHAPTER 1

INTRODUCTION

1.1 General Introduction

Increases in atmospheric concentrations of greenhouse gases (GHGs) such as carbon dioxide, methane, nitrous oxide, and carbon monoxide are the most significant cause of global warming; carbon dioxide already contributes to two-thirds of the enhanced warming impact (N.L. Ukwattage, P.G. Ranjith and X. Li, 2017). High levels of atmospheric CO_2 have the potential to cause major environmental harm as well as societal unrest when they reach 550 parts per million. Finding workable solutions to stabilise atmospheric CO_2 concentrations are therefore crucial. Furthermore, 2.6 gigatonnes of carbon dioxide are directly attributed to the iron and steel industry each year, greater than the emissions from all road freight combined and representing 7% of the world energy system's total emissions (IEA, 2020).

According to the World Association (2024), global steel demand will increase to 1,793 million metric tonnes (Mt) in 2024, an increase of 1.7%. In addition, a 1.2% increase is predicted for 2025, bringing demand to 1,815 Mt. Recently, greenhouse gas emissions have become a significant issue due to global warming. Global warming is caused by the steel and cement industries' massive CO_2 emissions. One efficient way to increase the utilisation of solid waste, thus reducing carbon emissions, and use less cement powder is to use steel industry waste, such as slag, to capture CO_2 in the exhaust gas from the steel industry and create appropriate construction materials (Amer Baras et al., 2023). A method that resembles the way rocks naturally weather. Equations 1.1, 1.2 and 1.3 represent the simplified chemical process for CO_2 mineralized storage:

$$(Ca, Mg)\,O + CO_2 \; \rightarrow \; (Ca, Mg)CO_3 \qquad (1.1)$$

$$(Ca, Mg)(OH)_2 + 2CO_2 \; \rightarrow \; 2(Ca, Mg)CO_3 \qquad (1.2)$$

$$(Ca, Mg)SiO_2 + 2CO_2 \; \rightarrow \; 2(Ca, Mg)CO_3 + SiO_2 \qquad (1.3)$$
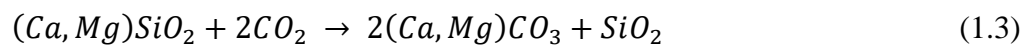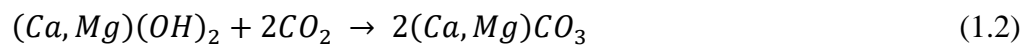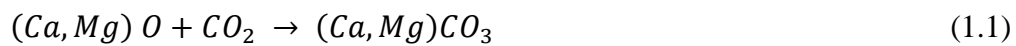
Due to the thermodynamic stability of the carbonate that is produced, mineral carbonation has been considered as a method that might enable the permanent disposal of the CO_2 (Lee et al., 2016). Carbonation of steel slag produces carbonate products that improve durability, lower the percentage of f-CaO/MgO,

and increase compressive strength in addition to storing CO_2. Consequently, a wider range of applications as building materials are made possible by the enhanced qualities of carbonated steel slag. This review summarises recent key results on the accelerated (Qifeng Song et al., 2021).

In recent years, there has been a growing interest in the use of waste products as resources for sustainable development. Slag waste, which is a result of several industrial operations, is one of these materials that has a great potential for carbon collection and utilisation by carbonation. When steel and impurities are separated in the steelmaking furnace, steel slag is created as a byproduct.

One important component that affects the efficiency and kinetics of carbonation processes is temperature. It is critical to comprehend how temperature affects CO_2 absorption and reaction efficiency in order to optimise the process and increase its feasibility for large-scale deployment (Ren & Li, 2023). Furthermore, the manufacturing of cement clinker can use steel slag, which lowers CO_2 emissions and the overall cost of the materials required.

According to Kalita-Jurowska and Jurowski (2020), improper disposal of steel slag can release trace metals and cause extremely alkaline drainage, which can have a negative impact on surface and groundwater. Steel production can have carbon dioxide intensities ranging from 0.45 to 1.97 tCO_2/t of crude steel, depending on the method employed. Slag is a rich resource as it may be created from a tonne of steel in the range of 0.13 to 0.2 tonne (Ukwattage, Ranjith and Li, 2017). As per Ukwattage, Ranjith, and Li (2017), the world's annual production of slag used in steel manufacturing has been around 200 Mt in recent times. Furthermore, future increases in steel demand will make by-product steel slag even more readily available. Slag is typically utilised in place of cement and other comparable materials as an additional cementitious ingredient.

1.2 Importance of the study

Global warming has grown to be a significant concern that highlights environmental problems. One of the primary functions of greenhouse gases is carbon dioxide. The study is crucial to the storage and capture of CO_2. Because the carbon dioxide will react chemically with the slags and generate a thermodynamically stable carbonate, the CO_2 may be permanently disposed of. Following capture, mineral sequestration transforms the carbon from gaseous CO_2 into stable, solid forms of carbonates (N.L. Ukwattage, P.G. Ranjith and X. Li, 2017). Furthermore, there won't be any easy chemical reactions between the carbonated slag and other substances. The final products of mineral carbonation are without a doubt a permanent method of fixing CO_2. Carbon dioxide emission rate and cost reduction are two features of mineral carbonation. Additional advantages include these waste products' cheap cost and wide availability.

In addition, the majority of steel slags are stored up or landfilled, taking up valuable land resources and allowing heavy metals to leak. Heavy metals may leach from steel slag as a result of some companies' improper handling of their waste slag. Direct disposal of steel slag or its buildup in landfills without proper treatment can seriously contaminate waterways and farms (Qifeng Song et al., 2021). Due to this waste management practice, a significant amount of mineral waste accumulates and is discarded in fields, seriously harming the local population's quality of life and polluting the environment (Humbert and Castro-Gomes, 2019). Reusing steel slag more efficiently by lowering its potential danger is achieved by making the discarded slag undergo carbonation. In construction, the pretreatment of steel slag is crucial.

The primary component needed to make concrete is cement. However, the cement sector contributes significantly to greenhouse gas emissions as well. Therefore, if less concrete is used in buildings, carbon dioxide emissions will gradually decline. Steel slag can be used to generate mortar if concrete quality is to be increased and construction codes are to be adhered to. The concrete's durability and mechanical qualities are enhanced by this modification. Moreover, employing eco-friendly materials such as rubberized lightweight foamed concrete can lower carbon emissions, encourage a more

environmentally friendly building sector, and help Malaysia become a carbon-neutral country.

However, the compressive strength test must be performed for the current structure. The test needs to be carried out carefully, making sure that it has no impact on the current framework. Effective early strength and response will be given underneath the mortar that is combined with steel slag. The mechanical strength of the system is not weakened by 10%–20% steel slag powder. Steel slag will therefore be managed efficiently and won't contaminate the environment. Better still, costs and carbon dioxide emissions may be decreased. A good way to increase the utilisation of solid waste, minimise carbon emissions, and use less cement clinker is to employ steel industry waste, such as steel slag, to absorb CO_2 in the steel industry waste gas and make appropriate building materials.

1.3   Problem statement

Steelmaking slag (SS), one of the most common industrial wastes, is a by-product of steel production. One ton of steel implies the production of 130–200 kg of slag, depending on the composition of the steel and the steel production process (Furlani, Tonello and Maschio, 2010). By 2016, approximately 832 million tons of steel were produced in China with an annual output of more than 100 million tons, which exceeded half of the total steel production worldwide. The utilization rate of steel slag in the United States, Germany and Japan is 50%, 30%, and 25%, respectively. However, China only uses 22% of the steel slags (Qifeng Song et al., 2021). The majority of steel slags are stored up or landfilled, using valuable land resources and harming the environment permanently.

Carbon dioxide emission also becomes an issue that everyone is concerned about. Of course, there are other problems, concentrations of greenhouse gases (GHGs) CO_2, CH_4N_2O and CO contribute to the greenhouse effect. However, carbon dioxide contributes to an important reason for the enhanced warming effect. If this situation is not treated well that will cause the possibility of great loss of the environment and social disruption will increase (Ukwattage, Ranjith and Li, 2017). Approximately 95% of global warming, according to Mongo, Belaïd, and Ramdani (2021), is caused by industrial

greenhouse gas emissions from the actions of humans. Iron and steel represent 6- 8% and cement and concrete 6% of global energy system combustion and industrial process CO_2 emissions (Bataille, 2020).

The stability and durability of formed carbonate minerals are evaluated under optimised temperature and CO2 conversion conditions to ensure the safety and effectiveness of carbon mineralisation as a secure carbon sequestration method. Understanding the behaviour of these carbonate minerals provides critical insights into the viability and efficacy of ex-situ mineralization as a long-term and dependable carbon-sequestration solution. Evaluate if there is an increase in the strength of mortars mixed with carbonate minerals.

1.4   Aim and Objective

This study aims to determine the optimal temperature conditions for accelerating the carbonation of waste slag. The primary focus is to enhance CO_2 absorption and reaction efficiency and evaluate the performance of mortar incorporating carbonated EAF slags. To achieve this, the research addresses three key objectives:To investigate how different temperatures influence the CO2 uptake capacity of waste slag during the carbonation process.

I.   Examine how varying temperatures impact the CO_2 absorption capacity of waste slag during carbonation, aiming to establish a quantifiable link between temperature and the efficiency of CO_2 uptake

II.   Examine the microstructural changes in waste slag during carbonation at various temperatures. By analyzing these changes, the research aims to understand how temperature affects the material properties of the slag.

III.   Investigate how incorporating carbonated steel slag affects the strength and durability of mortar. This objective evaluates the practical implications of using carbonated slag in construction applications.

1.5   Scope and limitation of the study

The scope of this study encompasses a comprehensive comparison of the mechanical properties of standard mortar and mortar mixed with steel slag, specifically focusing on the effects of heat on the carbonation process of the slag. The investigation aims to analyze the effectiveness of CO2 uptake by determining the optimal temperatures for carbonation. To achieve this, the study will utilize both standard oxygen furnace slag and electric arc furnace slag at temperatures of 10°C, 20°C, and 30°C. Additionally, the research will evaluate the chemical, physical, and structural properties of the slag, comparing the crystallographic structures of carbonated versus uncarbonated slag.

To investigate the material composition, the study will involve compressing slag powder into small cylinders, which will then be placed in a carbonation chamber for 24 hours. Post-carbonation, the internal structure and chemical composition of the slag crystals will be analyzed using appropriate analytical techniques.

For the mortar component of the study, specimens will be cast using different mould sizes to test various mechanical properties. Specifically, flexural strength will be evaluated using a 100 x 100 x 500 mm steel mould, compressive strength will be assessed with 150 mm x 150 mm x 150 mm moulds and load-bearing capacity will be tested with a 5/8" diameter tamping rod. Each test will correspond to a specific specimen size, with a total of 57 specimens prepared, incorporating a 40% replacement ratio of steel slag.

The study's limitations include potential challenges such as the lack of an appropriately sized carbonation chamber, which could extend the duration of the investigation and affect the carbonation process. Furthermore, the flexural strength test can only determine the maximum load until the specimen fails, and the mortar requires a 28-day curing period before testing, potentially impacting the overall timeline of the study.

1.6   Contribution of Study

This project contributes to sustainable construction materials and carbon capture by studying how to improve the carbonation of Electric Arc Furnace (EAF) slag, a by-product of steelmaking. The study examines how different conditions like temperature, humidity, and the concentration of carbon dioxide (CO_2) impact the process of turning CO_2 into minerals within the slag. By finding the best conditions for this carbonation, the project helps reduce CO_2 emissions and suggests ways to use slag more effectively in construction.

The project also looks at how carbonation changes the microscopic structure of the slag. Using techniques like Scanning Electron Microscopy (SEM), Energy-Dispersive X-ray spectroscopy (EDX), and X-ray Diffraction (XRD), the study identifies the new minerals formed during carbonation, such as calcite and vaterite. These minerals affect the durability and strength of the slag, making it more suitable for use in building materials.

Another key part of the study focuses on the strength of mortar made with carbonated slag. The results show improvements in compressive strength, flexural strength, and splitting tensile strength, which means the carbonated slag could be used as a strong and sustainable alternative in construction. This can reduce the need for traditional materials like natural aggregates, which are less eco-friendly.

Lastly, by promoting the reuse of waste materials, this study supports environmental goals like cutting down on industrial waste and CO_2 emissions. The findings may help scale up slag carbonation processes for broader use, encouraging eco-friendly construction solutions. This project highlights the potential of turning industrial by-products into valuable resources for the building industry.

1.7   Outline of the Report

This report comprises five chapters aimed at presenting a thorough investigation into optimizing temperature parameters to improve the mineralization process of waste slag. The primary goal is to maximize CO2 conversion efficiency while ensuring the stability of the formed carbonate minerals.

Chapter 1 sets the stage by offering an introduction to the study, outlining its importance, and defining the problem statement. It clearly states the aims and objectives of the research, discusses its scope and limitations, and highlights the contributions that the study intends to make to the field of mineral carbonation.

Chapter 2 delves into a comprehensive literature review, providing crucial background information relevant to the study. It covers the fundamentals of mineral carbonation, including reaction mechanisms and the factors influencing the mineralization process. Additionally, this chapter explores the various feedstocks suitable for carbonation, explains the crystalline polymorphs of carbonate minerals, and assesses their stability. It also reviews the analytical methods employed in the study, such as casting techniques, and includes a comparative analysis of the strength between mortars mixed with EAF slag and traditional mortar.

Chapter 3 details the methodology and work plan for the research. It describes the preparation of raw materials, pre-treatment procedures, and the mineralization process for EAF slag samples. The chapter also outlines the laboratory tests conducted to analyze the carbonated samples, which include Scanning Electron Microscopy (SEM), Energy-Dispersive X-ray Spectroscopy (EDX), X-ray Diffraction (XRD) analysis, and Thermogravimetric Analysis (TGA). Furthermore, it includes procedures for casting samples and testing their compressive strength, splitting tensile strength, and flexural strength.

Chapter 4 presents the results from the laboratory tests and provides a discussion of the findings. It includes qualitative observations from SEM and other analytical methods, as well as quantitative measurements shown in tables and graphs. This chapter illustrates the impact of temperature on the mineralization process and evaluates the thermal stability of the formed carbonate minerals. It also reports on the mechanical strength of the samples,

including compressive, splitting tensile, and flexural strength, highlighting how these properties are affected by the carbonation process.

Finally, Chapter 5 summarizes the study's findings in relation to the initial objectives. It offers valuable insights into the optimal temperature for achieving efficient CO2 conversion, assesses the thermal stability of the carbonate minerals formed, and evaluates the mechanical strength of EAF slag-based materials. This chapter concludes with a reflection on the study's contributions to the field and its implications for future research and practical applications.

CHAPTER 2

Literature Review

2.1   Introduction

The literature review compared the strengths of normal and mortar combined with slag, describes the thermal impacts of the slag carbonation management, and looks into efficient reactions to maximise CO_2 absorption. In this study, BOF and EAF are the slags used. Furthermore, the introduction and kinetics of carbonation are examined to investigate the ongoing studies. The purpose of this study is to demonstrate the need for an innovative and sustainable way to minimise excessive CO_2 emissions and excessive waste created in industries and construction. The foundation platform for this study is the literature review under the influence of temperature. In general, the purpose of the literature study is to demonstrate how waste slag may be used in place of cement to improve durability as well as encourage the growth of the sustainable building sector.

2.2   Introduction of Carbonation

The chemical process known as carbonation produces mostly carbonates when carbon dioxide in the air reacts with calcium hydroxide and hydrated calcium silicate in concrete. It has been observed that a little shrinkage occurs when CO_2 converts Ca(OH)2 into CaCO3 (Gopal Mishra, 2013). Since CO_2 is not reactive on its own, there will be further carbonation. When CO_2 is exposed to moisture, it transforms into diluted carbonic acid, which destroys the concrete and lowers its alkalinity—that is, its pH value. CO_2 is present in the air. According to Gopal Mishra (2013), the amount of CO_2 in rural air may be as little as 0.03 percent by volume. Carbonation is the process of using chemical processes to change carbon dioxide (CO_2) into carbonate minerals or other stable carbonates. This process takes place in geological formations like limestone spontaneously over extended periods of time. Carbonation, on the other hand, is used in the context of carbon capture and utilisation (CCU) to capture and store CO_2 emissions from industrial operations. As seen in the Figure 2.1, carbonation takes place on the concrete constructions' CO_2-exposed surfaces.
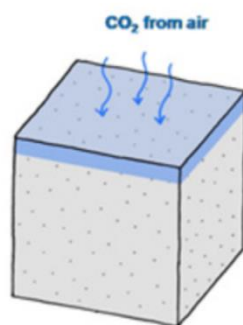
Figure 2.1:   Concrete undergoes carbonation when its exposed (CO2) surfaces
react with the concrete (www.ivl.se, n.d.)

The alkali concentration of cement determines the pH value of pore
water in cured concrete, which typically ranges from 12.5 to 13.5 (Gopal Mishra,
2013). Strong alkalinity surrounds the steel reinforcement, creating a thin
passivating coating that shields it from water and oxygen. Steel is resistant to
corrosion as long as it is kept in a very alkaline environment. This state is
referred to as passivation. When concrete is used, atmospheric carbon dioxide
seeps into it, carbonising it and lowering its alkalinity. In the cured cement paste,
the pH of the pore water decreases from around 13 to approximately 9.0.
Beginning with the exterior layers of the concrete, this procedure gradually
lowers its pH from around 13 to between 8 and 9. When it comes to reinforced
concrete construction, this pH shift can interfere with the steel reinforcement's
ability to passivate against corrosion. The steel reinforcing may then start to
corrode if oxygen and moisture are present. As a result, the concrete may lose
mechanical strength and develop spalling on its surface. Figure 2.2 show out an
illustration depicting a cross-section of reinforced concrete structure.
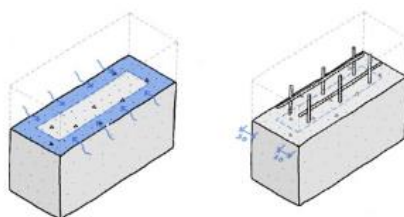
Figure 2.2:   An Illustration Depicting A Cross-Section of Reinforced Concrete
Structure (www.ivl.se, n.d.)

2.2.1 Effect of Carbonation on Waste Slag

Slag materials, which are usually obtained from industrial operations like metal smelting, coal combustion, or cement manufacture, undergo a reaction known as carbonation, in which carbon dioxide (CO_2) is introduced and combined with the alkaline components. Stable carbonate minerals are produced as a result of the reaction, principally carbonates of calcium and magnesium. The waste products left over after metallurgical processes such as extracting metals from their ores or refining them are known as slags. Untreated steel slag, however, causes detrimental expansion that compromises the integrity of steel slag concrete.

A regulated mixture of CO_2, temperature, pressure, and moisture content are usually applied to the slag material during the carbonation process. Due to this exposure, carbon dioxide (CO_2) can dissolve into the slag's pore spaces and combine with alkaline substances like magnesium oxide (MgO) and magnesium oxide (CaO) to generate carbonates (SUSHANTH KOMBATHULA, 2020). Equations 2.1 and 2.2 illustrate how the carbonation of CaO and MgO are:

$$CaO + CO_2 \rightarrow CaCo_3 \tag{2.1}$$

$$MgO + CO_2 \rightarrow MgCo_3 \tag{2.2}$$

These carbonate minerals' chemical stability and inertness allow the solid matrix of the slag material to efficiently capture carbon dioxide.

2.2.2 Effect of Carbonation in concrete

Calcium hydroxide interacts with airborne water and carbon dioxide when concrete is exposed to it. Equation 2.3 shows the reaction of :

$$Ca(OH)_2 + CO_2 \rightarrow CaCO_3 + H_2O \tag{2.3}$$
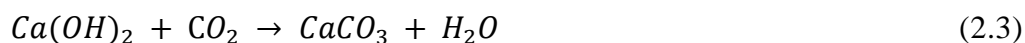
Carbonation causes the concrete's surface pH to drop to less than 8.3. This pH is enough in an industrial environment to cause the passive layer on the reinforcement to become unstable (GCCA, n.d.). As time passes, the depth of carbonation deepens, and the rate at which it occurs increases in proportion to relative humidity (RH). Low RH causes the most carbon dioxide to penetrate the concrete, but saturated concrete experiences the greatest penetration because

the reaction with Ca(OH)2 occurs in solution. The combination of these two causes carbonation to occur most quickly between 50 and 70 RH (GCCA, n.d.).

When concrete dries out quickly and gets regularly soaked by heavy rain, carbonation may have a significant role in determining how long it lasts in hot regions. In hot coastal locations, carbonation and chloride erosion can work in concert to cause significant issues (GCCA, n.d.). When enough concrete is utilised to cover the reinforcing steel, carbonation-induced corrosion is not a significant issue in northern North America (Concrete Construction, 1990).

2.3   Kinetics of Carbonation Reactions

Carbonation interactions between Ca- and Mg-containing compounds in steel slag occur during CO_2 curing, producing stable carbonate products that improve mechanical strength and structural density. The highest level of reactivity is exhibited by C_3S, and thermodynamic calculations verify that these events are spontaneous. Diffusion's impact on reaction kinetics and product generation is highlighted by kinetic studies that clarify the dissolving and carbonation behaviours of steel slag (Qifeng Song et al., 2021). Equation 2.4 to Equation 2.9 represent the primary chemical events that occur during carbonation (Qifeng Song et al., 2021).

$$2(2\text{CaO} \cdot \text{Si}O_2) + CO_2 + 3H_2O \rightarrow 3\text{CaO} \cdot 2\text{Si}O_2 \cdot 3H_2O + \text{Ca}CO_3 \quad (2.4)$$

$$2(3\text{CaO} \cdot \text{Si}O_2) + 3CO_2 + 3H_2O \rightarrow 3\text{CaO} \cdot 2\text{Si}O_2 \cdot 3H_2O + 3\text{Ca}CO_3 \quad (2.5)$$

$$\text{CaO} + H_2O \rightarrow \text{Ca}(OH)_2 \quad (2.6)$$

$$\text{Ca}(OH)_2 + CO_2 \rightarrow \text{Ca}(OH)_2 + H_2O \quad (2.7)$$

$$\text{MgO} + H_2O \rightarrow \text{Mg}(OH)_2 \quad (2.8)$$

$$\text{Mg}(OH)_2 + CO_2 \rightarrow \text{Mg}(OH)_2 + H_2O \quad (2.9)$$
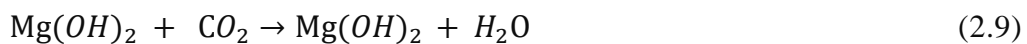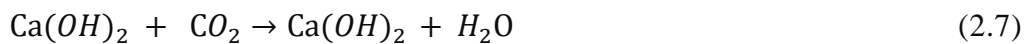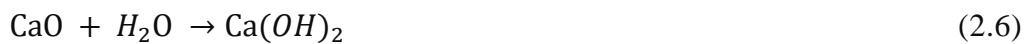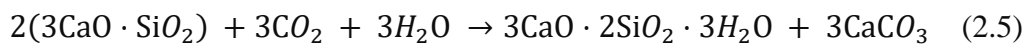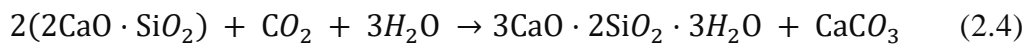
$\text{Ca}(OH)_2$ and f-CaO are found to be lost in the formation of $3\text{Ca}CO_3 3$ crystals. $3\text{Ca}CO_3$ can offer more nucleation sites for the hydration of C_3S and has good mechanical characteristics (Qifeng Song et al., 2021). Consequently, the products of carbonation and hydration fill in bigger spaces and bind cement gains or steel slag, making steel slag stronger and denser.

Steel slag's carbonation kinetics are determined by how quickly CO_2 from the environment ccombinewith the slag's calcium and magnesium oxides to produce carbonate minerals. Carbon dioxide is taken up and stored as solid

carbonate minerals during this process, which reduces its amount in the atmosphere. This is an essential step in the sequestration of carbon. CO_2 is first adsorbed onto the steel slag particles' surface. Later, carbon dioxide (CO_2) combines with magnesium oxide (MgO) and calcium oxide (CaO) to form magnesium carbonate (Mg CO_3) and calcium carbonate (Ca CO_3) during chemical processes. Heat is released during these exothermic processes.

The kinetics of the carbonation of steel slag involve several significant occurrences that impact the rate and efficiency of CO_2 gathering. Surface kinetics includes the adsorption of CO_2 onto the slag particles' surface as well as surface reactions in which CO_2 combines with the slag's calcium and magnesium oxides to generate carbonate minerals (Tamas´ Kurusta et al., 2023). As part of this process, the carbonate product that is produced is also desorption into the gas or liquid phase. The pace at which carbon dioxide diffuses out of slag pores and solid particles affects the rate at which carbonation proceeds overall. This resistance to pore diffusion is known as pore diffusion resistance. Carbonation is further facilitated by the rate of hydrolysis occurring on the particle surface and by transport mechanisms in a liquid layer. Together with the emission of heat, carbonate minerals are produced in the first chemical reaction (Equation 2.10) between the metal oxide (MO) in the slag and CO_2.

$$\text{MO} + CO_2 \rightarrow \text{M}CO_3 + \text{heat} \tag{2.10}$$

Compared to previous techniques, carbonation in solution can get a greater degree of carbonation more quickly, making it a viable option for sequestering CO_2. This multi-step technique offers the possibility of effective and quick carbon capture. It entails dissolving CO_2 in a liquid medium, then reacting it with the metal oxide to create carbonates (Tamas´ Kurusta et al., 2023).

2.4 Characteristics of Slag in Construction

Pig iron and crude steel production procedures yield important raw materials, such as iron and steel slags. The iron ore-based process and the scrap-based process are the two primary techniques of production (Ribbenhed, Thorén and Sternhufvud, 2008). The properties of slag might differ significantly based on the kind of feed, the temperature and duration of processing, the tapping environment, etc. The process of producing alloy steel results in a variety of

slags, similar to that of steelmaking (Nath, Randhawa, and Kumar, 2022). Figure 2.3 illustrates the procedures used in the steel industry that led to the creation of slag. Pig iron is created in a blast furnace using oxidic iron ores in the iron ore-based method. In the manufacturing variation that is solely dependent on scrap, steel scrap is recycled in electric arc furnace to make raw steel. Steelworks slag or blast furnace slag is the term used depending on which of these manufacturing techniques is employed. The phrases "electric furnace slag," "LD slag," and "blast furnace slag" (BFS) are interchangeable.
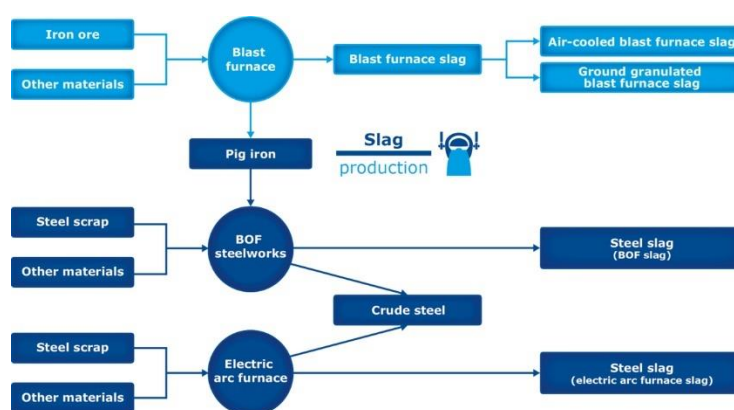
Figure 2.3:   The Steel Industry Processes Resulting in Slag Formation (www.recovery-worldwide.com, n.d.)

Blast furnace slag, which is produced during the iron-making process, is one of the main sources of slag in the building sector. Silicate and aluminate compounds, as well as leftover oxides of iron and other metallic elements, are commonly found in blast furnace slag. Slag can also come from steelmaking, copper, and nickel slag, each of which has a distinct composition and set of properties.

According to Yee Cheng Lim et al. (2020), Lightweight aggregates (LWA) have been utilised more frequently in concrete for high-rise structures and large-scale construction using waste glass and basic oxygen furnace (BOF) steel slag. Lightweight aggregates' low density can lower a structure's dead weight and save building expenses when used in concrete. Better acoustic and thermal insulation may be achieved by using the porous LWA to create room partitions. Figure 2.4 outlines the principal solid byproducts for each steelmaking process.

Main solid co-products per steelmaking route[2]
(average outputs in kg/tonne crude steel)
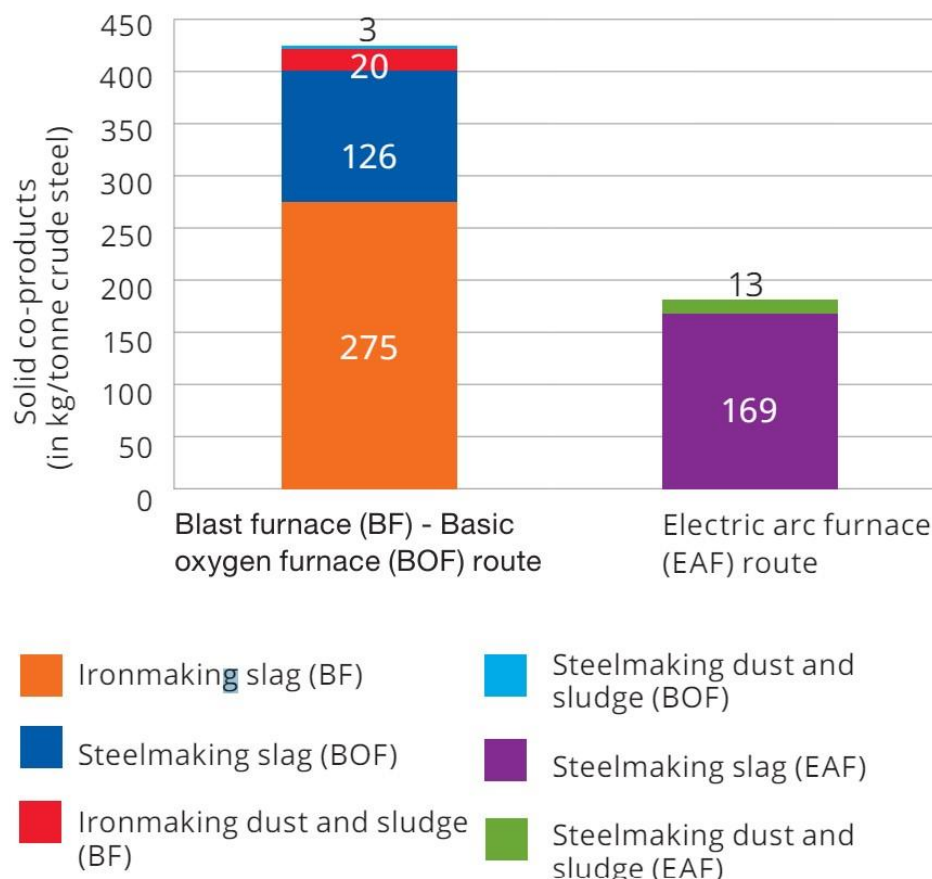
Figure 2.4: Principal Solid by Products for Each Steelmaking Process (average outputs in kg/tonne crude steel) (Steel Industry co-products Fact Sheet, n.d.)

2.4.1 Compressive Strength

According to Yu et al. (2016), the experiment on examining the impacts of adding several kinds of aggregates, such as waste glass, limestone, steel slag, and lightweight aggregate, to concrete mixes has advanced. Figure 2.5 shows the various varieties of concrete's compressive strengths. Figure 2.5 depicts various concrete mix proportions after 3, 7, and 28 days. Figure 2.5 shows that after 28 days, the coarse steel slag concrete 1 had a compressive strength of 23.0 MPa, which was similar with the 22.8 MPa of the reference mix normal concrete 1. The fc´-value for the second batch of coarse steel slag concrete (CSSC-2) at

28 days was found to be 40.5 MPa, which is lower compared to the 50.3 MPa value for the control mix, normal concrete 2 (NC-2).
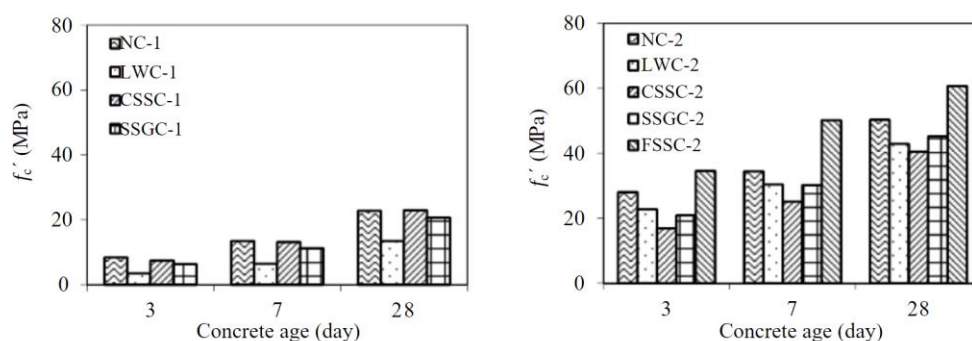
Figure 2.5:   Compressive Strength for Different Types of Concrete (Yu et al., 2016)

The unusually long time for the steel slag to weather is the reason why the second coarse steel slag concrete (CSSC-2) compression strength is not higher than regular concrete. Additionally, the coarse steel slag's relatively low quality prevented the concrete from becoming stronger. Throughout the weathering process, the slag's specific gravity dropped and its absorption capacity rose. According to Yu et al. (2016), when the steel slag weathered, the compressive strength of the concrete significantly dropped.

After 28 days, the mix FSSC-2, which uses fine steel slag in place of all the sand, has a compressive strength that is 20.7% higher at 60.7 MPa than the control mix NC-2's similar value. The fine steel slag's quality does not appear to have been harmed by prolonged weathering. Actually, by improving the conversion zone between the cement paste and the aggregate and boosting the interlocking of the porous steel slag with the paste of cement, the usage of fine steel slag boosted strength.

2.5   Basic Oxygen Furnace (BOF)

Crude steel production has increased globally in recent years; in 2021, 60 million tonnes of steel were produced globally, setting new production records. As a result, slags make about 90% of the mass of solid co-products, and their production rises along with steels. The basic oxygen furnace (BOF) slag route

produces, on average, more by-products than the Electric-Arc Furnace (EAF) slag route, which is created by high-power electric arcs.

The primary technique for producing steel is basic oxygen furnace (BOF) steelmaking. Based on statistical data, 70.8% of the world's steel output in 2018 came from crude steel produced by BOF (Wang et al., 2020). Precise estimation and management of the end-point carbon concentration in molten steel, as one of the primary processes, would significantly support high-quality, high-efficiency, and reliable production for the BOF steelmaking process.

The Basic Oxygen Furnace (BOF) technique for steelmaking is used to purify hot steel that contains different concentrations of sulphur, phosphorus, silicon, carbon, and manganese. In order to minimise slag emissions during melting, each BOF cycle, which lasts 30 to 40 minutes, includes introducing the hot metal and scrap metal into the converter, starting to blast oxygen to eliminate impurities, measuring the bath system and temperature, and blowing the metal ladle. High iron and basicity slag can be used as an earthwork or to make sinter (Wang et al., 2020). Before being stored, exhaust gases that contain dust and CO are cleaned. Figure 2.6 illustrates the BOF process.
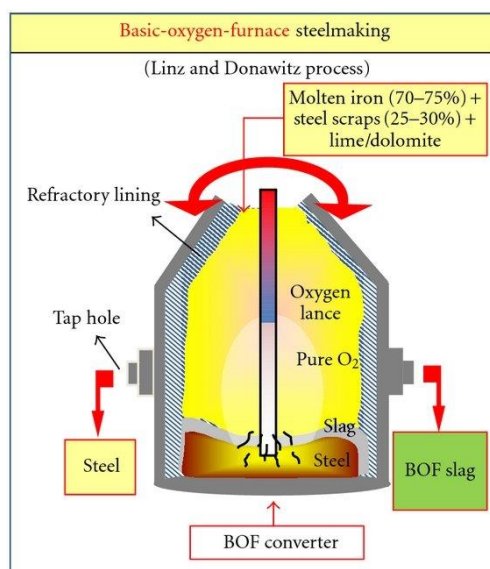
Figure 2.6: Basic-Oxygen Furnace Process (Yildirim and Prezzi, 2011).

Furthermore, a lot of study has been done on BOF slag in an attempt to find applications for it as aggregates for roads, embankments, reinforced

concrete parts, or high-performance concrete that binds well to reinforcements and is environmentally benign for prestressed concrete sleepers. Steel slag's unqualified qualities with the construction specification have prevented it from being widely used as aggregate for concrete production that is restricted by the specification.

2.5.1   Composition of BOF

According to Matthias Ruth (2004), BOF slag typically comprises 10–20% SiO_2, 40–50% CaO, 10% MgO, 10-15% iron (mixed oxides), 2-3% Al_2O_3, 10% manganese oxide (MnO), and other oxides. Significant mineralogical resemblance exists between the BOF slag and raw materials used in the production of cement, including olivine $[(Mg,Fe)_2(SiO_4)]$, merwinite $[Ca_3Mg(SiO_4)_2]$, $3CaO \cdot SiO_2$ (C3S), $3CaO \cdot SiO_2$ (C2S), and others. (Kaja and others, 2021).It is significant to highlight that phase identification is extremely challenging due to the extremely complex mineralogical composition of BOF slag, which has several overlapping peaks and distinct solid solutions of oxides (FeO and MgO). As a result, several overlapping mineral phases that were uncertain were classified as likely (Yildirim and Prezzi, 2011). Steel slag obtains its cementitious qualities from the presence of calcium silicates (C2S and C3S), tetracalcium aluminoferrite (C4AF), and other mineral constituents. BOF slag exhibits the α' and β polymorphs of the C2S phase (belite) (Kaja et al., 2021). Belite has relatively little hydraulic action in its early age when left untreated, either physically or chemically. Figure 2.7 and Figure 2.8 display the BOF slag sample and its SEM micrographs.

Figure 2.7: BOF Slag Sample (López-Díaz, Ochoa-Díaz and Grimaldo-León, 2018)
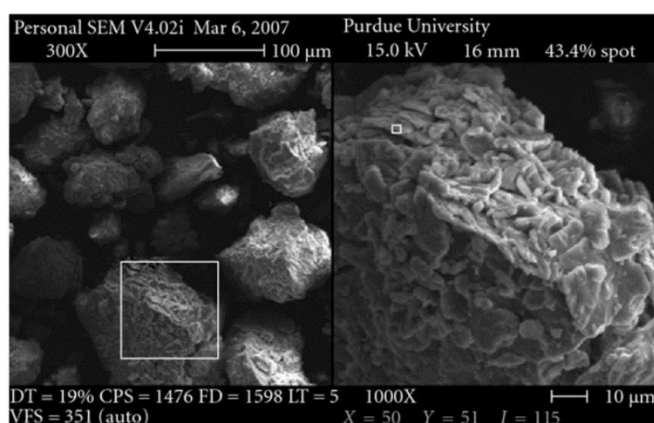
Figure 2.8: SEM Micrographs of BOF (Yildirim and Prezzi, 2011)

In addition, high specific gravity is exhibited by BOF slags, typically ranging from 3.1 to 3.7 g/cm3 (encyclopedia.pub, n.d.). The BOF slags are frequently used in concrete in construction. The purpose of BOF slags is to substitute natural aggregates. This is since specific gravity, shape, resistance to fragmentation, water absorption, wear resistance, and volumetric stability are among the crucial BOF qualities needed for concrete to work well. The characteristics of BOF slag aggregates are displayed in the table.

According to Table 2.1, BOF slag generally absorbs more water than sand and coarse aggregates, particularly for finer particle sizes. This can result in a greater need for water to keep the concrete's consistency when it's fresh, which raises the porosity of the concrete (encyclopedia.pub, n.d.). As a result of the crushing process and the mechanical strengths brought about by gradual

cooling, BOF slag has an uneven and angular form that improves the interlocking between the aggregates and the cement paste. On the contrary, extremely sharp edges may have the opposite effect, making concrete mixes with high replacement content less workable because they may cause particle segregation in the mixture and reduce concrete mobility (Sara Carvalho Zago, Vernilli and O. Cascudo, 2023).

Table 2.1: Properties of BOF Slag Aggregates (Sara Carvalho Zago, Vernilli and O. Cascudo, 2023).

Aggregates	Ap. Specific Gravity [g/cm^3]	Water Absorption [%]	Los Angeles Abras. Value [%]	f-CaO [%]	Reference
BOF SLAG	3.4	2	18	5.3	
Granite	2.7	0.5	20	N/A	[9]
Sand	2.6	0.8	-	N/A	
BOF SLAG	3.5	2.3	-	3.4	
Dolomite	2.8	1.8	-	N/A	[11]
Sand	2.7	1.5	-	N/A	
BOF SLAG	3.4	2.4	12.7	-	
Gravel	2.7	0.5	20.8	N/A	[15]
BOF SLAG	3.4	1–1.7	14–16	1.1	
Dolerite	2.8	0.3	14.8	N/A	[16]
BOF SLAG	3.1–3.7	0.2–1	17	-	
Granite	2.6–2.8	0.3–1.2	-	-	[17]
BOF SLAG	3.1–3.7	0.2–1	9–18	<10	
Basalt	2.6–2.8	0.3–1.2	15–20	N/A	[28]
BOF SLAG	3.3	1	22	<10	
Granite	2.5	<0.5	12	N/A	[29]
Gravel	2.6	<0.5	21	N/A	
BOF SLAG	3.4	1.9	12.9	1.9	
Limestone	2.7	0.9	-	N/A	[30]
Basalt	2.8	0.3	17.1	N/A	
BOF SLAG	3.4	1.8	11	-	
Limestone	2.6	1.1	25	-	[31]
Fine BOF SLAG	3.58	4.2	-	6.5	
Sand	2.56	4.0	-	N/A	
Coarse BOF SLAG	3.42	3.3	-	6.5	[32]
Limestone	2.49	1.7	-	N/A	

2.6   Electric Arc Furnace (EAF)

The Electric Arc Furnace (EAF) technique, sometimes referred to as tiny mills, uses high-power electric arcs in place of gaseous fuels to melt recycled steel waste and generate high-quality steel. Electric arcs produced by graphite electrodes are exposed to charged material, allowing electricity to flow through and heat the metal (Yildirim and Prezzi, 2011). Scrap baskets are used to meticulously select and put the scrap, which might be in shredded or heavy melt condition, into the furnace. Decarburization and dephosphorization are two refining processes that are carried out while the scrap melts, with the use of oxygen injections. To aid in the development of slag, which removes impurities from the steel, lime (CaO) is added. The addition of carbon powder to the slag creates froth, which increases refining efficiency.

Even with the usage of hot metal, the electric arc furnace can now melt a variety of charge compositions, ranging from 100% scrap to 100% DRI/HBI, and can do so in any combination between the two extremes (tenova.com, n.d.). EAFs are becoming more and more competitive in the steel production market, controlling a sizeable share of the industry's output. Machines can produce up to 300 tonnes of steel every cycle (Yildirim and Prezzi, 2011). The processes of ladle refining and electrical arc furnace steel production are illustrated in the figure 2.9.
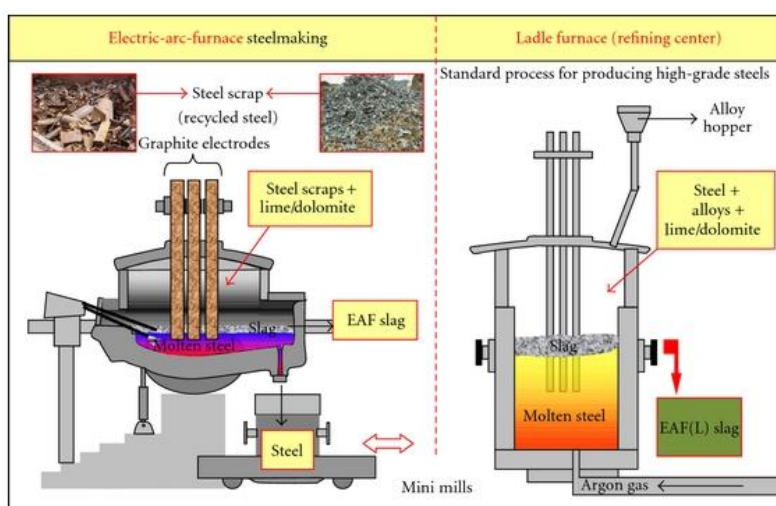
Figure 2.9:   The Electrical Arc Furnace Steel Making and Ladle Refining Process (Yildirim and Prezzi, 2011)

An industrial waste product of the steelmaking process is steel slag. This material's substantial quantity of strategic metals (SMs) makes it an essential curiosity economic resource. The continuous increase in the volume of steel produced by melting slag in the electric arc furnace (EAF) results in a considerable amount of EAF slag. According to Nour-Eddine Ménad et al. (2021), the different minerals contained in the BOF and EAF slags caused several overlapping peaks in their XRD patterns, which were described as being highly complicated

BOF slag and EAF slag are comparable in terms of their chemical makeup. The primary constituents of EAF slags exhibit significant variability. According to Nour-Eddine Ménad et al. (2021b), EAF slags usually have the following oxide contents: FeO (10–40%), CaO (22–60%), SiO2 (6–34%), Al2O3 (3–14%), and MgO (3–13). The 0 to ¾ inch treated EAF slag is shown on the left in Figure 2.10. For comparison, a gloved hand holding a range of EAF slag sizes is shown in the illustration on the right. Additionally, figure 2.11 shows particles of BOF and EAF slag.

Figure 2.10:   0 – ¾ Inch Processed EAF Slag and A Variety of EAF Slag Sizes in a Gloved Hand for a reference. (US EPA, 2021)
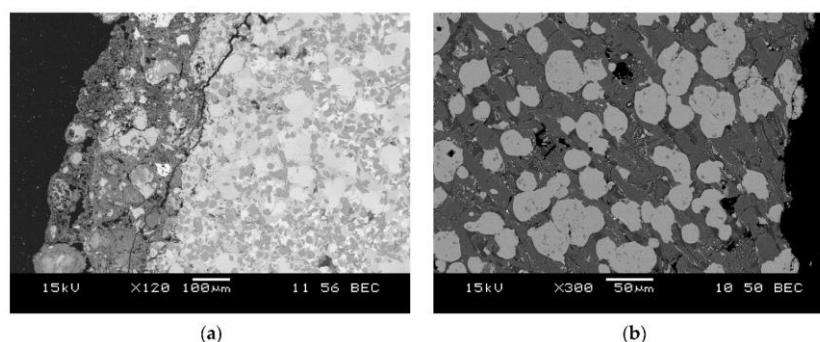
Figure 2.11:   (a) BOF Slag and (b) EAF Slag Particle (Brand and Fanijo, 2020)

Free MgO and CaO in the slag can cause swelling when hydrated, which is harmful to many civil engineering applications and causes slag volume to fluctuate over time (National Academies of Sciences et al., 2023). Due to this instability, several slag processing facilities alter the chemical and/or mineralogical features of the slag in order to reduce the volume instability brought on by the expansive components of steel slag.

2.7 Effect of Temperature on Reaction Mechanisms

2.7.1 Temperature

Comprehending the complex effects of temperature affecting steel slag's carbonation process is crucial to evaluating the way it absorbs CO_2. Heat treatment transforms lower-reactivity mineral elements into receptive ones and increases the reactive surface area of the slag, hence modifying its physical and chemical characteristics dramatically. However, high heat can also result in sintering, which reduces slag's porosity and reactivity and may stop carbonation (Baras et al., 2023).

The temperature at which steel slag carbonation undergoes possesses a major impact. Aqueous carbonation and dry carbonation methods behave differently with respect to the temperature at which carbonation occurs. The two studies are the aqueous carbonation and the dry carbonation of Electric Arc Furnace slag (EAF), according to Qifeng Song et al. (2021). The Figure 2.12 shows out the schematic diagram of carbonation setups, which are dry carbonation, aqueous carbonation.
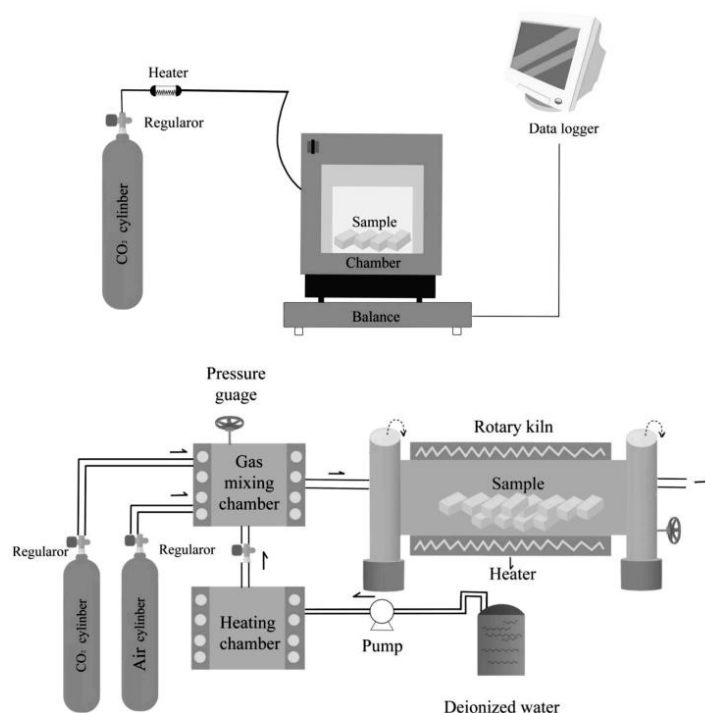
Figure 2.12:   Schematic Diagram of Carbonation Setups: Dry Carbonation Upper) and aqueous carbonation (Bottom) (Qifeng Song et al., 2021).

Higher temperatures improved the carbonation process but decreased CO_2 solubility in water, according to studies conducted on different particle sizes of BOF slag (Qifeng Song et al., 2021). On the other hand, the rate of carbonation decreased at temperatures over 200°C. Temperature affects the rate of slag component dissolving and CO_2 solubility of carbonation products in aqueous carbonation. Research has indicated that a rise in temperature stimulates the carbonation process to a particular point, beyond which the rate of carbonation diminishes. The optimal temperature for aqueous carbonation, for instance, was found to be around 200°C.

Steel slag undergoes dry carbonation when CO_2 reacts with it in the absence of water. Lower temperatures can occasionally result in greater absorption rates even though higher temperatures normally encourage CO_2 absorption, particularly at CO_2 concentrations of 50% or 75% (Qi Feng Song et al., 2021). On the other hand, high temperatures can cause CaCO_3 formation, which reduces slag surface area and reduces carbonation effectiveness. As a

result, temperature optimisation is essential to strike a balance between CO_2 absorption and any downsides.

2.7.2 Carbon Dioxide Levels and Pressure Variations

Important factors affecting the carbonation rate of steel slag are CO_2 concentration and pressure. For a given carbonation time, lower concentrations of CO_2 can attain equivalent or even higher conversion rates than high concentrations, which initially result in higher reaction rates. According to this, compressive strength and CO_2 capture capacity are positively associated, meaning that changing the CO_2 concentration can improve the performance of steel slag. In moderate circumstances, higher CO_2 concentrations and pressures tend to accelerate carbonation processes because they enhance CO_2 solubility and availability for interaction with steel slag components (Qifeng Song et al., 2021). On the other hand, very high CO_2 concentrations or pressures may cause the carbonate minerals to precipitate quickly, generating protective carbonate coatings on the slag surface that prevent more carbonation. (Qifeng Song et al., 2021).That is significant to highlight that even in situations where the concentration of CO_2 is either significantly higher than in the natural environment or relatively low, the complex metal compounds in steel slag act as catalysts to speed up the carbonation reaction. The reaction time as a function of CO_2 concentration is displayed in the Figure 2.13.
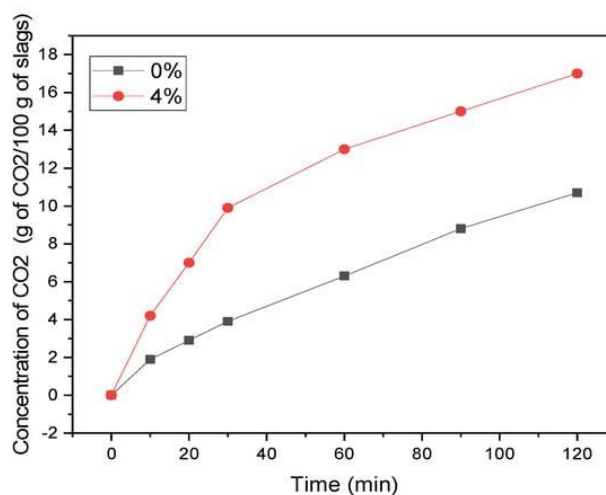
Figure 2.13: Effect of Reaction Time by Concentration CO_2 (Amer Baras et al., 2023)

Research findings indicate that steel slag may be evenly filled with calcium carbonate when CO_2 pressure is low. Research has demonstrated that when CO_2 concentration rises, the rate of carbonation conversion reduces, particularly at low concentrations of less than 50% (Baras et al., 2023). EAF slag exhibits greater reactivity and Ca utilisation than BOF slag, suggesting that other variables may also impact the rate of carbonation. Carbonation efficiency and CO_2 concentration have a complicated connection, and the ideal circumstances depend on a number of variables, including pressure and temperature (Baras et al., 2023). In the early stages of carbonation, temperature and CO_2 pressure interact in a time-dependent manner to promote CO_2 diffusion and increase the rate at which calcium is converted.

2.7.3   Particle size

Particle size has a major impact on how well carbonation works in steel slag. Studies have shown that reducing the size of the particles improves the specific surface area of the slag and leads to higher rates of carbonation conversion. Because they give carbonation more surface area, smaller particles boost the overall conversion extent (Qifeng Song et al., 2021). The link between carbonation efficiency and the size of particles is crucial in influencing the rate of dissolving of any substance. Conversely, CO_2 cannot diffuse because of the calcium carbonate coating that forms on the surface of the steel slag fragments during the carbonation process (Huang, Zhang, and Zhang, 2024).

Since grinding may reduce expenses and improve efficiency, grinding particles to the ideal size is a typical technique. The fineness of the powdered steel slag particles greatly affects the water content and carbonation of the active components in steel slag. As the steel slag particle size reduces, the rate of CO_2 absorption increases with specific surface area, increasing the overall amount of carbonation and improving the strength of the resulting steel slag products. For instance, the amount of free lime conversion elevated from 8% to 43% when the particle size of BOF slag reduced from 1.6 mm to 0.08 mm (Baras et al., 2023).

Moreover, finer particles have been observed to facilitate a higher uptake of CO_2, resulting in a more porous and looser product layer compared to

larger particles. This finer structure improves the overall performance of resulting materials, enhancing strength and optimizing pore structure. Additionally, it has been demonstrated that smaller particles allow for higher absorption of CO_2, resulting in a looser and more porous product layer. This finer structure optimises pore structure and strength while further enhancing the general functionality of the resulting materials. Agglomeration, however, usually occurs when the steel slag micro powders particular size becomes close to a certain threshold. The ideal fineness of steel slag facilitates the accomplishment of the best mechanical performance of steel slag products (Huang, Zhang and Zhang, 2024).

2.8   Effect of Temperature on Reaction and Kinetic on Slag

The basic oxygen furnace slag's (BOFS) carbonation kinetics are greatly influenced by temperature. First, it has been shown that BOFS's carbonation conversion rises with temperature, albeit the rate of rise may differ based on variables like rotation speed. Because of improved reaction kinetics, higher temperatures often result in quicker carbonation conversions. The process of carbonating steel slag is influenced by temperature in both wet and dry carbonation processes.

Among the other properties of the carbonation reaction, temperature affects the rate of dissolution of slag components, the solubility of CO_2, the nucleation of crystals, and the generation of carbonation products. Various studies have determined the ideal temperatures for carbonation processes, which may vary from 60°C to 200°C based on variables including particle size and liquid-solid ratio (Qifeng Song et al., 2021). Higher temperatures in dry carbonation usually result in more CO_2 being absorbed; however, there are some outliers, especially when the CO_2 concentration is between 50% and 75% (Qifeng Song et al., 2021). Raising the temperature facilitates quicker CaCO3 production by accelerating CO_2 diffusion into slag pores. Nevertheless, excessive CaCO3 buildup can obstruct more carbonation by filling the pores in the slag and covering its surface, which would ultimately lower the reaction rate (Qifeng Song et al., 2021).

Furthermore, there is a strong correlation between the surface coverage model—which describes these kinetics—and experimental data at various temperatures, demonstrating the model's dependability. According to SEM findings, carbonation processes mostly take place at the surface of BOFS particles, where they result in the formation of a protective CaCO3 carbon layer (Qifeng Song et al., 2021). Additionally, higher temperatures accelerate the leaching of calcium ions from BOFS into solution but delay the precipitation of calcium carbonate due to decreased CO_2 solubility. At lower temperatures, the rate-limiting step for carbonation is primarily the diffusion of reactants through the product layer (Pan et al., 2014). In general, temperature has a significant impact on reaction rates, surface coverage, and the process's rate-limiting phase when it comes to the kinetics of carbonation in BOFS.

2.9 Analytical Techniques for Characterizing Carbonation Reactions

2.9.1 X-Ray Diffraction (XRD) Analysis

Materials scientists use X-ray diffraction analysis (XRD) to determine the slag sample's mineralogical composition (Nour-Eddine Ménad et al., 2021a). In order to measure the intensities and scattering angles of the X-rays that leave a material, XRD first exposes the substance to incident X-rays. The foundation of all diffraction techniques is the production of X-rays in an X-ray tube. The diffracted beams from these X-rays are collected once they are directed towards the sample. The angle formed by the diffracted rays and the incident is a crucial factor in all diffraction. Beyond this, the equipment for powder and single crystal diffraction varies.

Tiny crystallites make up a wide variety of materials. These crystals' "phase" refers to their structural type and chemical makeup (Dutrow and Clark, 2019). Materials may consist of both crystalline and non-crystalline components and can be single-phase or multiphase combinations. The diffraction patterns produced by various crystalline phases in an X-ray diffractometer are distinct. Phase identification can be done by comparing reference database patterns to X-ray diffraction patterns acquired from unidentified materials (Malvern Panalytical, 2020). This method is comparable to the procedure of comparing

fingerprints at a crime scene. Figure 2.14 is showing X-ray Diffraction D8-Discover instrument.

Figure 2.14: X-ray Diffraction D8-Discover Instrument (Dutrow and Clark, 2019)

The XRD detector, sample container, and X-ray source are the three main parts of an X-ray apparatus. The sample is made visible by X-rays from the source of the radiation. The X-ray source illuminates the sample with X-rays, which then pass through the sample phase, are diffracted, and enter the detector (Dutrow and Clark, 2019). Diffraction data are captured and the intensity is quantified by shifting the tube, sample, and detector to alter the diffraction angle. The diffractometer's geometry and the kind of sample determine whether the angle between the incident beam and the sample is constant or changing. It is commonly matched with the diffracted beam angle. According to Bragg's rule, these waves contribute constructively in a few particular directions but cancel each other out destructively in most other directions. Equation 2.10 illustrate the formula of Bragg's rule:

$$2d\sin\theta = n\lambda \qquad (2.10)$$

The variables θ, n, d, and λ represent the incidence angle, variables, beam wavelength, and spacing between diffracting planes, respectively (Dutrow and Clark, 2019b). Reflections are the spots on the diffraction pattern that correspond to the specified directions. Thus, electromagnetic waves impinging on a regular array of scatterers produce X-ray diffraction patterns. The reason

X-rays are utilised to create the diffraction pattern is that their wavelength, λ, and the distance, d, between the crystal planes, are frequently of the same order of magnitude (1-100 angstroms) (Dutrow and Clark, 2019b). The figure 2.15 show out the X-ray powder diffractogram.
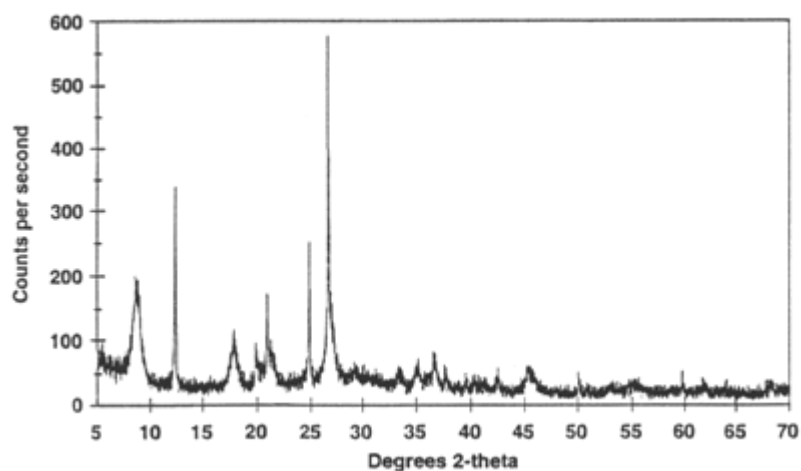
Figure 2.15: X-ray Powder Diffractogram (Dutrow and Clark, 2019b)

2.9.2 Thermogravimetric Analysis (TGA)

Numerous works deal with the use of thermogravimetric analysis (TGA) of plant biomass for determining thermal decomposition mechanisms (Marion Carrier et al., 2011). TGA cane coupled to a spectrometer for improving the understanding of the thermal decomposition mechanisms. The particular melting temperature of each component allows TGA to quantitatively resolve complicated mixes. Figure 2.16 show out the instrument of Thermogravimetric Analysis.

Figure 2.16: Instrument of Thermogravimetric Analysis (Made-in-China.com, n.d.)

A test used to assess structural, chemical, and physical changes in a material brought on by temperature variations is known as thermal analysis. Temperature is a fundamental state variable that influences most physical characteristics, structural changes, and chemical reactions (Watkins et al., 2015). In general terms, thermal analysis refers to any technical or scientific assessment of a material that involves varying temperature as an experimental parameter.

Nonetheless, this phase has historically been restricted to certain methods including thermogravimetric and calorimetric effects. The primary methods used in thermal analysis are now generally acknowledged to be differential thermogravimetry (DTA) between a sample and a reference, thermogravimetry (TG) and its derivative (DTG) for measuring weight loss, and differential scanning calorimetry (DSC) for determining heat flow (Watkins et al., 2015). Thermal analyses are frequently employed in conjunction with other methods to compute thermal diffusivity, specific heat, and thermal conductivity (Watkins et al., 2015). Depending on the objective, many methods or a mix of methods can be applied for assessing material properties. Figure 2.17 shows out the Thermal gravimetric analysis (TGA) data collected on the starting steel.
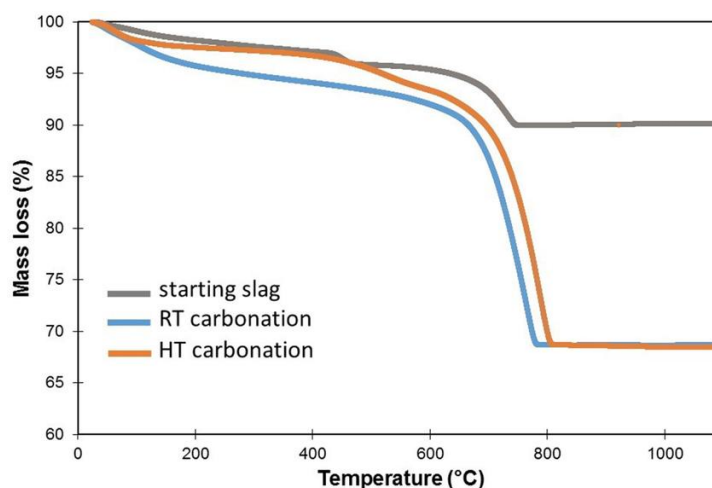
Figure 2.17: Thermal Gravimetric Analysis (TGA) Data Collected on the Starting Steel (Crouzet et al., 2017).

2.9.3 Scanning Electron Microscopy (SEM)

High-resolution pictures and comprehensive surface data about materials may be obtained using the incredibly flexible scanning electron microscopy technique. Information about the sample is disclosed by the signals that result from electron-sample interactions. This information includes the sample's exterior morphology (texture), chemical makeup, and the orientation and crystalline structure of the constituent components. Most applications include gathering data over a predetermined portion of the sample's surface, from which a two-dimensional picture is created to show the spatial changes in these characteristics (Nanoscience Instruments, 2018).

This kind of electron microscopy creates pictures at a far higher resolution than optical microscopy by scanning a specimen's surface with a concentrated electron beam. The resolution of SEM instruments can range from < 1 nanometer up to several nanometers (Swapp, 2017). Using a concentrated electron beam, this kind of electron microscopy scans a specimen's surface to provide pictures with far higher resolution than optical microscopy. SEM equipment have resolutions ranging from less than one nanometer to several nanometers (Swapp, 2017).

The surface of a sample is exposed to a concentrated stream of electrons in a scanning electron microscope (SEM), which uses specialised detectors to gather the various signals it produces. Information on the topography and

composition of the surface may be obtained by using the different signals produced by the interaction between the electrons in the beam and the atoms in the sample. Immediate view image observing on an external monitor is made possible by software that correlates the position of the beam with the electron intensity detected by the detector or detectors.

High-resolution imaging in a scanning electron microscope (SEM) is often achieved using two types of detectors: backscattered electron detectors (BSD) and secondary electron detectors (SED). Surface component microscopy can be obtained by the use of energy-dispersive X-ray spectroscopy (EDS) detectors (Nanoscience Instruments, 2018). The SEM's unique configuration ultimately affects the accuracy and available picture techniques. The SEM instrument is seen in the image below. Figure 2.18 below shows the SEM instrument.

Figure 2.18: SEM Instrument (Swapp, 2017)

Scanning Electron Microscopy (SEM) is a powerful technique used to obtain magnified images revealing the topography, morphology, size, shape, and composition of materials. By integrating an Energy Dispersive X-ray Spectrometer (EDS) with SEM, elemental composition analysis can be performed. EDS utilizes X-ray spectra emitted when a sample is bombarded with electrons to provide localized chemical analysis (Ural, N, 2021). This allows for qualitative and quantitative analysis through point, line, and area scans, enabling researchers to characterize materials and identify their

crystallographic structures. Figure 2.19 show out the SEM-EDS analysis with the area scan of clay.
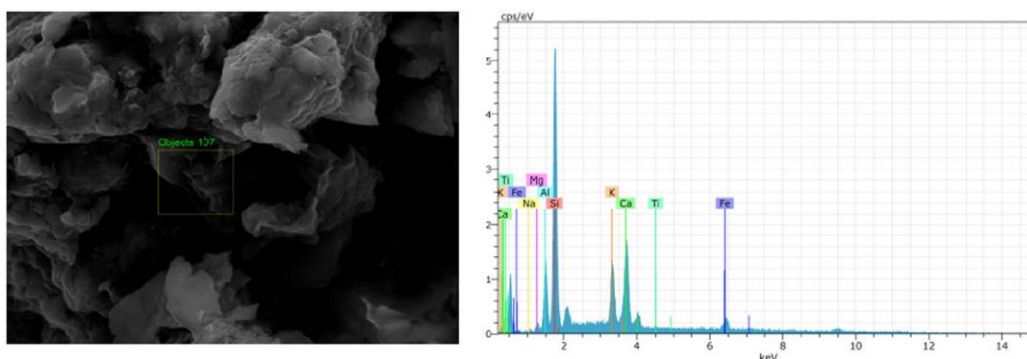
Figure 2.19:   SEM-EDS Analysis with Area Scan of Clay. (Ural, N, 2021)

2.9.4   Energy Dispersive X-Ray Spectroscopy (EDX)

EDS/EDX (Energy Dispersive X-ray Spectrometer) is a technique for elemental and compositional analysis based on the information from the X-rays produced by electron irradiation (Oxford, 2023). EDS functions with three major parts: an emitter, a collector, and an analyzer. These parts are typically equipped on an electron microscope such as SEM (Gaston and Protter, 2019). It is an analytical technique for finding the elements present in the sample. It relies on an interaction of some source of X-ray excitation and a sample.Figure 2.20 show the instrument of EDX-SEM.

Figure 2.20: Instrucment of EDX-SEM (www.mst.or.jp, n.d.)

A higher energy outer-shell electron then proceeds to fill its place, releasing the difference in energy as an X-ray that has a characteristic spectrum based on its atom of origin (www.thermofisher.com, n.d.). This allows for the compositional analysis of a given sample volume that has been excited by the energy source. The position of the peaks in the spectrum identifies the element, whereas the intensity of the signal corresponds to the concentration of the element (www.thermofisher.com, n.d.). In this, highly energetic particles like electrons or an X-ray beam is allowed to fall on the sample. This excites the electron of the inner energy level thereby creating a hole in it. The electron of the outer energy level now can transit to this inner energy level by releasing the excess energy in the form of X-ray photons (Ma et al., 2016). The number and energy of these X-ray photons are measured by an energy-dispersive

The EDS data is presented as a graph with KeV on the x-axis and peak intensity on the y-axis. The peak location on the x-axis is converted into the atoms that the energy changes represent by a computer program (Gaston and Protter, 2019). Figure 2.21 shows the data collected from EDX.
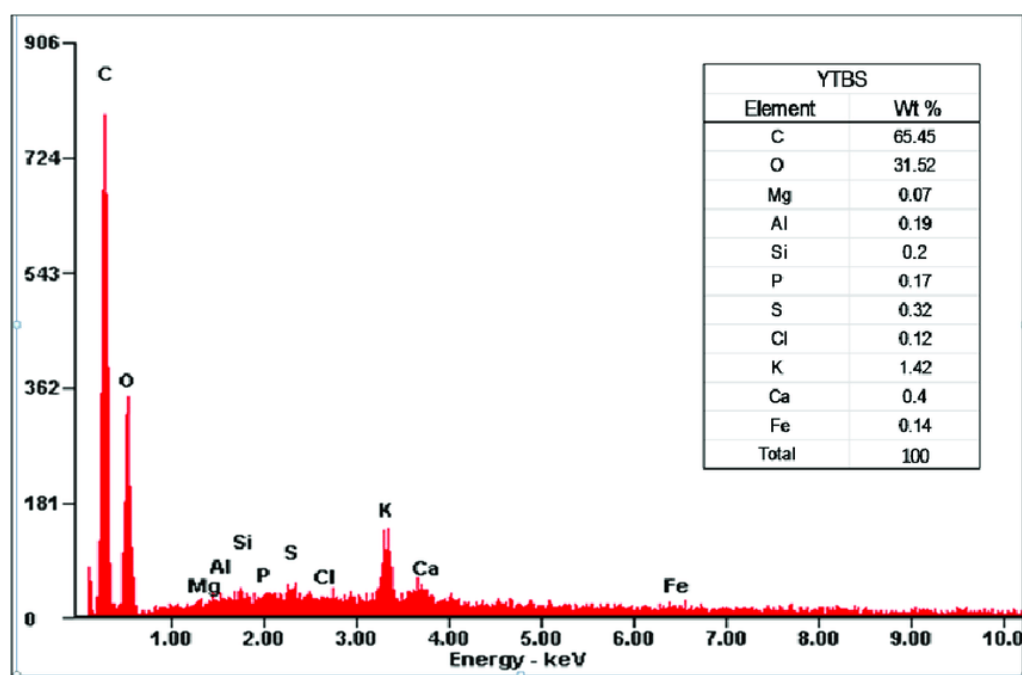
Figure 2.21: The Data collected from EDX (Asuquo, Martin and Nzerem, 2018)

Energy dispersive X-ray spectroscopy (EDX) is one of the important techniques to characterize the material in terms of its purity and

stoichiometricity (Ma et al., 2016). It is an analytical technique for finding the elements present in the sample. It relies on an interaction of some source of X-ray excitation and a sample. It works on the principle that the unique atomic structure will have unique X-ray emission spectrum peaks. In this, highly energetic particles like electrons or an X-ray beam are allowed to fall on the sample. This excites the electron of the inner energy level thereby creating a hole in it. The electron of the outer energy level now can transit to this inner energy level by releasing the excess energy in the form of X-ray photons. The number and energy of these X-ray photons are measured by an energy-dispersive spectrometer. This spectrometer data gives information on the composition of the sample.

2.10   Effect of Steel Slag on Mortar

Most of the published studies assessed the mechanical and physical properties of mortars and concretes neglecting the effects on the durability-related properties and the necessity of a pre-treatment on the steel slag aggregate (Nunes et al., 2024). The steel slag can be separate as BOF slag fines and EAF slag fines.

BOF slag fines were used as an alternative material for cementitious mortars. On the other hand, all the BOF slag particles were ground to pass through a 0.15 mm mesh and also used to produce cementitious mortars (Tung Hsuan Lu et al., 2018).

Electric Arc Furnace Dust collected from two different steelwork plants is used as secondary raw material in the production of self-compacting mortars (Lozano-Lunar et al., 2019). Higher replacement levels of EAF Dust affected fresh and early hardened concrete properties that retarded the setting time of concrete and lower compressive strength at an early age (R Syahyadi et al., 2020).

2.10.1   Compressive Strength

Figure 2.22 shows the average values of compressive strength for mortar specimens. According to Figure 2.22, the compressive strength of mortar mixed with sand and non-carbonated BOF, smaller than 1.6 mm, is better than the reference mortar.   Besides, the compressive strength of mortar mixed with carbonated BOF is better than non-carbonated BOF. From this, the only mortar specimen that obtained similar consistency, soundness and compressive strength values as the reference mortar specimen, was the one with carbonated BOF slag of <0.5 mm particle size (Bodor et al., 2016).
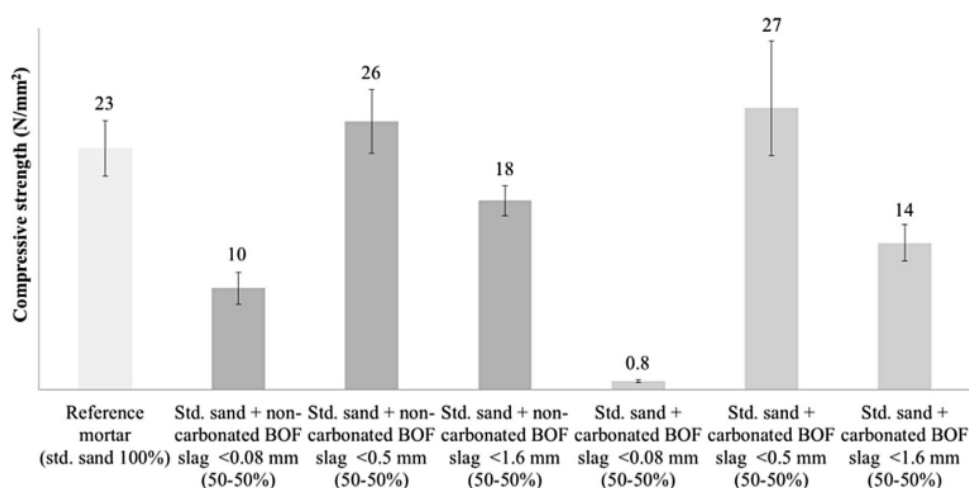
Figure 2.22: Average values of compressive strength for all mortar specimens (reference, non-carbonated BOF slag aggregate replacement, and carbonated BOF slag aggregate) (Bodor et al., 2016)

According to da Silva Magalhães et al. (2017), the experiment compares the three material contents, normal mortar, mortar contains 5 % EAF dust and mortar contains 10% EAF dust. Data shown in Figure 2.23 highlight that, in most cases, compressive strength increases when 5% of EAFD is used as supplementary cementing material, whereas it decreases at 10% of substitution, regardless of the w/b ratio and the age of curing.

The maximum observed strength gain in M01 mortars with 5% of EAFD is 5.2% at 7 days, and 2.8% at 28 days; conversely, the highest loss in M02 mortars with 10% of EAFD is 3% at 7 days, and 4.3% at 28 days. It is worth noting that even at 7 days of curing, the retardant effect in strength

development is not observed at the lowest EAFD dosage (da Silva Magalhães et al., 2017).
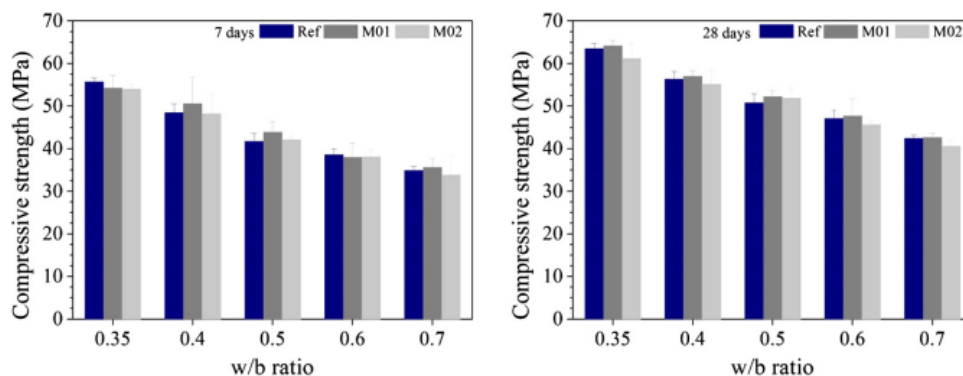
Figure 2.23: Experimental compressive strength of tested mortars, with varying w/b ratios, at 7 and 28 days (da Silva Magalhães et al., 2017).

2.11   Summary

A substitute material for mortar has been investigated: waste slag. The review focuses on the differences in the slag's crystallographic structure, the effects of temperature, thermal decomposition mechanisms, and crystallographic structures under different settings of carbonation. The studies also address which test is better for comparing waste slags that have been carbonated or uncarbonated. In addition, this study discusses the role of waste slag as well as how mortar differs from normal mortar in terms of compressive strength, flexural strength, and load bearing. In addition, the studies discuss about the how much strength improve for the mortar under adding steel slag.

CHAPTER 3

Methodology and Work Plan

3.1 Introduction

This chapter overviews the methodology for examining the chemical composition and internal structure between crystallized uncarbonated waste slag and carbonated waste slag. Then, the progress of carbonation of the steel slag and the progress. This study also discusses the progress of mixing the normal mortar and mortar which have BOF and EAF. Besides, the study also overviews the compressive strength, flexural strength and load bearing of the mortar mixed with BOF, EAF and normal mortar. Figure 3.1 shows the flowchart of the methodology.

Raw Materials Preparation (EAF, BOF)

↓

Oven-Dry the Slag (BOF, EAF)

↓

Sieve Analysis for the slag (BOF, EAF)

↓

Examine the steel slag by EDX, XRD SEM and TGA

↓

Compressive steel slag under 2 mm into small cylinder sample

↓

Carbonation of the steel slag which compressed and some steel slag follow the settings

↓

Examine the steel slag which compressed into small cylinder carbonated slag by EDX, XRD and SEM

Do casting mortar which mixes with carbonated steel slag under settings

↓

After casting for 1 day, demould, weigh and curing 28 days in the tank.

↓

Dry, Product and Laboratory Test
1. Compressive Strength Test
2. Flexural Strength Test
3. Load Bearing Test

↓

Examine the powder of mortar which mix with steel slag under settings by EDX, XRD, TGA and SEM

Figure 3.1: Flowchart of the Methodology

3.2   Raw Material Preparation

3.2.1   Electric Arc Furnace Slag (EAF)

Electric arc furnace (EAF) slags, which were bought from Penang state, were selected as the sample material for the mineralization experiment. The reasons was their relevance to the local context and availability. Figure 3.2 illustrates that EAF slags have a dark, metallic appearance, attributed to the presence of iron oxides and other metal compounds. Several steps are undertaken to prepare the EAF slags for the subsequent mineralization process. These steps are crucial to ensure the accuracy and reliability of the experimental results.

Figure 3.2: EAF slags

3.2.2   Ordinary Portland Cement

Ordinary Portland Cement (OPC), manufactured by YTL Cement Sdn. Bhd. and marketed under the name "ORANG KUAT," was the cement used in this investigation. Approved by MS EN 197-1, CEM 1 52.5, the cement is designed as a high-strength OPC that makes handling simple and early de-moulding possible. The product is especially appropriate for high-strength precast components. High early strength, quick setting, and reliable product quality are among its advantages, which make it appropriate for a variety of general-purpose uses like precast and brick production. To assure compliance with ASTM C150 requirements, sieving is required before mortar mixing, with OPC passing through a 600 μm sieve. Figure 3.3 shows ORANG KUAT Ordinary Portland Cement (OPC).
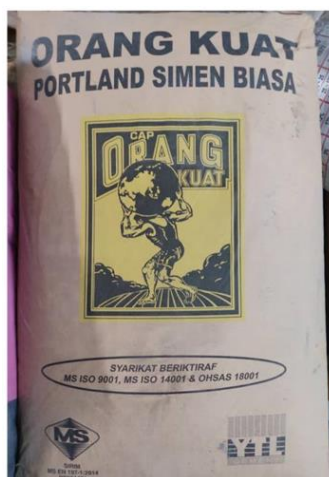
Figure 3.3: ORANG KUAT Ordinary Portland Cement (OPC)

3.2.3 Fine Aggregates

The fine aggregate utilized in the study adhered to standards ASTM C778 and ASTM C136. Initially, the fine aggregate, which consisted of sand, underwent oven drying at temperatures ranging from 100°C to 110°C to eliminate excess moisture content, ensuring no additional water would be introduced into the fine aggregate mix. Subsequently, the fine aggregates underwent sieve analysis according to ASTM C136 to verify its particle size, ensuring it did not exceed 600 μm as specified in ASTM C778. This meticulous process ensured the fine aggregate met the required standards for use in the mortar mixture, enhancing the overall quality and performance of the resulting material. Figure 3.4 shows out the fine aggregates.

Figure 3.4: Fine Aggregate

3.2.4 Water

Following ASTM C1602 guidelines, the water used in the study was pure and free of contaminants including acid, alkali, oil, salt, and other organic and inorganic materials that may have harmed the mortar's qualities and consequently impacted the study's findings. Both potable and non-potable water were considered suitable for use in mixing mortar; however, in this case, laboratory tap water was used. The crucial C-S-H gel, or calcium silicate hydrate gel, is formed during the hydration process, which is sped up using a proportion of water to cement of 0.55 to give the mortar workability during casting. Furthermore, the investigation included the creation of water in five distinct ratios, spanning from 0.5 to 0.7, with a 0.05 increment rate, guaranteeing a thorough examination of the water-cement interaction.

3.3 Sieve Analysis

The sieve analysis was done with steel slag (BOF slag and EAF slag). A total of 2 kg was measured to perform the particle size distribution curve. The sizes of the sieve analysis are 5 mm, 4.75 mm, 3.35 mm, 2.36 mm, 2 mm and 0.8mm were arranged in descending order from top to bottom and the steel slag sample was placed on top sieves. Afterwards, the overall sieve was placed on the sieve shaking machine and the cover plates were tightened. The sieve shaking machine was switched on and operated for 4 minutes. After 4 minutes, the material retained in each sieve and each sieve pan was weighted and the particle size distribution curve was plotted to determine the fineness modulus of steel slag. Figure 3.5 shows the arrangement of the sieve analysis pan on the sieve shaking machine.

Figure 3.5: The Photo of Sieve Analysis Pan on Sieve Shaking Pan

3.4 Carbonation Chamber

The steel slag carbonation samples are made easier by the controlled functioning of the carbonation chamber. To replicate real-world carbonation conditions, the chamber is usually built to maintain particular parameters including temperature, pressure, and gas composition. Figure 3.6 shows the photo of the manual pallet press. Steel slag powder was compressed into little pieces as the Figure 3.8 before entering the carbonation chamber. After that, some steel slag was also put in the carbonation chamber for carbonation. Here are the steps involved in operating a carbonation in the carbonation chamber:

1.   Prepared slag samples.

2.   Oven-dried the steel slag.

3.   Sieve the steel slag.

4.   Weighted steel slag under 2 mm weighted 10.00g and were compressed slags into small pieces by manuel pellet press.

5.   Placed samples inside the carbonation chamber.

6.   Set the condition of the condition as table 3.1.

7.   Sealed the chamber to create a controlled environment.

8.   Monitored and recorded temperature, pressure, humidity and time.

9.   Allowed carbonation reaction to occur over 1 day.

10. Opened chamber after completion of the reaction.

11. Removed slag and crushed the samples for analysis.

12. Analyzed results by EDX, XRD and SEM.

The conditions used in this study for slag were divided into two types of slag. Table 3.1 shows the condition required in the apparatus. Figure 3.6 shows the manual pallet press. Figure 3.7 shows the photo of the Carbonation Chamber. All the samples would be put inside the chamber to have a carbonation reaction.

Figure 3.6: Manual Pallet Press

Figure 3.7: Carbonation Chamber

Figure 3.8: Compated Steel Slag Sample

Table 3.1: The Condition Required in the Apparatus

Temperature	Humidity	CO2 concentration	Temperature	Humidity	CO2 concentration	Temperature	Humidity	CO2 concentration
10	40	10	20	40	10	30	40	10
10	40	20	20	40	20	30	40	20
10	40	30	20	40	30	30	40	30

Temperature	Humidity	CO2 concentration	Temperature	Humidity	CO2 concentration	Temperature	Humidity	CO2 concentration
10	60	10	20	60	10	30	60	10
10	60	20	20	60	20	30	60	20
10	60	30	20	60	30	30	60	30

Temperature	Humidity	CO2 concentration	Temperature	Humidity	CO2 concentration	Temperature	Humidity	CO2 concentration
10	80	10	20	80	10	30	80	10
10	80	20	20	80	20	30	80	20
10	80	30	20	80	30	30	80	30

3.5 Mix Ratio for Mortar

Table 3.4 and Table 3.5 illustrate the proportion of materials used to produce the normal mortar and mortar mixed with EAF slags. Table 3.3 shows the proportion of normal mortar and the proportion of mortar mixed with EAF slags is also shown in Table 3.4. Table 3.4 serves as a summary and the user guide to produce the mortar in which cement proportion is replaced by EAF slags. The total volume of mortar's material is used for three specimens cube, cylinder and prism. The replacement ratio of the cement by steel slag is 30%. The proportion of all the mortar includes the wastage of 20% to 30%. In this study, the target density of the mortar is 2000 kg/m^3. Table 3.2 illustrates the replacement percentage of each raw material, and the total replacement percentage of the mortar is 2.604. Equation 3.1 also shows the formula to calculate the volume per unit of each raw material.

Table 3.2: Replacement Percentage of Raw Material

Raw Material	Replacement Percentage, %
Cement	1.000
Sand	0.7
Slag	0.354
Water	0.550
Total:	2.604

$$\text{Volume per Unit} = \text{Target Weight} \left(\frac{\text{Replacement Percentage}}{\text{Combined Proportion of Material}} \right) \quad (3.1)$$

Table 3.3: Proportion of Normal Mortar

Material	Volume for 1 cube (kg)	Total Volume (kg)
Cement	3.97	11.91
Sand	3.97	11.91
Water	2.18	6.55

Table 3.4: The Proportion of Mortar Mixed with EAF

Material	**Proportion of Percentage (%)**
Cement	13.841
and	9.689
BOF Steel Slags	3.673
Water	7.612

Table 3.5: Density of Mortar's Material

Material	Density (kg/m3)
Steel slag	2135
Sand	2650
Cement	3150

3.4   Mortar Mixing

The mortar specimen was produced by mixing all the raw materials. First, the amount of Ordinary Portland cement, steel slag, sand and tap water was calculated before being weighed. Then, put all the material except water into the mixer. Figure 3.9 shows the photo of the mixer and Figure 3.10 illustrates the photo of the preparation of raw materials. The cement, sand and carbonated slags under settings conditions were poured and mixed in dry conditions according to the proportion. Next, add in water slowly. Using a 1-liter container, the mixer's fresh density was determined. Make sure the density of freshly blended mortar is between 2000 ± 50 g/L. The procedure was repeated mortar which was mixed with other settings of BOF and EAF. The normal mortar also follows the procedure. Figure 3.11 shows the process of wet mix.

Figure 3.9: Photo of Mixer

Figure 3.10: Photo of Preparation of Material

Figure 3.11: Wet Mix of Material

3.6 Mortar Casting

Before the mortar casting, the steel mould was checked to ensure no leakage would occur during the mortar pouring. Next, the mould oil was applied to the mould to ease the demoulding process afterwards. The specimen was subsequently poured after the freshly blended mortar material was placed in the mould. The mould used was steel mould, which is the specimen size was 100 x 100 x 500 mm prism steel mould, 150 mm × 150 mm × 150 mm cube mold and 5/8" diameter cylinder mould. Next, tampering and tapping were applied to ensure the mixture's homogeneity. After that, the trowel was used to flatten the surface of the specimen. After the surface flattening work, the mortar specimen was left for one day for initial hardening. Figures 3.12, 3.13 and 3.14 shows the mortar casting process.

Figure 3.12: The Photo of Prism Steel Mould

Figure 3.13: The Photo of Cube Mould

Figure 3.14: The Photo of Cylinder Mould

3.7   Curing Process

One day after casting, the mortar was cured. First, the desired specimens were demolded and tagged with specific settings of steel slag based on the mortars mixed with which type of steel slag. After that, two sets of the previously mentioned mortar cube, cylinder and prism specimens were made. All the sample total of 171 samples were produced.

The mortar test specimens for the second set of specimens and weigh the samples following demolding and were allowed to cure for 28 days. Lastly, the mortar specimens were air dried by the oven the day before testing. In order to allow the mortar samples to air dry, the specimens were finally taken out the day before the test. Figure 3.15 illustrates the photo of mortar curing.

Figure 3.15: The Photo of Mortar Curing

3.8   Mortar Cube Specimen Test

Three methods were used for the mortar which was mixed with slags. There are compressive strength, flexural strength and load bearing. Mould size needs to attention because each experiment test corresponds to a different mould.

3.8.1   Compressive Strength Test

The first set of specimens was tested for compressive strength at 28 days using a compression test machine, as shown in Figure 3.16. The compressive strength test by using the compression test machine was based on the standard of BS EN 12390–4. The concrete cube specimen must be undrained, and the cross-section area of the specimen must be measured before the compressive strength test. The procedure to conduct the test was to place the concrete cube specimen at the centre of the plate of the compression test machine, as shown in Figure 3.13. Before placing the specimen on the platen, the platen was cleaned. Start the test by applying loading on the concrete cube specimen until cracking happens as Figure 3.17. The maximum loading applied on the concrete cube specimen was recorded. Before testing, the cube needed to be oven-dried for 1 day and the weight of the cube sample was recorded.

Figure 3.16: The Photo of Compression Test

Figure 3.17: The Photo of Mortar Cube Crack in Compressive Strength Test

3.8.2 Splitting Tensile Strength Test

The splitting tensile strength test was conducted to obtain the splitting tensile strength of the cylindrical specimens for 28 days. A universal compression machine is utilized to carry out the test as shown in Figure 3.18. The cylindrical specimens were oven-dried and the saturated concrete was weighed. Packing strips were placed at the top and the bottom of the specimen that was subjected to the surface of compression and adjusted to the centre of the machine's base plate. Start the test by applying loading on the cylinder specimen until cracking

Figure 3.18: The Photo of Load Bearing

3.8.3   Flexural Strength Test

The four-point flexural test was used in this study. Flexural strength test was used to identify the testing samples' flexural strength and modulus. The test could be identified as the amount of bending force that the sample can resist. For the four-point flexural strength test, the sample was set up as Figure 3.19. Figure 3.20 illustrates the sample in which the line was drawn and Figure 3.21 shows the photo of the flexural strength test.
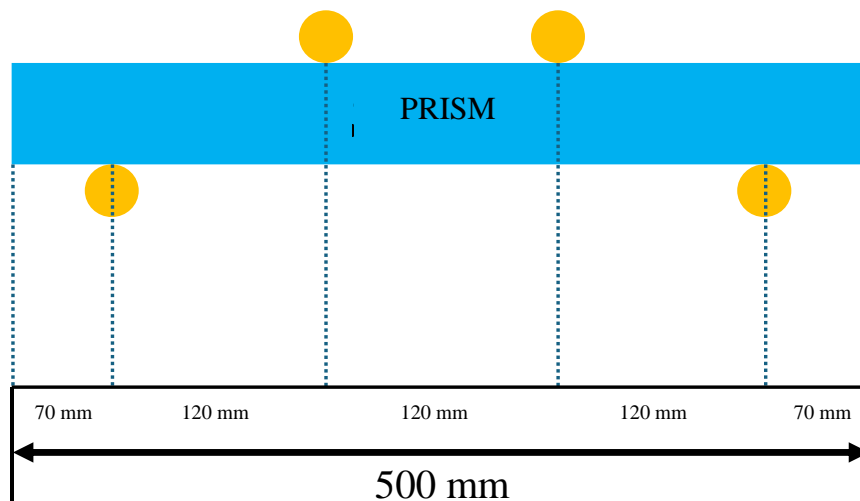
Figure 3.19: Plan View of the Sample Set up on the Flexural Strength Machine

Figure 3.20: The Sample in which The Line was Drawn

Figure 3.21: The Photo of Flexural Test

3.9 Laboratory Tests

3.9.1 X-ray Diffraction (XRD)

X-ray Diffraction (XRD) is a versatile non-destructive analytical technique used to analyze physical properties such as phase composition, crystal structure and orientation of the sample. The source illuminates the sample with X-rays. After that, the material passes through the sample phase and into the detector. The intensity is measured and diffraction data are recorded by moving the tube or sample and detector to alter the diffraction angle (2θ), which is the angle between the incident and diffracted beams. The angle between the incident beam and the sample can be either constant or variable, depending on the diffractometer's geometry and the kind of sample. This angle is often associated with the diffracted beam angle. The photo of X-ray Diffraction (XRD) is shown in Figure 3.22.

Figure 3.22: The photo of X-ray Diffraction (XRD)

In the procedure for preparing samples for X-ray Diffraction (XRD) analysis, the first step involved further grinding the small particles of carbonated slag samples and mortar after the test until they reached a powdered form. Figure 3.23 illustrates the photo of the apparatus which grinds the samples into powder. Once the sample was finely powdered, it was filled into the concave on the sample specimen holder, as shown in Figure 3.24. Subsequently, manual compression was applied using a piece of glass to ensure that the sample was tightly compacted within the concave. This compression was crucial to prevent the sample from falling out during scanning in the XRD machine.

Figure 3.23: The Photo of the Apparatus Grinds the Sample into Powder.
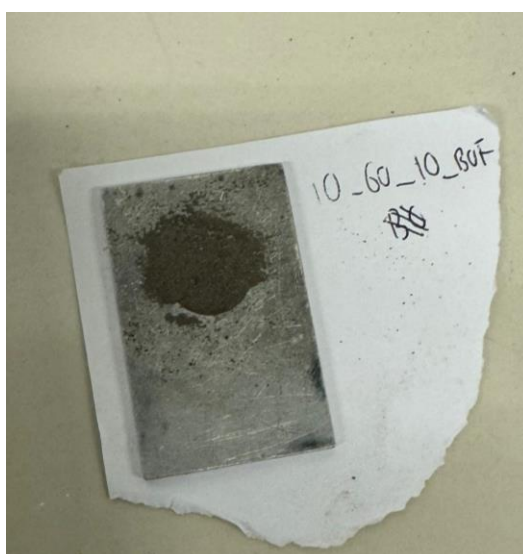
Figure 3.24: XRD Sample Specimen Holder

During the scan, the sample was rotated from a specific angle to another, depending on the scanning range determined for the analysis. In this study, the scanning range spanned from 5 ° to 85 ° and the entire XRD analysis was expected to take approximately 40 minutes to complete.

3.9.2 Scanning Electron Microscopy (SEM)

Scanning electron microscopy, also known as SEM, is a powerful imaging technique to examine the microstructure of materials at high magnification to capture high-resolution images of the surface material. By scanning a focused beam of electrons across the sample surface, the surface image was generated by the emission of photons. SEM is particularly useful for characterizing the surface topography, particle size, shape, and distribution of materials. To perform elemental analysis of the sample, SEM might be combined with energy-dispersive X-ray spectroscopy (EDX), which would further expand its capabilities. Figure 3.25 shows the SEM and EDX specimen stubs and mounts and Figure 3.26 illustrates the photo of scanning electron microscopy.

Figure 3.25: SEM and EDX Specimen Stubs and Mounts

Figure 3.26: Scanning Electron Microscope

3.9.3 Energy dispersive X-ray (EDX)

EDS, also known as energy-dispersive X-ray spectroscopy, allows for an elemental composition of the sample. The premise for the functioning of EDS is the ability of high-energy electromagnetic radiation (X-rays) to discharge "core" electrons. The working principle of EDX is the same as SEM. Figure 3.27 shows out the photo of energy dispersive X-ray.
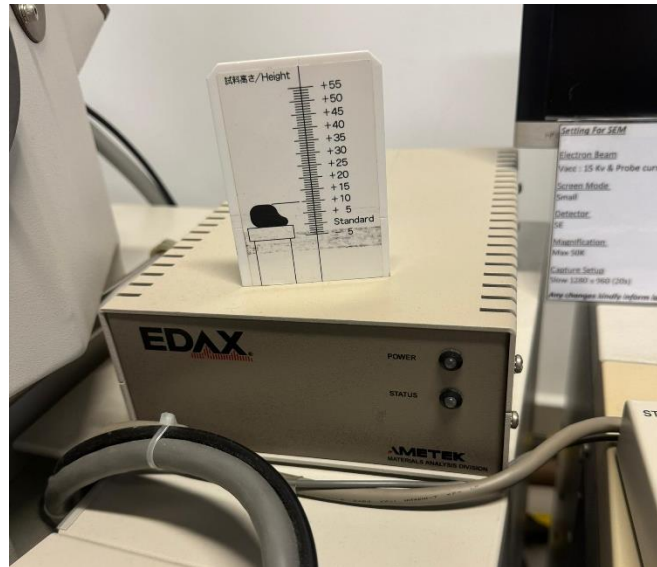
Figure 3.27: The Photo of Energy Dispersive X-ray

The elemental composition of a sample may be determined analytically through energy dispersive X-ray (EDX) testing, which focusses on elements including carbon (C), oxygen (O), silicon (Si), magnesium (Mg), calcium (Ca), and aluminium (Al). The interaction of the X-ray excitation with the sample is what allows for the analysis of the sample; the X-rays that are released provide information about the availability of particular elements in the sample.

3.9.4 Thermogravimetric analysis (TGA)

Thermogravimetric analysis (TGA) instrument measures the amount and rate of change in the mass of a sample as a function of temperature and time in a controlled atmosphere. The technique is used to characterize materials that exhibit either mass loss or gain due to loss of volatiles, decomposition, and oxidation. The instrument was versatile and can be used to investigate various thermal processes, including decomposition kinetics, phase transitions, and stability. TGA can be used to determine the composition, thermal stability of materials. Figure 3.28 shows the Thermogravimetric analyzer used in this study

Figure 3.28: Thermogravimetric analyzer

During the thermal analysis of the carbonated samples, specific conditions were set to facilitate accurate measurement of the sample's thermal properties. The analysis was conducted under a nitrogen (N2) atmosphere, with a continuous flow rate of 50 ml/min. Additionally, a purge gas was employed at a flow rate of 20 ml/min to maintain a stable environment within the TGA instrument. The heating rate is set to 10 °C/min, ensuring a gradual increase in temperature over time. The temperature range spanned from 30 °C to 900 °C, covering a broad spectrum to capture any changes in sample mass throughout the heating process. These controlled conditions enabled precise characterization of the thermal behavior and decomposition kinetics of the samples during TGA analysis.

3.10   Summary

The study focuses on the carbon mineralization process of Electric Arc Furnace (EAF) slag, aiming to produce calcium carbonate and magnesium carbonate due to their abundance in the slag composition. The investigation involved preparing 10 g samples of EAF slag, compacted into cylindrical shapes (20 mm diameter, 10 mm height) using a hydraulic compaction machine. These samples were then subjected to the mineralization process for 24 hours in a carbonation chamber at temperatures of 40 °C, 60 °C, and 80 °C. To ensure a comprehensive approach, the process was also conducted under different CO_2 concentrations (10%, 20%, and 30%) and humidity levels (40%, 60%, and 80%), resulting in a total of 27 carbonated slag samples. Various analytical methods were employed to evaluate the outcomes of the mineralization process. Scanning Electron Microscopy (SEM) and Energy Dispersive X-ray (EDX) were used to investigate the slag's microstructure and elemental composition. Additionally, X-ray Diffraction (XRD) helped identify mineral compounds and crystalline structures, while Thermogravimetric Analysis (TGA) assessed the thermal stability of the carbonated slag samples. In summary, the study explores the engineering properties of carbonated EAF slag, with a focus on understanding the physical and chemical stability of the slag under varied conditions of temperature, CO_2 concentration, and humidity.

CHAPTER 4

Result and Discussion

4.1 Introduction

This chapter presents the results and explanations of several laboratory tests performed to assess the effects of varying temperatures on the mineralization process, CO2 conversion efficiency, and the thermal stability of carbonate minerals formed within electric arc furnace (EAF) slag. The tests conducted include Scanning Electron Microscopy (SEM), Energy-Dispersive X-ray spectroscopy (EDX), X-ray diffraction (XRD), Thermogravimetric Analysis (TGA), as well as mechanical strength tests like compressive strength, flexural strength, and splitting tensile strength for mortar mixed with carbonated EAF slag.

SEM was utilized to study the morphology and microstructure of the EAF slag before and after carbonation. The results allowed the identification of specific crystalline structures that indicated the formation of carbonate minerals. EDX analysis provided information on the elemental composition of the samples, particularly focusing on the changes in carbon content before and after mineralization. XRD analysis helped identify the precise crystalline structures and mineral phases in both untreated and carbonated EAF slags, offering insights into the purity and crystallinity of the carbonates formed.

TGA was employed to evaluate the thermal stability of the carbonated minerals, tracking changes in sample weight under controlled temperature variations. This provided insights into decomposition processes, phase transitions, and the overall stability of the carbonate phases formed in the slag. In addition to these tests, three mechanical strength tests were conducted on mortar mixed with carbonated slag to evaluate its performance under different stresses:

1. **Compressive Strength Test**: This test assessed the mortar's ability to withstand axial loads, providing data on the load-bearing capacity of the material. The results offer valuable insights into the structural performance of mortar with carbonated slag under compression, which is critical for construction applications.

2. **Flexural Strength Test**: This test measured the mortar's resistance to bending forces. By applying a bending load until failure, the test determined how well the mortar can handle flexural stresses, which is crucial for materials subject to bending or flexing in structural applications.

3. **Splitting Tensile Strength Test**: This test evaluated the material's ability to resist tensile stresses, simulating conditions that could lead to cracking or splitting. By subjecting the mortar to tensile forces, the test results provide information on its durability and resistance to tensile failure.

The combined outcomes from these mechanical strength tests, alongside SEM-EDX, XRD, and TGA analyses, offer a comprehensive understanding of the effectiveness of CO2 uptake, optimal conditions for carbonation, and the stability of carbonate minerals formed in EAF slag. These findings provide essential data for evaluating the suitability of carbonated slag as a sustainable and durable material in construction.

4.2 Sieve Analysis (EAF)

In this section, sieve analysis is conducted to determine the particle size distribution of a granular material. This method classifies particles into various size ranges by passing the material through a series of sieves with progressively smaller mesh sizes. Sieve analysis is significant as it aids in selecting filter materials, ensuring uniform powder sizes in manufacturing, and classifying ores in mining for efficient processing. This technique is essential for optimizing material performance and quality across various industries.

The methodology of sieve analysis involves passing the materials through different mesh sizes, starting from the largest to the smallest. In this study, sieve sizes of 6.3 mm, 5 mm, 4.75 mm, 3.35 mm, 2.36 mm, 2 mm, and 0.8 mm were utilized. The material analyzed in this section is EAF slag, and the weight retained on each sieve is measured to determine the particle percentages within specific ranges. Figure 4.1 illustrates the graduation curve of EAF slags.
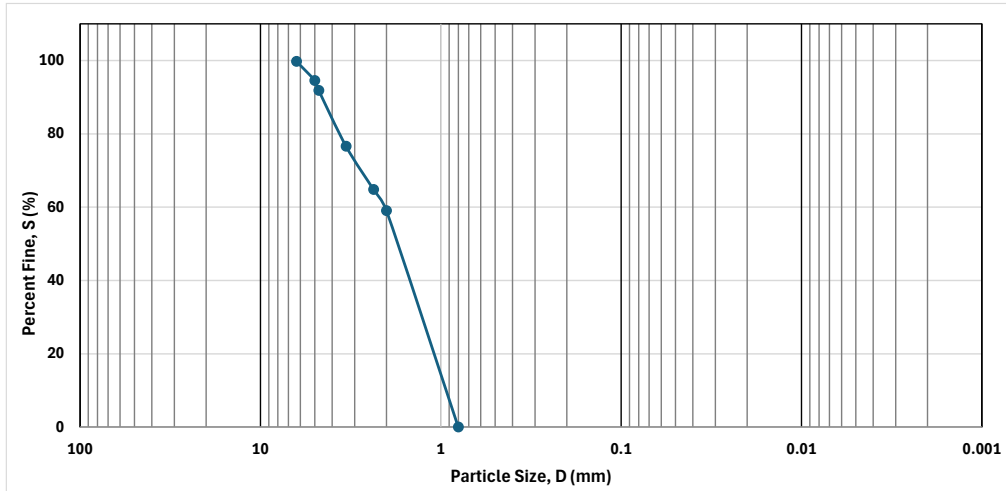
Figure 4.1: Graduation Curve for EAF Slag.

The fineness modulus of the slag is calculated to be 5.86, with the first sieve size set at 0.8 mm. According to ASTM C33 criteria for slag grinding, a coefficient of uniformity (Cu) greater than 6 and a curvature coefficient (Cc) between 1 and 3 are required for the slag to be classified as well-graded. However, the values obtained in this study are Cu = 2.06 and Cc = 0.97, which do not meet the ASTM standards. As a result, the slag is classified as poorly graded. Table 4.1 summarizes the calculated values for fineness modulus, coefficient of uniformity, and curvature coefficient.

Table 4.1:   Summary of Parameters in Sieve Analysis

Material	Parameter					
	Fineness Modulus	d_{10}	d_{30}	d_{60}	C_u	C_C
EAF slag	5.86	1.00	1.41	2.06	2.06	0.97

4.3   SEM Analysis

SEM analysis provides insights into the surface and microstructure of samples at high magnification. In this study, SEM was utilized to investigate the crystalline structures of uncarbonated EAF slag, carbonated EAF slag, and mortar mixed with carbonated EAF slags.

Figure 4.2 presents the SEM images of uncarbonated EAF slag at a magnification of 1.5k. The images reveal a rough surface texture characterized by protrusions and variations in height and size. Notably, the structure of

uncarbonated EAF slag lacks distinct crystal formations, which can be attributed to its non-uniform particle size and loose structure. In contrast, the smoother and less crystalline appearance of carbonated EAF slag may result from the carbonation process, which fills surface voids and reacts with the material, ultimately altering the surface texture and reducing roughness.
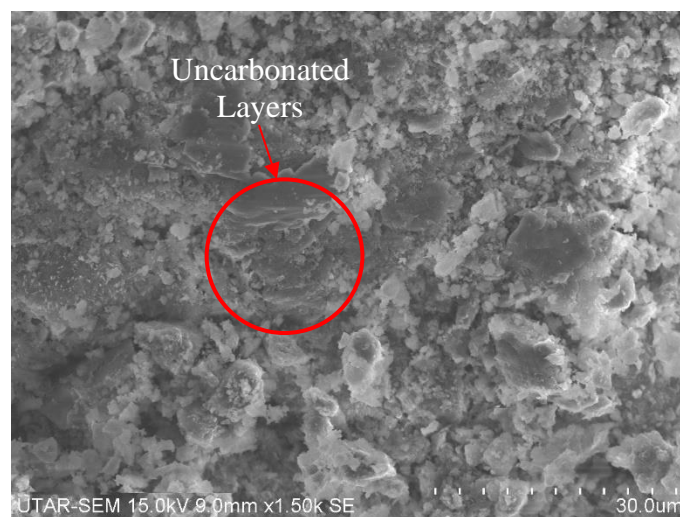
Figure 4.2: SEM Image of Uncarbonated EAF Slags

Figure 4.3 (a) to (c) presents the SEM results of EAF slag under conditions set at 20_40_10, 20_40_20, and 20_40_30, focusing on temperature, humidity, and CO_2 concentration, all observed at a magnification of 1.5 kV. The findings indicate that the surfaces of carbonated EAF slag are rougher compared to those of uncarbonated slag. Additionally, the crystalline structure of carbonated slag is more pronounced than that of uncarbonated slag. For samples mineralized at 20 °C, the crystal structure increased in correlation with rising CO_2 concentrations. Similarly, temperature increases also contributed to enhanced crystalline formation. However, the development of crystalline structures is influenced by other factors, such as CO_2 concentration and humidity. This suggests that carbonation can significantly alter the mineralogical characteristics of EAF slag. Factors including slag type, carbonation process, and mineral composition play crucial roles in these changes (Wang et al., 2021).

a)

b)

c)
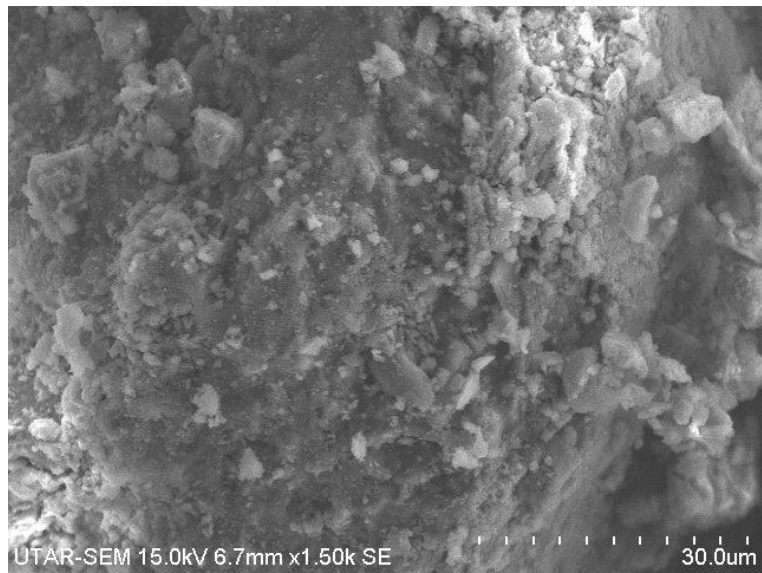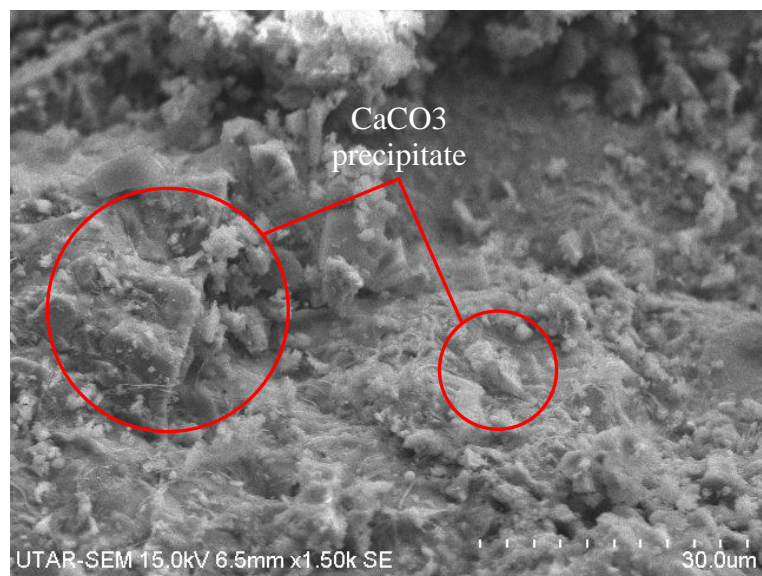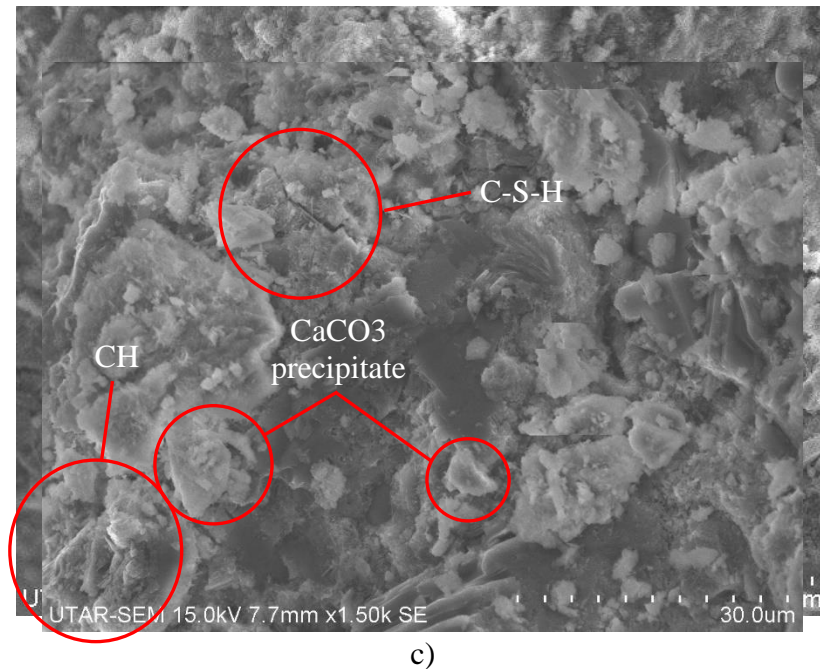
Figure 4.3: SEM Images of Carbonated EAF Slag under Various Conditions: a) 20_40_10; b) 20_40_20 c)20_40_30.

Figure 4.4 displays the SEM images of mortar mixed with EAF slags under the condition 20_40_30 at a magnification of 1.5 kV. In contrast, Figure 4.3 illustrates the crystalline structure of carbonated slag, highlighting its significant influence on the crystalline structure of mortar. Figures 4.4 and 4.5 present SEM images of normal mortar for comparison. The crystalline structure of mortar mixed with carbonated EAF slags is notably more pronounced than that of normal mortar. Similar observations were noted under various experimental conditions, and XRD results further confirmed the presence of $CaCO_3$ on the surface of the EAF slag.

Figure 4.4: The SEM Images of Mortar Mixed with EAF Slags under condition
20_40_30
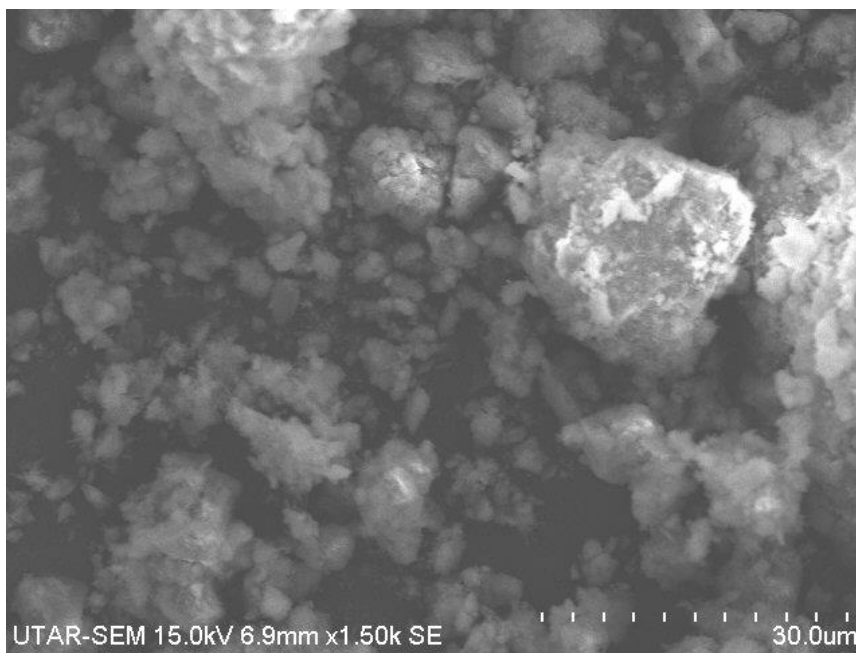
Figure 4.5: The SEM Images of Normal Mortar

4.4   EDX Analysis

EDX (Energy Dispersive X-ray Spectroscopy) analysis is commonly paired with SEM (Scanning Electron Microscopy) to identify and characterize the elemental composition of a sample, providing detailed surface information. The results obtained from EDX analysis involve detecting the X-rays emitted from a sample when bombarded with electrons, which allows for the determination of the specific elements present and their relative abundances.

In this research, EDX was utilized to analyze the elemental composition of electric arc furnace (EAF) slags both before and after mineralization. The aim was to evaluate the CO_2 conversion efficiency of the mineralization process under various temperature parameters and simulated conditions.

Table 4.2 presents the elemental composition of EAF slags before carbonation, reported as weight percentages. The analysis reveals the presence of oxygen, calcium, magnesium, aluminum, and silicon, with mean weight percentages of 16.27%, 62.72%, 2.63%, 4.82%, and 13.2%, respectively. Notably, no carbon element was detected in the samples prior to mineralization.

Table 4.2:   Elemental Composition of EAF Slags with Particle Sizes Ranging from 0.8mm to 2.36mm.

Element	(wt%)
O	16.27
Ca	62.72
Mg	2.63
Al	4.82
Si	13.2

According to Librandi et al. (2019), calcium, magnesium, and aluminum are present as metal oxides, including CaO, SiO_2, MgO, Al_2O_3, and FeO. From Table 4.2, calcium is found to be the most abundant element in the EAF slags, followed by silicon. However, silicon does not readily react with CO_2 or other substances. Wahyu S. Putro et al. (2021) note that converting SiO_2 is challenging due to the strength of the Si-O bonds and the thermodynamic

stability of the SiO_2 structure. Additionally, the carbothermal reduction of SiO_2 to silicon metal requires extremely high temperatures (around 1900 °C). Although magnesium reacts more easily than calcium, its proportion in the EAF slag is minimal. Therefore, the majority of reactions involving CO_2 are primarily attributed to calcium.

The CO_2 conversion efficiency of the mineralization process can be assessed by measuring the change in carbon concentration in EAF slag samples before and after the process. Specifically, the changes in elemental carbon content reflect the chemical reaction between calcium oxide and CO_2, resulting in the formation of calcium carbonate. Table 4.3 displays the elemental composition of carbon in the EAF slag samples.

Table 4.3: Elemental Composition of Carbon in Carbonated EAF Slag Samples

Stimulated Condition	Sample No	Temperature (°C)	Humidity Level (%)	CO2 Concentration (%)	Elemental Composition of Carbon (wt%)
1	1	10	40	10	2.83
	2	20			3.59
	3	30			4.9
2	4	10	40	20	6.34
	5	20			8.65
	6	30			9.95
3	7	10	40	30	12.21
	8	20			13.98
	9	30			14.87
4	10	10	60	10	2.94
	11	20			3.78
	12	30			5.22

5	13	10	60	20	7.44
	14	20			9.53
	15	30			10.23
6	16	10	60	30	13.72
	17	20			14.73
	18	30			15.68
7	19	10	80	10	3.43
	20	20			4.53
	21	30			5.71
8	22	10	80	20	8.46
	23	20			10.13
	24	30			11.57
9	25	10	80	30	14.86
	26	20			15.34
	27	30			16.97

The tabulated data has been plotted into three graphs depicting carbon element content (wt%) versus temperature (°C) for better analysis, as illustrated in Figures 4.6 to 4.8. These figures show a clear trend of increasing carbon content with rising temperature across all simulated conditions. For instance, at a temperature of 30°C, the carbon element content for conditions 1, 2, and 3 reaches 4.9%, 9.95%, and 14.87%, respectively. This indicates that higher temperatures significantly enhance CO_2 conversion efficiency in the mineralization process, regardless of variations in CO_2 concentrations.
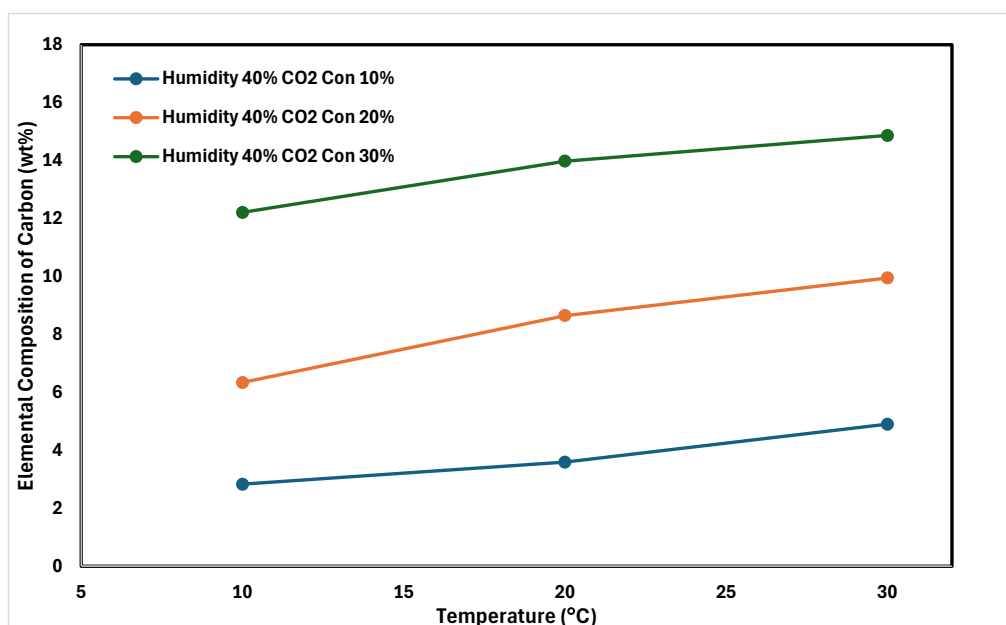
Figure 4.6: Graph of Carbon Element Content versus Temperature under 10%, 20%, 30% CO2 Concentration at Relative Humidity of 40%.

Temperature plays a critical role in the efficiency of CO_2 mineralization, as demonstrated in Figure 4.6. As the temperature increases, the CO_2 conversion rate also rises, particularly at moderate humidity levels and CO_2 concentrations. Under conditions of 40% humidity and 30% CO_2 concentration, the highest efficiency in CO_2 conversion was observed at elevated temperatures, indicating that temperature is a key factor in accelerating the carbonation process. Furthermore, Figure 4.7 illustrates that higher temperatures consistently lead to an increase in carbon content, confirming that elevated temperatures enhance the mineralization process and promote the formation of more stable carbonates.
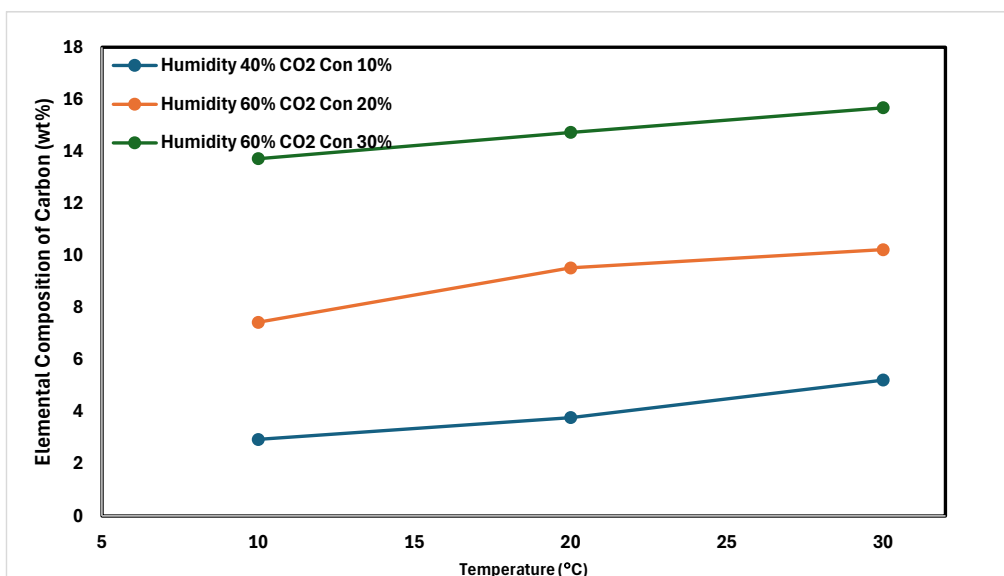
Figure 4.7: Graph of Carbon Element Content versus Temperature under 10%,
20%, 30% CO2 Concentration at Relative Humidity of 60%.

Figure 4.7 illustrates the relationship between elemental carbon content
and temperature for simulated conditions 7, 8, and 9. The plots indicate that the
elemental carbon composition did not increase with rising temperatures. Among
all samples, the condition 20_80_20 exhibited the best CO_2 conversion rate at
14.87%. Figure 4.8 presents the graph of carbon element content versus
temperature under 10%, 20%, and 30% CO_2 concentrations at a relative
humidity of 80%.
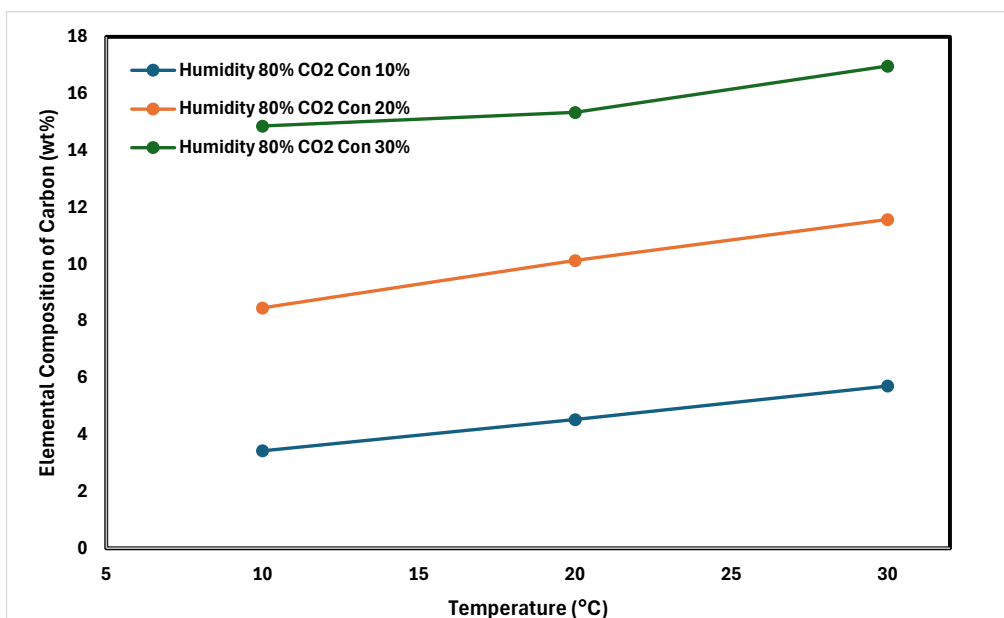
Figure 4.8: Graph of Carbon Element Content versus Temperature under 10%, 20%, 30% CO2 Concentration at Relative Humidity of 80%.

The carbonation process in steel slag is closely related to temperature, with carbon content exhibiting a direct correlation to temperature increases. As the temperature rises, the carbonation reaction accelerates, resulting in a higher rate of CO_2 absorption and mineral formation. This relationship is evident in the increase in carbon content observed under varying temperature conditions. At elevated temperatures, the enhanced dissolution of calcium ions and CO_2 diffusion promotes a more efficient reaction, facilitating greater carbon uptake within the slag. Consequently, higher temperatures facilitate the formation of stable carbonate minerals, thereby improving overall carbonation efficiency.

Generally, as temperature increases, the carbon content of EAF slags rises due to more efficient carbonation reactions. Elevated temperatures enhance the reaction between calcium oxide (CaO) and CO_2, leading to a greater formation of calcium carbonate ($CaCO_3$) and an increase in the carbon content of the slag. However, if the temperature exceeds a certain threshold, CO_2 uptake efficiency may decrease, adversely affecting the carbon content (Li, Zhong, and Ling, 2022). Therefore, optimizing the temperature for effective carbonation is crucial for maximizing carbon retention in EAF slag. Table 4.4 shows the elemental composition of carbon in mortar mixed with carbonated EAF slag samples.

Table 4.4:   Elemental Composition of Carbon in Mortar Mixed with Carbonated EAF Slag Samples

Simulated Condition	Sample No	Temperature	Humidity Level	Concentration of CO2	Elemental Composition of Carbon (wt%)
1	1	10	40	10	3.32
	2	20			4.21
	3	30			5.75
2	4	10	40	20	7.44
	5	20			10.16
	6	30			11.68
3	7	10	40	30	14.33
	8	20			16.41
	9	30			17.46
4	10	10	60	10	3.45
	11	20			4.44
	12	30			6.13

5	13	10	60	20	8.73
	14	20			11.19
	15	30			12.01
6	16	10	60	30	16.11
	17	20			17.29
	18	30			18.41
7	19	10	80	10	4.03
	20	20			5.32
	21	30			6.70
8	22	10	80	20	9.93
	23	20			11.89
	24	30			13.58
9	25	10	80	30	17.45
	26	20			18.01
	27	30			19.92

When EAF slags are mixed with cement, the carbon content in the mixture increases as the carbonation process continues. The calcium oxide (CaO) present in the EAF slag reacts with CO_2 from the cement to form calcium carbonate ($CaCO_3$), which enhances the carbon content in the mixture. This increase in $CaCO_3$ not only stabilizes the carbon within the cement matrix but also contributes to the overall durability of the material. The interaction between the carbonated slag and the cement enhances the amount of CO_2 sequestered, resulting in a higher carbon content in the final product.

Table 4.5: Comparison of Elemental Composition of Carbon of Slags and Mortar Mixed with Carbonated EAF Slags

Simulated Condition	Condition	Element Composition of Carbon in EAF Slags (wt %)	Elemental Composition of Carbon in mortar Mixed with Carbonated EAF slags (wt %)
7	10_40_30	12.21	14.33
8	20_40_30	13.98	16.41
9	30_40_30	14.87	17.46
16	10_60_30	13.72	16.11
17	20_60_30	14.73	17.29
18	30_60_30	15.68	18.41
25	10_80_30	14.86	17.45
26	20_80_30	15.34	18.01
27	30_80_30	16.97	19.92

4.5   XRD Analysis

In this study, X-ray diffraction (XRD) analysis was employed to identify and characterize the crystalline phases in electric arc furnace (EAF) slag before and after carbonation. The XRD analysis confirmed the formation of carbonate minerals, such as calcite and vaterite, while assessing the crystallinity and phase purity of the carbonated slag. It also enabled comparisons between uncarbonated and carbonated slag, highlighting how carbonation enhances the material's stability and its potential for construction applications. This analysis was crucial for evaluating the effectiveness of the carbonation process. The results were obtained from the XRD tests and analyzed using the X'Pert Highscore Plus software. Figure 4.8 illustrates the XRD results from test 6. Figures 4.9 (parts a to c) display the XRD graphs of carbonated EAF slag samples that underwent mineralization at temperatures of 10°C, 20°C, and 30°C, respectively, under consistent conditions of 60% humidity and 30% CO_2 concentration.

The XRD graphs in Figures 4.9 (parts a to c) provide essential data about calcium carbonate crystals, including peak positions and intensities. These peaks correspond to the crystallographic planes in the analyzed material and are observed when X-rays diffract off the crystal lattice at specific angles, known as Bragg angles, according to Bragg's law. The intensity of these peaks reflects the magnitude of the diffracted X-rays at those angles, with higher intensities indicating a greater concentration or crystallinity of the corresponding phases within the sample. This intensity is measured by the number of X-ray photons detected at each diffraction angle. In this study, the X-ray diffraction (XRD) results were analyzed using X'Pert HighScore Plus software. This tool was crucial in identifying the mineral phases present in the carbonated slag samples by interpreting the diffraction patterns and intensities with precision.
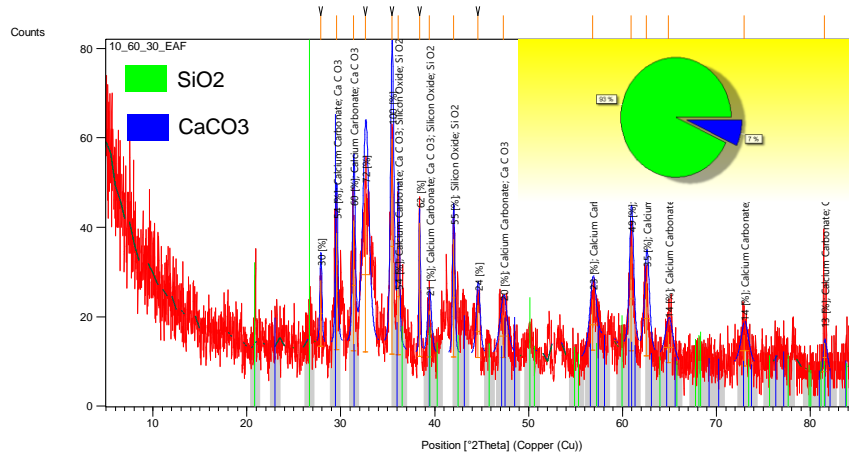
a)
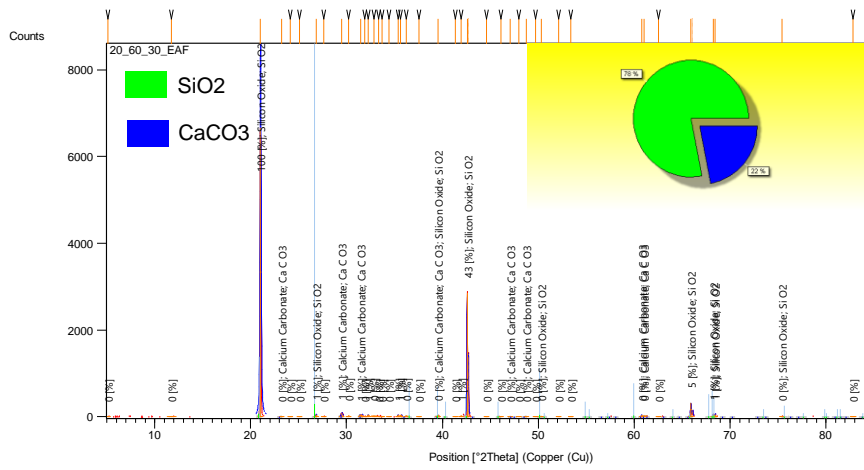
b)
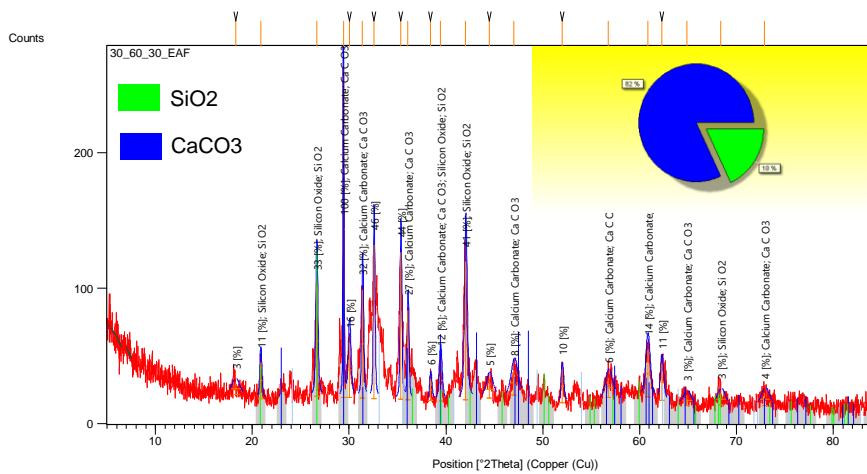
c)

Figure 4.9: XRD Graph of Carbonated EAF Slags that Underwent Mineralization under Various Conditions: a) 10_60_30; b) 20_60_30; c) 30_60_30.

Since the SEM test cannot accurately determine the calcium carbonate polymorphs in the sample, the quantification chart feature in X'Pert Highscore Plus software was used for analysis. This tool helps quantify the relative amounts or concentrations of different phases present based on X-ray diffraction (XRD) data, providing insights into the proportions of various crystalline phases in the sample. This allows researchers to better understand the material's composition and mineralogy. In an XRD graph, different 2θ positions correspond to various crystallographic planes within the material, which reflect the different phases or compositions of elements and compounds present, as shown in Figure 4.9 (parts a to c).

Figures 4.9 (a to c) demonstrate that the proportion of $CaCO_3$ increases with temperature. The proportions of $CaCO_3$ shown in these figures are 7%, 22%, and 82%, respectively. This increase is attributed to the reaction between the CaO component of the EAF slag and atmospheric CO_2. As the temperature rises, the CaO in the slag gains more kinetic energy, enhancing its reaction with CO_2. On the other hand, SiO_2 remains relatively stable and does not easily react with CO_2, except under specific conditions.

Figures 4.10 (a to c) present the XRD graphs of mortar mixed with carbonated EAF slag samples, which were mineralized at temperatures of 10°C, 20°C, and 30°C, respectively. The process occurred under controlled conditions of 60% humidity and 30% CO_2 concentration. Table 4.6 provides a comparison of the carbon content between the carbonated slags and the mortar mixed with EAF slags.
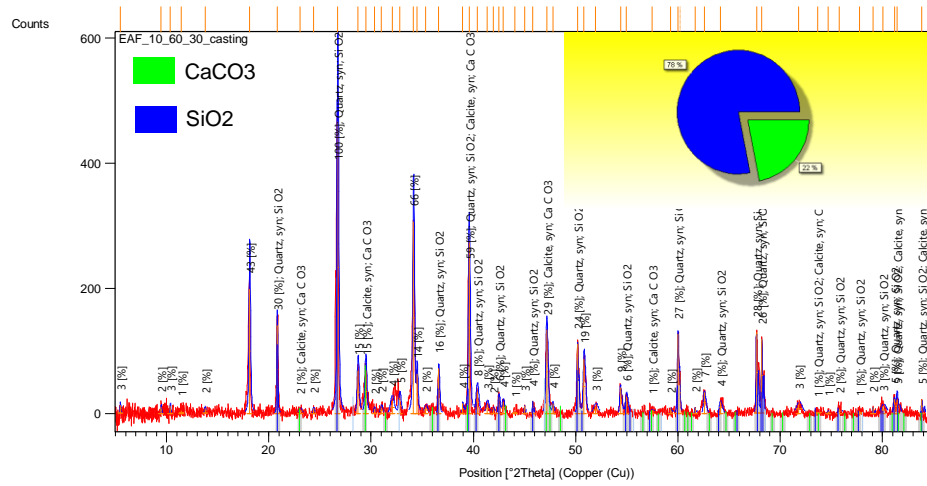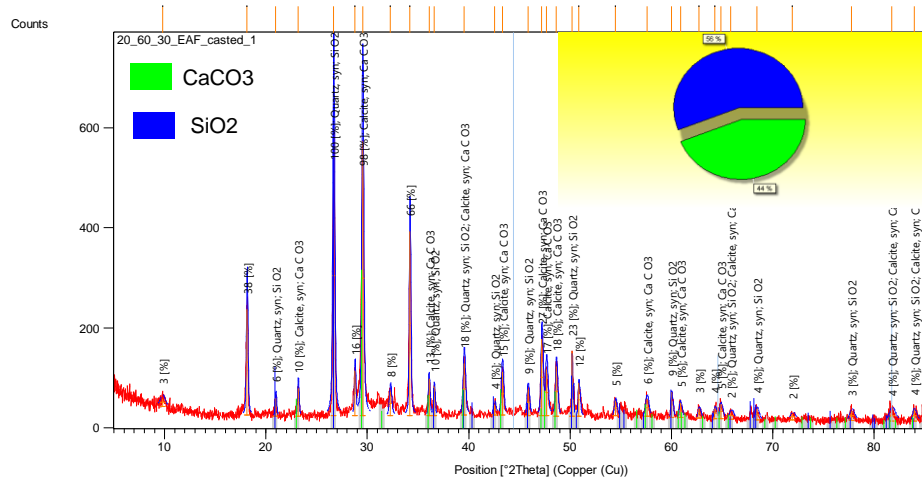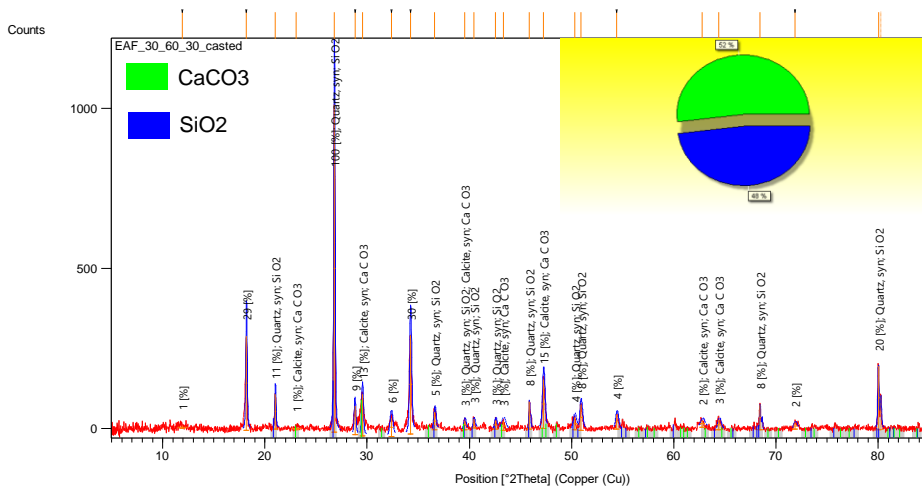
Figure 4.10: XRD Graph of Carbonated EAF Slags that Underwent Mineralization under Various Conditions: a) 10_60_30; b) 20_60_30; c) 30_60_30.

Table 4.6: Comparison of Carbon Content between Carbonated Slags and Mortar Mixed with EAF Slags

Conditions	Carbon Content Percentages of Carbonated EAF Slags (%)	Carbon Content Percentages of Mortar Mixed with Carbonated EAF Slags (%)
10_60_30	17	22
20_60_30	22	44
30_60_30	82	52

The carbon content in carbonated EAF slags and mortar mixed with carbonated slags increases, as shown in Table 4.6. The carbon content rises with temperature, and after mixing carbonated EAF slag with mortar, it also increases. Although the carbonated EAF slags under the condition 30_60_30 show a decrease in certain components, the carbon content still increases. This is because cement contains various compounds such as CaO, SiO_2, Al_2O_3, Fe_2O_3, and others (Lea, 2024), which lower the percentage of other elements.

The increase in carbon content after mixing carbonated slags with mortar is mainly due to the presence of high levels of calcium carbonate. This results from the reaction between calcium-rich materials, like cement, and carbon dioxide from the environment. During the hydration process, calcium hydroxide ($Ca(OH)_2$), a byproduct of cement hydration, reacts with CO_2 in the air to form calcium carbonate ($CaCO_3$) through a process known as carbonation. This reaction typically occurs over time as the mortar cures and is exposed to the atmosphere, leading to a higher concentration of calcium carbonate in the hardened mortar (von Greve-Dierfeld et al., 2020).

4.6 TGA Analysis

In this study, TGA (Thermogravimetric Analysis) was conducted to measure weight changes in materials during heating, assessing their thermal stability and composition. The thermal properties of carbonated slag samples were measured over a wide temperature range, from 30°C to 900°C, to capture any mass changes during the heating process. The analysis was performed in a nitrogen (N_2) atmosphere with a continuous flow rate of 50 ml/min. A purge gas, at a flow rate of 20 ml/min, was used to maintain a stable environment within the TGA instrument. The heating rate was set at 10°C/min, allowing for a gradual increase in temperature. Due to limited laboratory resources, only 9 out of the 27 carbonated samples were tested using TGA.

Figures 4.11 to 4.13 present the TGA graphs of carbonated samples under the conditions 10_60_30, 20_60_30, and 30_60_30, respectively. Prior to TGA testing, these samples underwent a mineralization process at 60% humidity and 30% CO_2, with temperature parameters set at 10°C, 20°C, and 30°C, respectively. Figure 4.11 shows that the sample mass decreases until it reaches 700°C. After 700°C, the weight loss rate increases, and the mass stabilizes after 750°C. In Figure 4.12, the sample mass starts to decrease gradually from 100% as the temperature rises, reaching 700°C. At this point, there is a slight increase in mass, from approximately 82.5% to 83% or 84%. Figure 4.13 shows a small increase in sample mass to 100.1% of its original mass as the temperature rises from 0°C to about 50°C. It then decreases gradually to 100% as the temperature reaches 80°C. At 400°C, the mass decreases, followed by a gradual rise until 600°C, where it starts to decrease again. Upon reaching 750°C, the sample mass increases, with the rate of increase accelerating until 830°C. At around 880°C, the sample mass suddenly drops, followed by a small additional decrease.
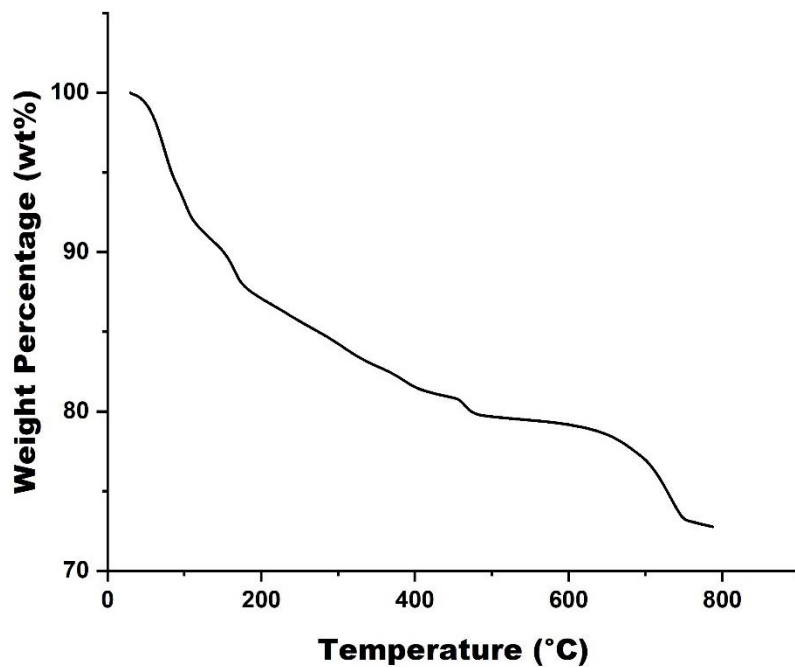
Figure 4.11: TGA Gaph of Carbonated EAF Slag under 10_60_30
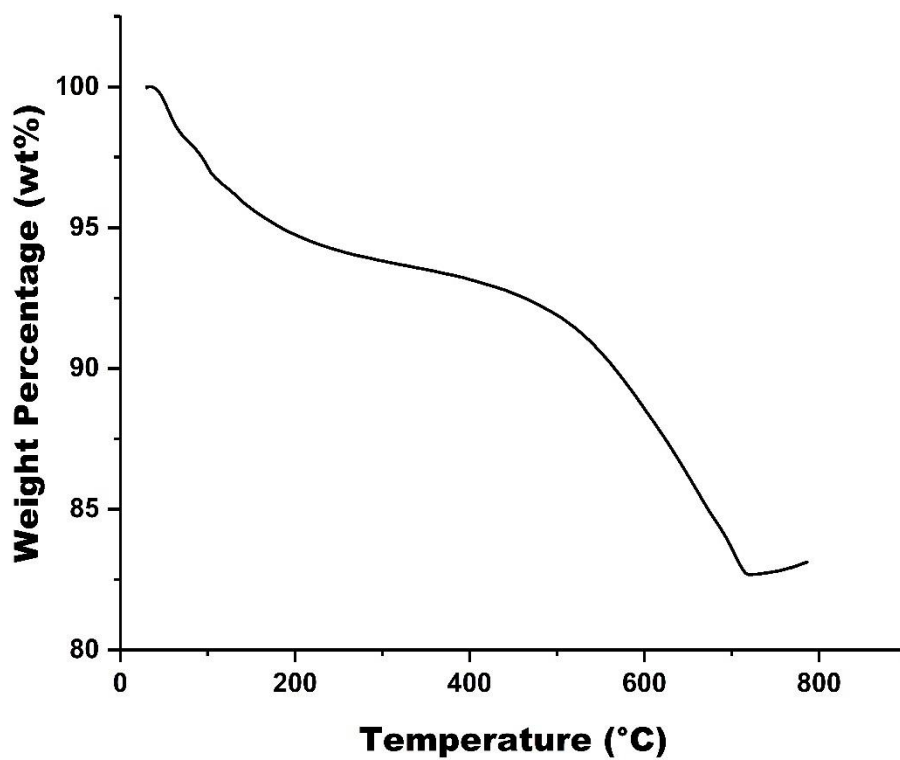
Figure 4.12: TGA Gaph of Carbonated EAF Slag under 20_60_30
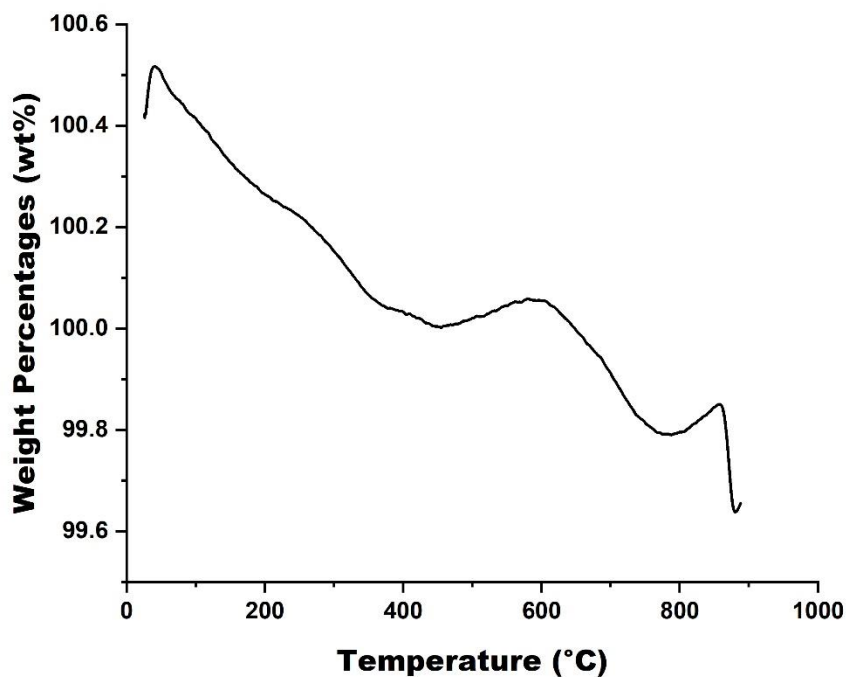
Figure 4.13: TGA Gaph of Carbonated EAF Slag under 30_60_30

Figure 4.14 demonstrates the TGA (Thermogravimetric Analysis) graphs of mortar mixed with carbonated EAF slags under the conditions of 10_60_30 (10°C, 60% humidity, and 30% CO2 concentration). Figure 4.12 shows that the mass decreases slowly until approximately 420°C, with the rate of decrease changing from 95% to 92%, and then stabilizing until 600°C. After this point, the mass decreases significantly, from 95% to 85%, between 750°C and 800°C, and then stabilizes again. Comparing the TGA analysis between carbonated slags and mortar mixed with slags, the weight loss percentage of the mortar is greater than that of the carbonated slags. This is due to the decomposition of $CaCO_3$ in the mortar. Additionally, the weight loss in the mortar is attributed to the loss of combined water caused by the dehydration of calcium silicate hydrate (Shaikh and Supit, 2014).
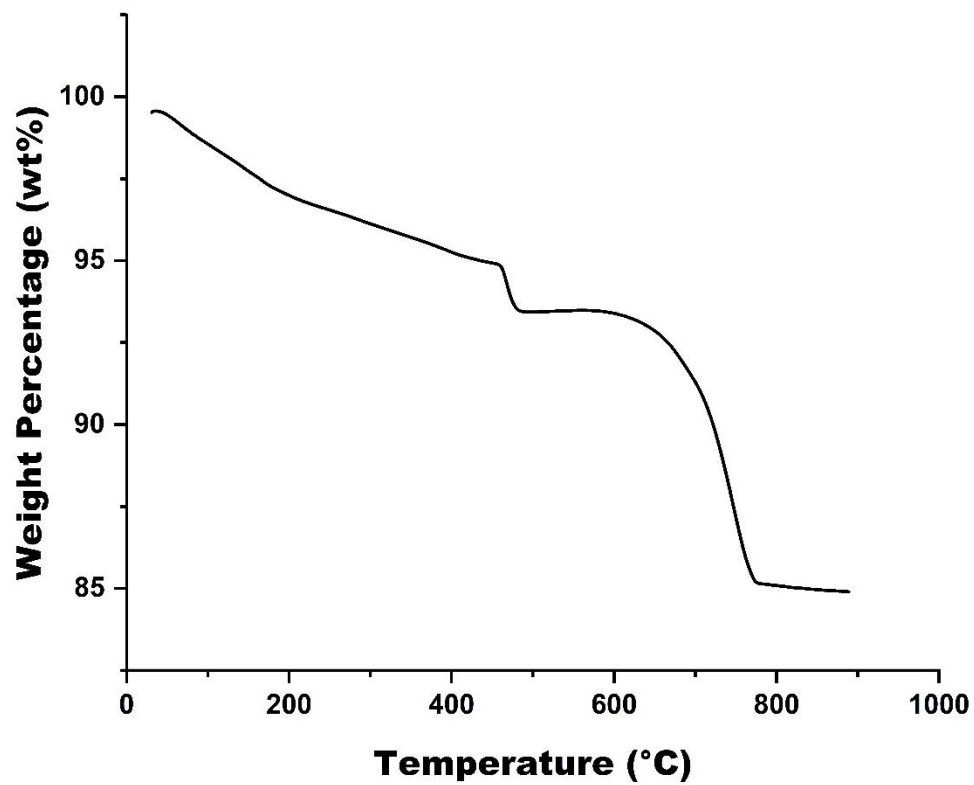
Figure 4.14: TGA Gaph of Mortar Mixed with Carbonated EAF Slags under 10_60_30

4.7   Compression Strength Test Analysis

The compressive strength test measures a material's ability to resist crushing under an applied load. This test involves placing a sample, typically a cube, under a compression machine that gradually applies force until the sample fractures. The maximum load at which the sample fails is recorded, and the compressive strength is calculated by dividing this load by the cross-sectional area of the sample. The test helps determine the material's structural integrity and suitability for construction or other load-bearing applications. Tables 4.7 and 4.8 show the average compressive strength of normal mortar and mortar mixed with EAF slags. Table 4.7 indicates that the compressive strength of normal mortar is 15.69 kN, 14.86 kN, and 16.43 kN, with an average compressive strength of 15.66 kN. Figures 4.15 (parts a to c) illustrate the compressive strength of mixtures with carbonated slags under the following conditions: (a) Humidity 40% with CO_2 concentration at 30%, (b) Humidity 60% with CO_2 concentration at 30%, and (c) Humidity 80% with CO_2 concentration at 30%. The figures also compare which temperature yields the highest compressive strength.

Table 4.7:   Average Compressive Strength of Normal Mortar

Name	Sample 1 (kN)	Sample 2 (kN)	Sample 3 (kN)	Average Strength (kN)
Control Sample	15.69	14.86	16.43	15.66

Table 4.8: Compressive Strength of Mortar Mixed with EAF Slags

No	Type of Slag	Temperature	Humidity	CO2	Weight (B)	Weight (A)	Density (B)	Density (A)	compressive, Mpa
1	EAF	10			6.84	6.36	2026.67	1884.44	19.72
2	EAF	20	40	10	6.90	6.26	2044.44	1854.81	20.70
3	EAF	30			7.14	6.48	2115.56	1920.00	21.85
4	EAF	10			6.43	6.02	1905.19	1783.70	20.43
5	EAF	20	60	10	6.92	6.44	2050.37	1908.15	21.10
6	EAF	30			6.66	6.34	1973.33	1878.52	22.06
7	EAF	10			6.44	5.45	1908.15	1614.81	20.63
8	EAF	20	80	10	7.16	6.90	2121.48	2044.44	21.36
9	EAF	30			6.90	6.46	2044.44	1914.07	24.98
10	EAF	10			6.10	5.98	1807.41	1771.85	24.17
11	EAF	20			6.90	6.26	2044.44	1854.81	24.37
12	EAF	30	40	20	7.04	6.60	2085.93	1955.56	25.31

13	EAF	10			7.04	6.06	2085.93	1795.56	25.61
14	EAF	20	60	20	6.96	6.54	2062.22	1937.78	23.98
15	EAF	30			6.54	6.00	1937.78	1777.78	25.31
16	EAF	10			6.74	6.14	1997.04	1819.26	24.18
17	EAF	20	80	20	7.44	7.00	2204.44	2074.07	24.92
18	EAF	30			6.96	6.46	2062.22	1914.07	28.94
19	EAF	10			6.60	5.88	1955.56	1742.22	27.81
20	EAF	20	40	30	6.72	6.46	1991.11	1914.07	27.43
21	EAF	30			7.16	6.88	2121.48	2038.52	26.82
22	EAF	10			6.66	5.96	1973.33	1765.93	26.41
23	EAF	20	60	30	7.24	6.90	2145.19	2044.44	26.24
24	EAF	30			6.72	6.10	1991.11	1807.41	25.90
25	EAF	10			6.82	6.14	2020.74	1819.26	26.82
26	EAF	20	80	30	6.64	6.13	1967.41	1816.30	26.41
27	EAF	30			7.00	6.16	2074.07	1825.19	25.33
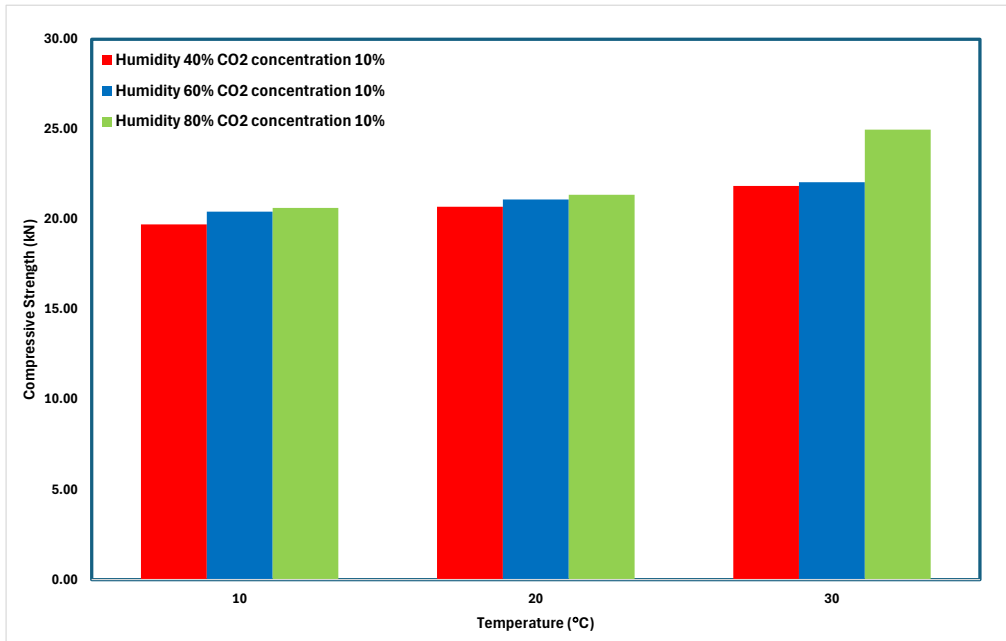
a)
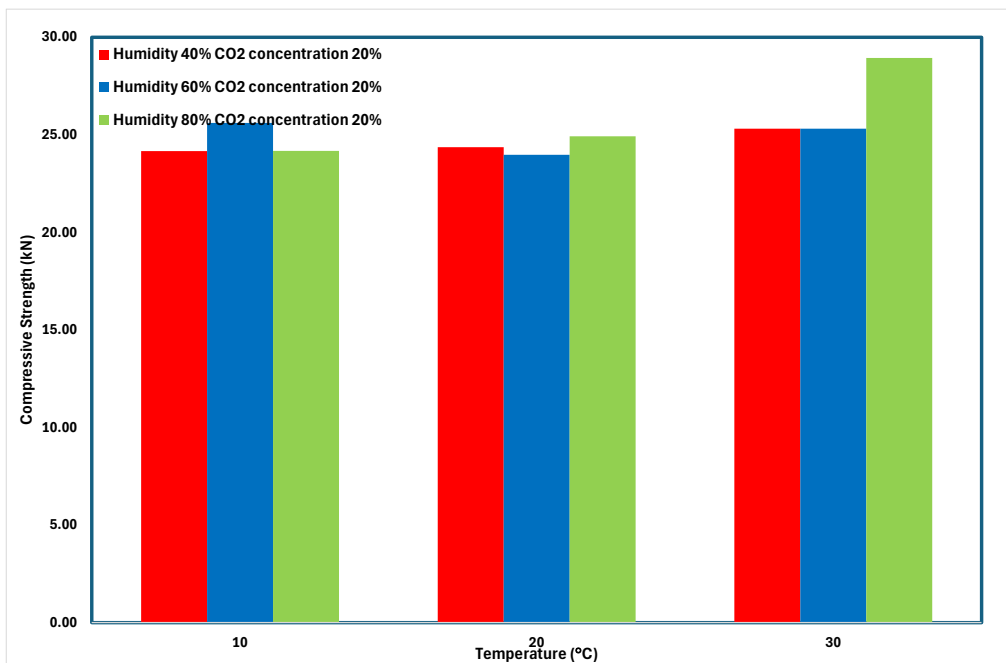
b)
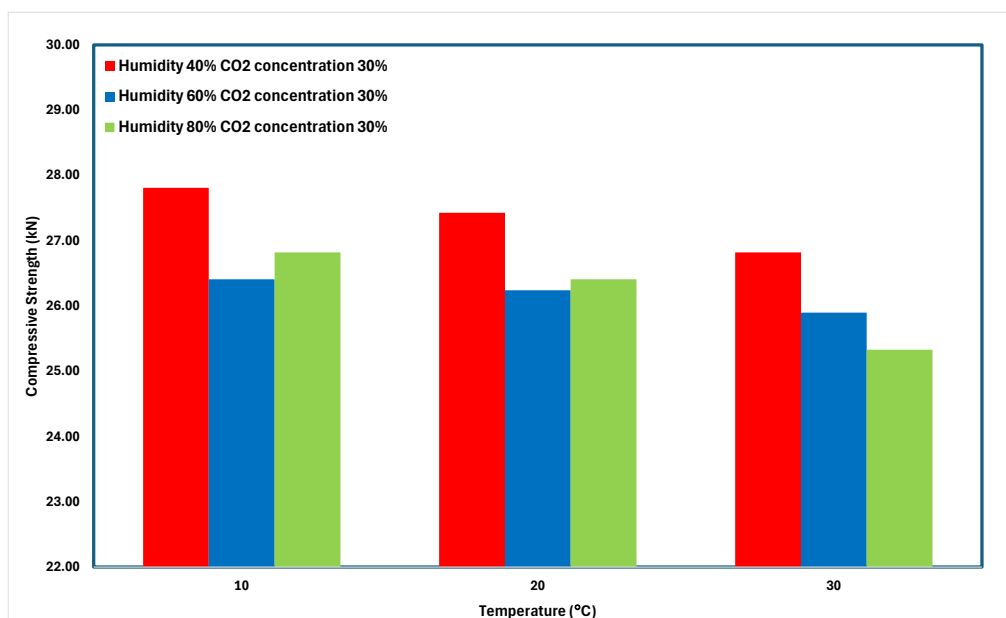
c)

Figure 4.15: Compressive Strength of Mortar Mixed with Carbonated EAF Slags Subjected to Mineralization at 10°C, 20°C, and 30°C: a) 40% Humidity, 30% CO2; b) 60% Humidity, 30% CO2; c) 80% Humidity, 30% CO2.

The addition of EAF slags can improve the compressive strength of mortar, as seen in Tables 4.7 and 4.8. The compressive strength reported in Table 4.8 is higher than that of normal mortar, as shown in Table 4.7. The optimal condition for enhancing strength is 30_80_20, with a compressive strength of 28.94 kN. Figure 4.14 (part a) shows that compressive strength increases with carbonation temperatures. The best condition in Figure 4.15 (part a) is 30_80_10, with a compressive strength of 24.98 kN. Figure 4.15 (part b) indicates that 30_80_20 is the most effective condition overall, with a compressive strength of 28.94 kN. Figure 4.15 (part c) identifies 10_40_20 as the optimal condition, with a compressive strength of 27.81 kN. The least effective condition, as noted in Table 4.7, is 10_40_10, with a compressive strength of 19.72 kN.

4.8   Splitting Tensile Strength Test Analysis

The splitting tensile strength test is essential for determining the tensile properties of mortar mixed with carbonated slag. In this test, a compressive load is applied along the diameter of a cylindrical specimen until failure, allowing the material's tensile strength to be calculated indirectly. For mortar containing carbonated slag, the test assesses the material's ability to withstand tensile forces, providing insights into how carbonation influences its tensile properties and durability. This data is valuable for optimizing the mechanical performance of mortars in construction applications. Tables 4.9 and 4.10 show the average splitting tensile strength of normal mortar and mortar mixed with carbonated slags. Table 4.9 indicates that the compressive strength of normal mortar is 11.16 kN, 9.38 kN, and 9.13 kN, with an average compressive strength of 9.89 kN as shown in Table 4.7. Figures 4.16 (parts a to c) illustrate the splitting tensile strength of mixtures with carbonated slags under the following conditions: (a) Humidity 40%, 60%, 80% with CO_2 concentration at 10%, (b) Humidity 40%, 60%, 80% with CO_2 concentration at 20%, and (c) Humidity 40%, 60%, 80% with CO_2 concentration at 30%. The figures also compare which temperature yields the highest compressive strength.

Table 4.9:   Average Splitting Tensile Strength of Normal Mortar

Name	Sample 1 (kN)	Sample 2 (kN)	Sample 3 (kN)	Average Strength (kN)
Control Sample	11.16	9.38	9.13	9.89

Table 4.10: Splitting Tensile of Mortar Mixed with EAF Slags

Number	Type of Slag	Temperature	Humidity	CO2	Weight (B)	Weight (A)	Density (B)	Density (A)	Splitting tensile
1	EAF	10			6.84	6.36	2026.67	1884.44	7.83
2	EAF	20	40	10	6.90	6.26	2044.44	1854.81	9.57
3	EAF	30			7.14	6.48	2115.56	1920.00	11.05
4	EAF	10			6.43	6.02	1905.19	1783.70	7.46
5	EAF	20	60	10	6.92	6.44	2050.37	1908.15	9.78
6	EAF	30			6.66	6.34	1973.33	1878.52	13.44
7	EAF	10			6.44	5.45	1908.15	1614.81	9.02
8	EAF	20	80	10	7.16	6.90	2121.48	2044.44	9.78
9	EAF	30			6.90	6.46	2044.44	1914.07	11.32
10	EAF	10			6.10	5.98	1807.41	1771.85	8.19
11	EAF	20			6.90	6.26	2044.44	1854.81	9.40
12	EAF	30	40	20	7.04	6.60	2085.93	1955.56	10.48

13	EAF	10			7.04	6.06	2085.93	1795.56	11.41
14	EAF	20	60	20	6.96	6.54	2062.22	1937.78	8.02
15	EAF	30			6.54	6.00	1937.78	1777.78	11.00
16	EAF	10			6.74	6.14	1997.04	1819.26	7.49
17	EAF	20	80	20	7.44	7.00	2204.44	2074.07	9.92
18	EAF	30			6.96	6.46	2062.22	1914.07	15.48
19	EAF	10			6.60	5.88	1955.56	1742.22	11.46
20	EAF	20	40	30	6.72	6.46	1991.11	1914.07	9.35
21	EAF	30			7.16	6.88	2121.48	2038.52	8.48
22	EAF	10			6.66	5.96	1973.33	1765.93	11.16
23	EAF	20	60	30	7.24	6.90	2145.19	2044.44	9.51
24	EAF	30			6.72	6.10	1991.11	1807.41	7.54
25	EAF	10			6.82	6.14	2020.74	1819.26	14.74
26	EAF	20	80	30	6.64	6.13	1967.41	1816.30	11.10
27	EAF	30			7.00	6.16	2074.07	1825.19	9.74
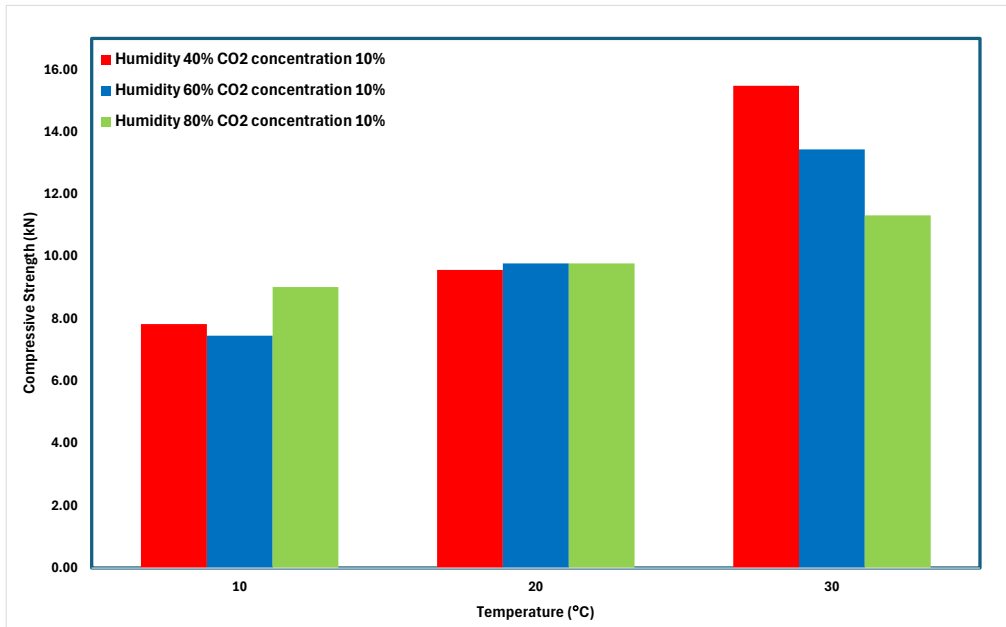
a)
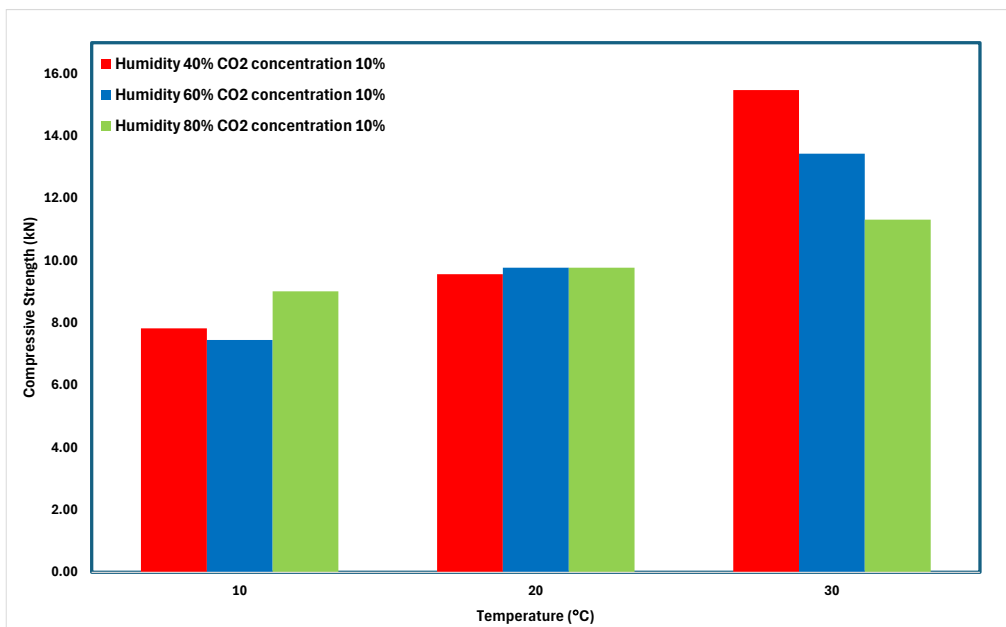
b)
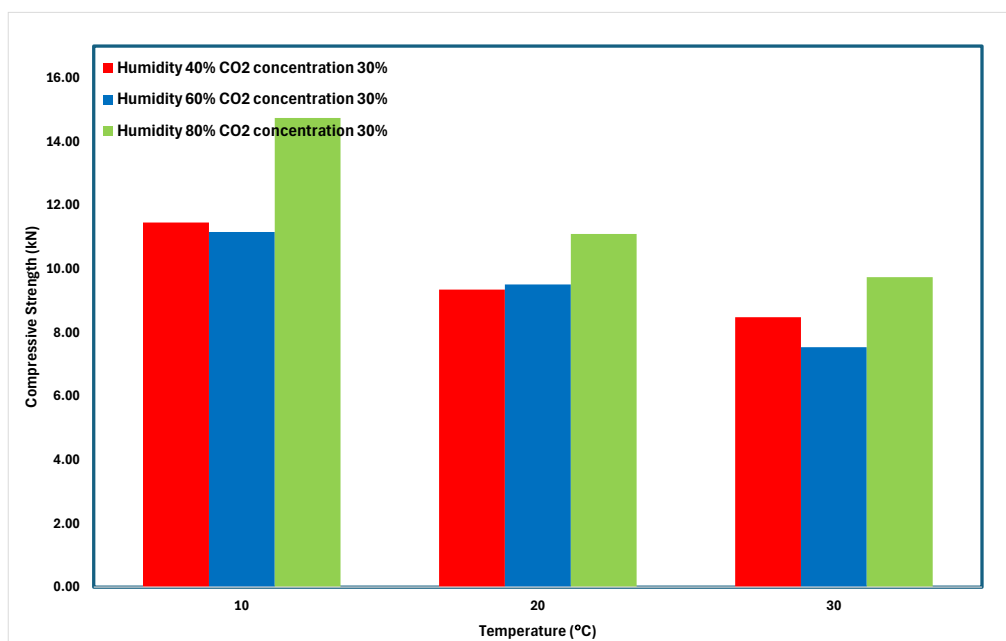
c)

Figure 4.16: Splitting Tensile Strength of Mortar Mixed with Carbonated EAF
Slags Subjected to Mineralization at 10°C, 20°C, and 30°C: a) 40%
Humidity, 30% CO2; b) 60% Humidity, 30% CO2; c) 80%
Humidity, 30% CO2.

The addition of EAF slags can enhance the splitting strength of the
mortar, as compared to Tables 4.9 and 4.10. Table 4.10 shows a higher splitting
strength than the normal mortar in Table 4.9. The optimal condition for
increasing strength is 30_80_20, where the splitting strength reaches 15.48 kN.
In Figure 4.15 (part a), the best condition noted is 30_40_10, with a splitting
strength of 11.05 kN. Figure 4.15 (part b) indicates that the most effective
condition is 30_80_20, which proves to be the best overall, achieving a splitting
strength of 15.48 kN. Figure 4.15 (part c) shows that the best condition is
10_40_30, with a splitting strength of 14.74 kN. The least effective condition,
as noted in Table 4.10, is 10_60_10, with a splitting strength of 7.46 kN.

4.9   Flexural Strength Test Analysis

The flexural strength test is used to evaluate the bending strength of mortar mixed with carbonated slag. In this test, a beam-shaped mortar specimen is subjected to a load applied at its midpoint until it fractures, measuring the material's resistance to deformation under flexural stress. For carbonated slag-mixed mortar, the test helps assess improvements in tensile performance and rigidity, highlighting the influence of carbonation on the mortar's structural stability and its potential application in construction, where bending resistance is crucial. Tables 4.11 and 4.12 show the average flexural strength of normal mortar and mortar mixed with carbonated EAF slags. Table 4.7 presents the compressive strength of normal mortar as 4 kN, 3.22 kN, and 2.67 kN, with an average compressive strength of 3.3 kN. Figures 4.17 (parts a to c) illustrate the flexural strength of mixtures with carbonated slags under the following conditions: (a) Humidity 40%, 60%, 80% with CO_2 concentration at 10%, (b) Humidity 40%, 60%, 80% with CO_2 concentration at 20%, and (c) Humidity 40%, 60%, 80% with CO_2 concentration at 30%. The figures also compare which temperature yields the highest compressive strength.

Table 4.11: Average Flexural Strength of Normal Mortar

| Name	Sample 1 (kN)	Sample 2 (kN)	Sample 3 (kN)	Average Strength (kN)
Control Sample	4.00	3.22	2.67	3.30

Table 4.12: Flexural Strength of Mortar Mixed with EAF Slags

Number	Type of Slag	Temperature	Humidity	CO2	Weight (B)	Weight (A)	Density (B)	Density (A)	Flexural
1	EAF	10			6.84	6.36	2026.67	1884.44	3.71
2	EAF	20	40	10	6.90	6.26	2044.44	1854.81	3.20
3	EAF	30			7.14	6.48	2115.56	1920.00	4.00
4	EAF	10			6.43	6.02	1905.19	1783.70	3.00
5	EAF	20	60	10	6.92	6.44	2050.37	1908.15	3.20
6	EAF	30			6.66	6.34	1973.33	1878.52	4.31
7	EAF	10			6.44	5.45	1908.15	1614.81	2.21
8	EAF	20	80	10	7.16	6.90	2121.48	2044.44	2.41
9	EAF	30			6.90	6.46	2044.44	1914.07	2.84
10	EAF	10			6.10	5.98	1807.41	1771.85	3.91
11	EAF	20			6.90	6.26	2044.44	1854.81	4.13
12	EAF	30	40	20	7.04	6.60	2085.93	1955.56	4.22

13	EAF	10			7.04	6.06	2085.93	1795.56	4.58
14	EAF	20	60	20	6.96	6.54	2062.22	1937.78	3.64
15	EAF	30			6.54	6.00	1937.78	1777.78	4.33
16	EAF	10			6.74	6.14	1997.04	1819.26	3.17
17	EAF	20	80	20	7.44	7.00	2204.44	2074.07	3.62
18	EAF	30			6.96	6.46	2062.22	1914.07	5.03
19	EAF	10			6.60	5.88	1955.56	1742.22	4.83
20	EAF	20	40	30	6.72	6.46	1991.11	1914.07	2.43
21	EAF	30			7.16	6.88	2121.48	2038.52	2.46
22	EAF	10			6.66	5.96	1973.33	1765.93	4.02
23	EAF	20	60	30	7.24	6.90	2145.19	2044.44	3.56
24	EAF	30			6.72	6.10	1991.11	1807.41	3.17
25	EAF	10			6.82	6.14	2020.74	1819.26	4.16
26	EAF	20	80	30	6.64	6.13	1967.41	1816.30	3.40
27	EAF	30			7.00	6.16	2074.07	1825.19	3.04
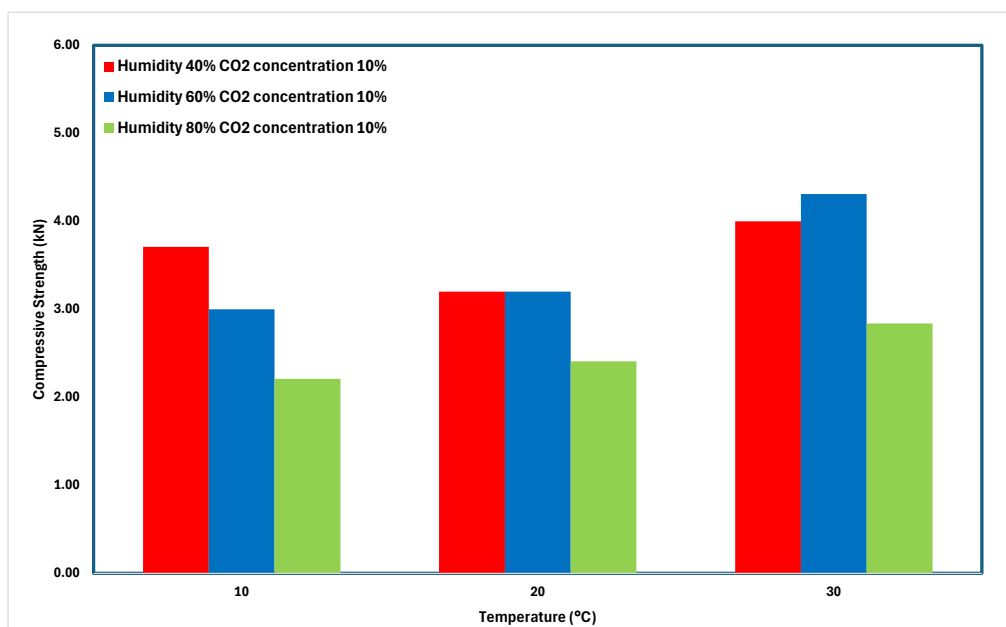
a)
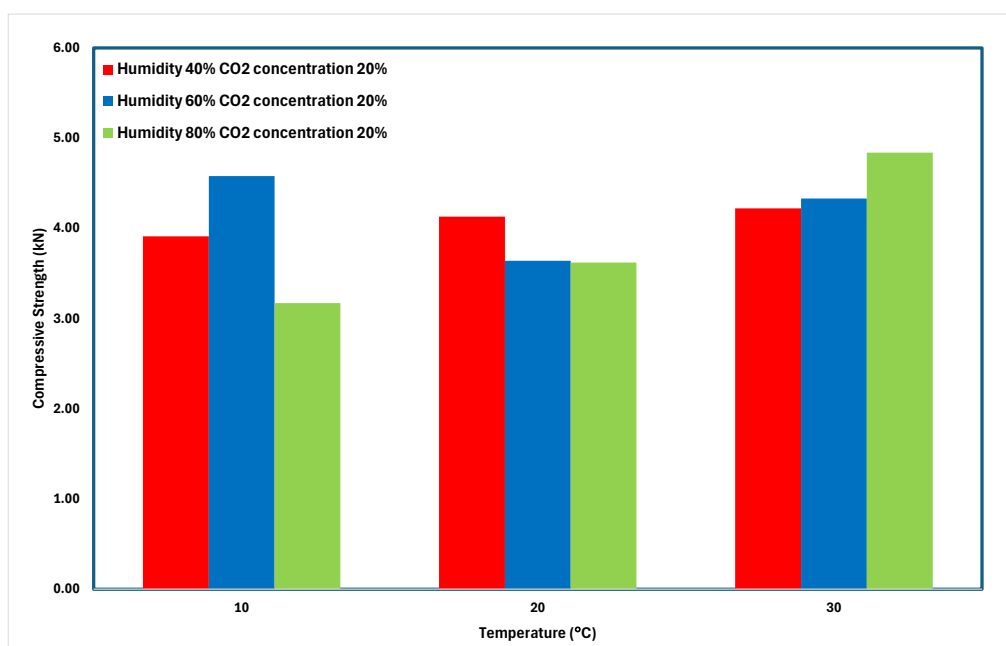
b)
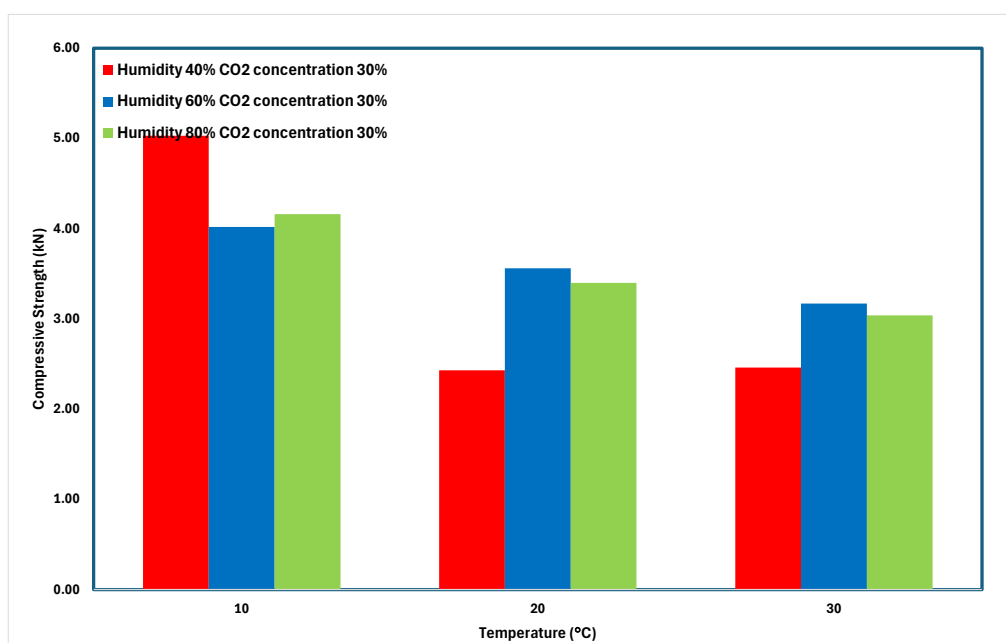
c)

Figure 4.17: Splitting Tensile Strength of Mortar Mixed with Carbonated EAF
Slags Subjected to Mineralization at 10°C, 20°C, and 30°C: a) 40%
Humidity, 30% CO2; b) 60% Humidity, 30% CO2; c) 80%
Humidity, 30% CO2.

The incorporation of EAF slags enhances the flexural strength of the
mortar, as shown in Tables 4.11 and 4.12. The flexural strength reported in
Table 4.12 surpasses that of normal mortar, as detailed in Table 4.11. The
optimal condition for improving strength is 30_80_20, with a flexural strength
of 5.03 kN. In Figure 4.17 (part a), the most favorable condition is 30_60_10,
yielding a flexural strength of 4.31 kN. Figure 4.17 (part b) shows that the best
condition is again 30_80_20, with a flexural strength of 4.84 kN, proving to be
the best overall. In contrast, Figure 4.17 (part c) identifies 10_40_30 as the
optimal condition, with a flexural strength of 27.81 kN. The lowest performance
is observed in Table 4.12, under the condition 10_40_10, with a flexural strength
of 4.83 kN.

4.10 Relationship Between Carbon Content and Mechanical Strength

EAF slags have a definite increase in mortar strength. Carbonated temperature does not directly affect the mechanical strength of the mortar mixed with carbonated EAF slags. Instead, the carbon content direct effect on mechanical strength. Figure 4.18 shows the graph of the relationship between carbon content and mechanical strength. Table 4.13 shows the mechanical properties and carbon content of EAF slags under various mineralization conditions.
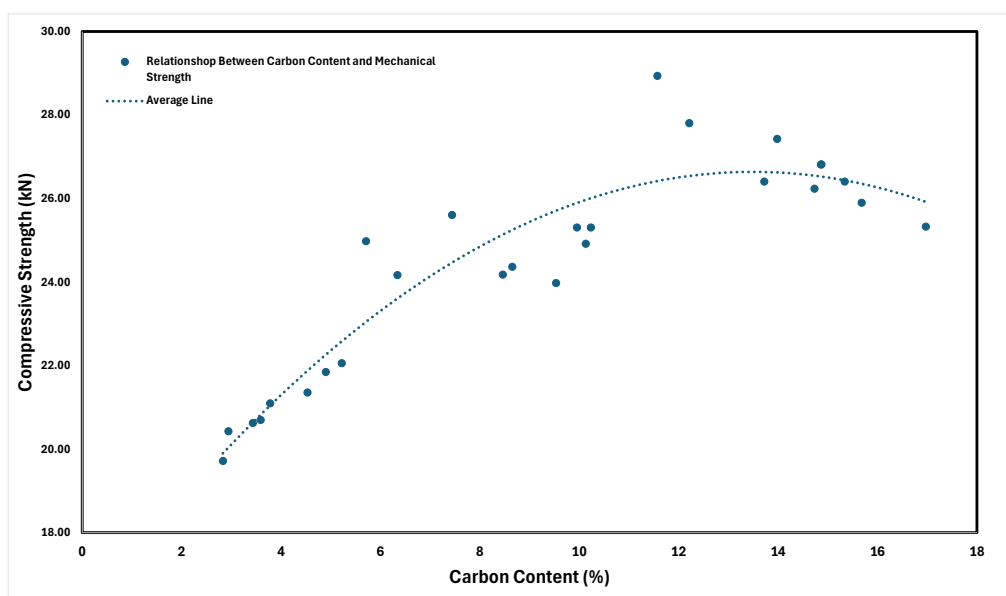
Figure 4.18:   Graph of the Relationship between Carbon Content and Mechanical Strength

Table 4.13: Mechanical Properties and Carbon Content of Carbonated EAF Steel Slag Under Various Mineralization Conditions

Number	Type of Slag	Temperature	Humidity	CO2	Compressive Strength, (kN)	Splitting Tensile (kN)	Flexural Strength (kN)	Carbon content (%)
1	EAF	10			19.72	7.83	3.71	2.83
2	EAF	20	40	10	20.70	9.57	3.20	3.59
3	EAF	30			21.85	11.05	4.00	4.9
4	EAF	10			20.43	7.46	3.00	2.94
5	EAF	20	60	10	21.10	9.78	3.20	3.78
6	EAF	30			22.06	13.44	4.31	5.22
7	EAF	10			20.63	9.02	2.21	3.43
8	EAF	20	80	10	21.36	9.78	2.41	4.53
9	EAF	30			24.98	11.32	2.84	5.71
10	EAF	10			24.17	8.19	3.91	6.34
11	EAF	20	40	20	24.37	9.40	4.13	8.65
12	EAF	30			25.31	10.48	4.22	9.95
13	EAF	10			25.61	11.41	4.58	7.44
14	EAF	20	60	20	23.98	8.02	3.64	9.53
15	EAF	30			25.31	11.00	4.33	10.23
16	EAF	10			24.18	7.49	3.17	8.46
17	EAF	20			24.92	9.92	3.62	10.13
18	EAF	30	80	20	28.94	15.48	5.03	11.57

19	EAF	10			27.81	11.46	4.83	12.21
20	EAF	20	40	30	27.43	9.35	2.43	13.98
21	EAF	30			26.82	8.48	2.46	14.87
22	EAF	10			26.41	11.16	4.02	13.72
23	EAF	20	60	30	26.24	9.51	3.56	14.73
24	EAF	30			25.90	7.54	3.17	15.68
25	EAF	10			26.82	14.74	4.16	14.86
26	EAF	20	80	30	26.41	11.10	3.40	15.34
27	EAF	30			25.33	9.74	3.04	16.97

Table 4.13 demonstrates that the optimal conditions for carbonating EAF slags in mortar involve a temperature of 30°C, 80% humidity, and a CO2 concentration of 20%, resulting in the best performance. The compressive, splitting tensile and flexural strength of mortar are 28.94 kN, 15.48 kN and 5.03 kN. Figure 4.17 presents that compressive strength starts to decrease when carbon content reaches approximately 12%, the strength starts to decrease. A certain amount of carbon content can increase the strength of mortar, but beyond a fixed point, it can be counterproductive. Table 4.13 presents the carbon contents of mortar between 11.57% and 12.51%, with the mechanical strength approximately starting to decrease in the middle of carbon contents.

The increase in compressive strength is primarily due to the carbonation process, which leads to the formation of calcium carbonate (CaCO3) crystals. These crystals fill the pores within the mortar, making it more compact and reducing internal voids, which strengthens the material. Additionally, the rough surface of the steel slag fine aggregate improves bonding with the cement, further enhancing strength (Liu, Tang and Wang, 2023). On the other hand, the decrease in compressive strength, especially at higher steel slag fine aggregate replacement ratios, is linked to the uncarbonated steel slag fine aggregate. The hydration of free CaO (f-CaO) in uncarbonated steel slag fine aggregate can lead to expansion, causing internal stress and micro-cracking, which weakens the structure and reduces strength (Liu, Tang and Wang, 2023).

CHAPTER 5
Conclusions and Recommendations

5.1   Conclusions

This study investigates how effectively Electric Arc Furnace slag can capture and store CO_2, a process known as carbonation. The research examines how different temperatures (10°C, 20°C, 30°C), CO_2 concentrations (10%, 20%, 30%), and humidity levels (40%, 60%, 80%) impact this process, aiming to pinpoint the optimal conditions for maximizing CO_2 uptake and reaction efficiency. Additionally, the study evaluates the performance of mortar incorporating carbonated EAF slags, exploring its potential for forming stable carbonate minerals.

The research pursues three main objectives:

I.   Determine the influence of temperature on CO_2 uptake during carbonation. Energy-dispersive X-ray Spectroscopy analysis reveals a positive correlation between temperature and CO_2 conversion efficiency, indicating that higher temperatures lead to increased carbonation.

II.   Analyze the microstructural changes in waste slag during carbonation at various temperatures. Scanning Electron Microscopy imaging confirms the presence of visible crystal structures in EAF slag at 30°C. X-ray Diffraction analysis shows that all samples consist of approximately 82% calcium carbonate ($CaCO_3$) and 18% silicon dioxide (SiO_2). Thermogravimetric Analysis demonstrates an approximately 18% weight reduction in samples carbonated under optimized temperature and CO_2 conversion efficiency when heated to approximately 900°C.

III.   Evaluate the impact of incorporating carbonated steel slag on the strength and durability of mortar. Compressive strength tests demonstrate that mortar containing carbonated slag exhibits superior mechanical performance compared to control samples. This improvement is attributed to the formation of stable calcium carbonate ($CaCO_3$) within the slag, which enhances bonding within the mortar matrix.

5.2   Recommendation for Future Work

This study focused on optimizing CO2 conversion and carbonate mineral stability in electric arc furnace (EAF) slag within a temperature range of 40°C to 80°C, using a single type of slag. Future research should broaden the temperature range and intervals to understand their effects on mineralization further. Additionally, exploring various slag types can enhance the generalizability of optimal temperature findings. Further studies should also evaluate the mechanical properties of mortar mixed with carbonated EAF slag, including compressive and flexural strength, to assess its practical applications in construction. Therefore, it is essential to investigate a broader range of temperature parameters and their effects on the mineralization of different slags. Here are some recommendations for future works:

I.   Conduct experiments using a wider range of temperatures beyond the 40°C to 80°C range explored in this study. Testing at both lower and higher temperatures will provide a more comprehensive understanding of how temperature affects CO2 conversion efficiency and mineralization kinetics. This broader approach will help identify critical temperature thresholds where carbonation processes are optimized or hindered, offering deeper insights into the thermal behavior of EAF slag.

II.   Within the expanded temperature range, use smaller temperature increments to capture subtle variations in CO2 conversion efficiency and mineralization behavior. This finer resolution will enable precise identification of optimal temperature thresholds and facilitate a detailed analysis of how temperature impacts the carbonation process.

III.   Explore a variety of steel slags from different sources and compositions to validate the optimal temperature conditions for CO2 conversion efficiency. Examining diverse slag types will provide a more complete understanding of how slag composition influences carbonation kinetics and CO2 uptake,

ensuring that findings are applicable to a broader range of slag materials.

REFERENCES

Amer Baras, Jiajie Li , Wen Ni, Zahid Hussain and Michael Hitch (2023). Evaluation of Potential Factors Affecting Steel Slag Carbonation. [online] doi: https://doi.org/10.1016/B0-12-176480-X/00371-5.

Asuquo, E., Martin, A. and Nzerem, P. (2018). Evaluation of Cd(II) Ion Removal from Aqueous Solution by a Low-Cost Adsorbent Prepared from White Yam (Dioscorea rotundata) Waste Using Batch Sorption. *ChemEngineering*, 2(3), p.35. doi: https://doi.org/10.3390/chemengineering2030035.

Baras, A., Li, J., Wen, N., Hussain, Z. and Hitch, M. (2023). Evaluation of Potential Factors Affecting Steel Slag Carbonation. *Processes*, 11(9), pp.2590–2590. doi: https://doi.org/10.3390/pr11092590.

Bataille, C. (2020). Low and zero emissions in the steel and cement industries: Barriers, technologies and policies. *RePEc: Research Papers in Economics*, [online] pp.5–6. Available at: https://www.oecd.org/greengrowth/GGSD2019_IssuePaper_CementSteel.pdf [Accessed 20 Apr. 2024].

Bodor, M., Santos, R.M., Cristea, G., Salman, M., Özlem Cizer, Remus Ion Iacobescu, Yi Wai Chiang, Koenraad Van Balen, Vlad, M. and Tom Van Gerven (2016). Laboratory investigation of carbonated BOF slag used as partial replacement of natural aggregate in cement mortars. *Cement & Concrete Composites*, 65, pp.55–66. doi: https://doi.org/10.1016/j.cemconcomp.2015.10.002.

Brand, A.S. and Fanijo, E.O. (2020). A Review of the Influence of Steel Furnace Slag Type on the Properties of Cementitious Composites. *Applied Sciences*, 10(22), p.8210. doi: https://doi.org/10.3390/app10228210.

Crouzet, C., Brunet, F., Montes-Hernandez, G., Recham, N., Findling, N., Ferrasse, J.-H. and Goffé, B. (2017). Hydrothermal Valorization of Steel Slags—Part I: Coupled H2 Production and CO2 Mineral Sequestration. *Frontiers in Energy Research*, 5. doi:https://doi.org/10.3389/fenrg.2017.00029.

da Silva Magalhães, M., Faleschini, F., Pellegrino, C. and Brunelli, K. (2017). Cementing efficiency of electric arc furnace dust in mortars. *Construction and Building Materials*, 157, pp.141–150. doi: https://doi.org/10.1016/j.conbuildmat.2017.09.074.

Dutrow, B. and Clark, C. (2019). *X-ray Powder Diffraction (XRD)*. [online] Techniques. Available at: https://serc.carleton.edu/research_education/geochemsheets/techniques/XRD.html.

encyclopedia.pub. (2024). *Basic Oxygen Furnace Slag Characteristics and Properties*. [online] Available at: https://encyclopedia.pub/entry/43979 [Accessed 2 Mar. 2024].

Furlani, E., Tonello, G. and Maschio, S. (2010). Recycling of Steel Slag and Glass Cullet from Energy Saving Lamps by Fast Firing Production of Ceramics. *Waste Management*, 30(8-9), pp.1714–1719. doi: https://doi.org/10.1016/j.wasman.2010.03.030.

Gaston, B. and Protter, C. (2019). *Energy-Dispersive X-ray Spectroscopy (EDS)*. [online] Chemistry LibreTexts. Available at: https://chem.libretexts.org/Courses/Franklin_and_Marshall_College/Introduction_to_Materials_Characterization__CHM_412_Collaborative_Text/Spectroscopy/Energy-Dispersive_X-ray_Spectroscopy_(EDS).

Humbert, P.S. and Castro-Gomes, J. (2019). CO2 activated steel slag-based materials: A review. *Journal of Cleaner Production*, [online] 208, pp.448–457. doi: https://doi.org/10.1016/j.jclepro.2018.10.058.

IEA (2020). *Iron and Steel Technology Roadmap – Analysis*. [online] IEA. Available at: https://www.iea.org/reports/iron-and-steel-technology-roadmap.

Kaja, A.M., K. Schollbach, Melzer, S., van, Brouwers, H.J.H. and Yu, Q. (2021). Hydration of potassium citrate-activated BOF slag. *Cement and Concrete Research*, 140, pp.106291–106291. doi: https://doi.org/10.1016/j.cemconres.2020.106291.

Kaleta-Jurowska, A. and Jurowski, K. (2020). The Influence of Ambient Temperature on High Performance Concrete Properties. *Materials*, 13(20), p.4646. doi: https://doi.org/10.3390/ma13204646.

Lea, F. (2024). *Cement - The major cements: composition and properties*. [online] Encyclopedia Britannica. Available at: https://www.britannica.com/technology/cement-building-material/The-major-cements-composition-and-properties.

Lee, S., Kim, J.-W., Chae, S., Bang, J.-H. and Lee, S.-W. (2016). CO2 sequestration technology through mineral carbonation: An extraction and carbonation of blast slag. *Journal of CO2 Utilization*, 16, pp.336–345. doi: https://doi.org/10.1016/j.jcou.2016.09.003.

Li, L., Zhong, X. and Ling, T.-C. (2022). Effects of accelerated carbonation and high temperatures exposure on the properties of EAFS and BOFS pressed blocks. *Journal of Building Engineering*, [online] 45, p.103504. doi: https://doi.org/10.1016/j.jobe.2021.103504.

Librandi, P., Nielsen, P., Costa, G., Snellings, R., Quaghebeur, M. and Baciocchi, R. (2019). Mechanical and environmental properties of carbonated steel slag compacts as a function of mineralogy and CO2 uptake. *Journal of CO2 Utilization*, 33, pp.201–214. doi: https://doi.org/10.1016/j.jcou.2019.05.028.

Liu, G., Tang, Y. and Wang, J. (2023). Effects of carbonation degree of semi-dry carbonated converter steel slag on the performance of blended cement mortar – Reactivity, hydration, and strength. *Journal of Building Engineering*, 63, p.105529. doi: https://doi.org/10.1016/j.jobe.2022.105529.

López-Díaz, A., Ochoa-Díaz, R. and Grimaldo-León, G.E. (2018). Use of BOF slag and blast furnace dust in asphalt concrete: an alternative for the construction of pavements. *DYNA*, 85(206), pp.24–30. doi: https://doi.org/10.15446/dyna.v85n206.70404.

Lozano-Lunar, A., Raposeiro da Silva, P., de Brito, J., Fernández, J.M. and Jiménez, J.R. (2019). Safe use of electric arc furnace dust as secondary raw material in self-compacting mortars production. *Journal of Cleaner Production*, 211, pp.1375–1388. doi:https://doi.org/10.1016/j.jclepro.2018.12.002.

Ma, X., Li, Y., Shi, L., He, Z. and Wang, Z. (2016). Fabrication and CO2 capture performance of magnesia-stabilized carbide slag by by-product of biodiesel during calcium looping process. *Applied Energy*, 168, pp.85–95. doi: https://doi.org/10.1016/j.apenergy.2016.01.080.

Made-in-China.com. (2024). *[Hot Item] Skz1053 1200c 1350c Thermo Gravimetric Tga Analysis Thermogravimetric Analyzer Tg Thermogravimetric Analysis Tga Thermal Gravimeter*. [online] Available at: https://skzindustrial.en.made-in-china.com/product/iZCtUVRvCgYk/China-Skz1053-1200c-1350c-Thermo-Gravimetric-Tga-Analysis-Thermogravimetric-Analyzer-Tg-Thermogravimetric-Analysis-Tga-Thermal-Gravimeter.html [Accessed 16 Apr. 2024].

Malvern Panalytical (2020). *X-ray Diffraction | XRD | XRPD*. [online] Malvernpanalytical.com. Available at: https://www.malvernpanalytical.com/en/products/technology/xray-analysis/x-ray-diffraction.

Marion Carrier, Anne Loppinet-Serani , Dominique Denux, Jean-Michel Lasnier, Fre´de´rique Ham-Pichavant , Franc¸ois Cansell and Cyril Aymonier (2011). Thermogravimetric analysis as a new method to determine the lignocellulosic composition of biomass. *Biomass and Bioenergy*, [online] 35(1), pp.298–307. doi: https://doi.org/10.1016/j.biombioe.2010.08.067.

Matthias Ruth (2004). Steel Production and Energy. *Encyclopedia of Energy*, [online] pp.695–706. doi:https://doi.org/10.1016/B0-12-176480-X/00371-5.

Mongo, M., Belaïd, F. and Ramdani, B. (2021). The effects of environmental innovations on CO2 emissions: Empirical evidence from Europe. *Environmental Science & Policy*, 118, pp.1–9. doi: https://doi.org/10.1016/j.envsci.2020.12.004.

Nanoscience Instruments (2018). *Scanning electron microscopy - nanoscience instruments*. [online] Nanoscience Instruments. Available at: https://www.nanoscience.com/techniques/scanning-electron-microscopy/.

Nath, S.K., Randhawa, N.S. and Kumar, S. (2022). A review on characteristics of silico-manganese slag and its utilization into construction materials. *Resources, Conservation and Recycling*, 176, p.105946. doi: https://doi.org/10.1016/j.resconrec.2021.105946.

National Academies of Sciences, E., Studies, D. on E. and L., Toxicology, B. on E.S. and and Uses, C. on E.A.F.S.U.H.H.R. from U. (2023). *Electric Arc Furnace Steelmaking and Slag Formation, Composition, and Distribution*. [online] www.ncbi.nlm.nih.gov. Available at: https://www.ncbi.nlm.nih.gov/books/NBK599051/# [Accessed 16 Apr. 2024].

Nour-Eddine Ménad, Kana, N., Seron, A. and Ndue Kanari (2021a). New EAF Slag Characterization Methodology for Strategic Metal Recovery. *Materials*, 14(6), pp.1513–1513. doi: https://doi.org/10.3390/ma14061513.

Nour-Eddine Ménad, Kana, N., Seron, A. and Ndue Kanari (2021b). New EAF Slag Characterization Methodology for Strategic Metal Recovery. *Materials*, 14(6), pp.1513–1513. doi: https://doi.org/10.3390/ma14061513.

Nunes, V.A., Cimentada, A., Thomas, C. and Paulo H.R. Borges (2024). Pre-treatment of BOF steel slag aggregates and effect on the mechanical and microstructure properties of alkali-activated mortars. *Journal of building engineering*, pp.109562–109562. doi: https://doi.org/10.1016/j.jobe.2024.109562.

Nurazzi, N.M., Asyraf, M.R.M., Rayung, M., Norrrahim, M.N.F., Shazleen, S.S., Rani, M.S.A., Shafi, A.R., Aisyah, H.A., Radzi, M.H.M., Sabaruddin, F.A., Ilyas, R.A., Zainudin, E.S. and Abdan, K. (2021). Thermogravimetric Analysis Properties of Cellulosic Natural Fiber Polymer Composites: A Review on Influence of Chemical Treatments. *Polymers*, 13(16), p.2710. doi: https://doi.org/10.3390/polym13162710.

Oxford (2023). *What is EDS/EDX? - Nanoanalysis - Oxford Instruments*. [online] Oxford Instruments. Available at: https://nano.oxinst.com/campaigns/what-is-eds/edx.

Pan, S.-Y., Chiang, P.-C., Chen, Y.-H., Tan, C.-S. and Chang, E.-E. . (2014). Kinetics of carbonation reaction of basic oxygen furnace slags in a rotating packed bed using the surface coverage model: Maximization of carbonation conversion. *Applied Energy*, 113, pp.267–276. doi: https://doi.org/10.1016/j.apenergy.2013.07.035.

Qifeng Song, Ming-Zhi Guo, Lei Wang and Tung-Chai Ling (2021). Use of Steel Slag as Sustainable Construction materials: a Review of Accelerated Carbonation treatment, Resources, Conservation and Recycling,. *Use of Steel Slag as Sustainable Construction materials: a Review of Accelerated Carbonation Treatment*, pp.0921-3449. https://doi.org/10.1016/j.resconrec.2021.105740.

R Syahyadi, A Fauzi, E Majuar, F Rizal, Reza, M. and Fajri, dan (2020). Effect of Electric Arc Furnace Dust Treatment on the Properties of Fresh and Hardened Mortar. *IOP conference series. Materials science and engineering*, 739(1), pp.012032–012032. doi:https://doi.org/10.1088/1757-899x/739/1/012032.

Ren, Z. and Li, D. (2023). Application of Steel Slag as an Aggregate in Concrete Production: A Review. *Materials*, [online] 16(17), pp.5841–5841. doi:https://doi.org/10.3390/ma16175841.

Ribbenhed, M., Thorén, M. and Sternhufvud, C. (2008). CO2 Emission Reduction Costs for Iron ore-based Steelmaking in Sweden. *Journal of Cleaner Production*, 16(1), pp.125–134. doi:https://doi.org/10.1016/j.jclepro.2006.11.007.

Sara Carvalho Zago, Vernilli, F. and O. Cascudo (2023). The Reuse of Basic Oxygen Furnace Slag as Concrete Aggregate to Achieve Sustainable Development: Characteristics and Limitations. 13(5), pp.1193–1193. doi: https://doi.org/10.3390/buildings13051193.

Sha, F., Li, H., Pan, D., Liu, H. and Zhang, X. (2020). Development of steel slag composite grouts for underground engineering. *Journal of materials research and technology/Journal of Materials Research and Technology*, 9(3), pp.2793–2809. doi:https://doi.org/10.1016/j.jmrt.2020.01.014.

Shaikh, F.U.A. and Supit, S.W.M. (2014). Mechanical and durability properties of high volume fly ash (HVFA) concrete containing calcium carbonate (CaCO3) nanoparticles. *Construction and Building Materials*, 70, pp.309–321. doi:https://doi.org/10.1016/j.conbuildmat.2014.07.099.

Steel Industry Co Products Fact Sheet. (2024). Available at: https://worldsteel.org/wp-content/uploads/Fact-sheet-Steel-industry-co-products.pdf.

SUSHANTH KOMBATHULA (2020). *Sequestration of carbon dioxide in steel slag SUSHANTH KOMBATHULA KTH ROYAL INSTITUTE OF TECHNOLOGY SCHOOL OF INDUSTRIAL ENGINEERING AND MANAGEMENT*. [online] Available at: https://www.diva-portal.org/smash/get/diva2:1466343/FULLTEXT01.pdf [Accessed 14 Apr. 2024].

Swapp, S. (2017). *Scanning Electron Microscopy (SEM)*. [online] Geochemical Instrumentation and Analysis. Available at: https://serc.carleton.edu/research_education/geochemsheets/techniques/SEM.html.

Tamas ´ Kurusta, Gábor Mucsi, Sanjay Kumar and Ferenc Kristály (2023). Carbon-dioxide Sequestration by Mechanical Activation of Linz-Donawitz Steel slag; the Effect of Water on CO2 Capture. *Fuel*, [online] Volume 352, pp.0016-2361. Available at: https://www.sciencedirect.com/science/article/pii/S0016236123015648 [Accessed 17 Apr. 2024].

tenova.com. (2024). *Electric Arc Furnaces (EAF) | Tenova*. [online] Available at: https://tenova.com/technologies/electric-arc-furnaces-eaf [Accessed 3 Sep. 2024].

Tung Hsuan Lu, Ying Liang Chen, Pai Haung Shih and Juu En Chang (2018). Use of basic oxygen furnace slag fines in the production of cementitious mortars and the effects on mortar expansion. *Construction and Building Materials*, 167, pp.768–774. doi: https://doi.org/10.1016/j.conbuildmat.2018.02.102.

Ukwattage, N.L., Ranjith, P.G. and Li, X. (2017). Steel-making slag for mineral sequestration of carbon dioxide by accelerated carbonation. *Measurement*, 97, pp.15–22. doi: https://doi.org/10.1016/j.measurement.2016.10.057.

Ural, N (2021). The Significance of Scanning Electron Microscopy (SEM) Analysis on the Microstructure of Improved clay: an overview. Open Geosciences. [online] Vol. 13(Issue 1), pp.197–218. Available at: https://doi.org/10.1515/geo-2020-0145 [Accessed 17 Apr. 2024].

US EPA, O. (2021). *Electric Arc Furnace (EAF) Slag*. [online] www.epa.gov. Available at: https://www.epa.gov/smm/electric-arc-furnace-eaf-slag.

von Greve-Dierfeld, S., Lothenbach, B., Vollpracht, A., Wu, B., Huet, B., Andrade, C., Medina, C., Thiel, C., Gruyaert, E., Vanoutrive, H., Saéz del Bosque, I.F., Ignjatovic, I., Elsen, J., Provis, J.L., Scrivener, K., Thienel, K.-C., Sideris, K., Zajac, M., Alderete, N. and Cizer, Ö. (2020). Understanding the carbonation of concrete with supplementary cementitious materials: a critical review by RILEM TC 281-CCC. *Materials and Structures*, 53(6). doi: https://doi.org/10.1617/s11527-020-01558-w.

Wahyu S. Putro, Vladimir Ya Lee, Kazuhiko, Jun-Chul Choi and Norihisa Fukaya* (2021). From SiO2 to Alkoxysilanes for the Synthesis of Useful Chemicals. *From SiO2 to Alkoxysilanes for the Synthesis of Useful Chemicals*. [online] Available at: https://pubs.acs.org/doi/full/10.1021/acsomega.1c05138 [Accessed 8 Sep. 2024].

Wang, Y.-J., Tao, M.-J., Li, J.-G., Zeng, Y.-N., Qin, S. and Liu, S.-H. (2021). Carbonation of EAF Stainless Steel Slag and Its Effect on Chromium Leaching Characteristics. *Crystals*, 11(12), p.1498. doi: https://doi.org/10.3390/cryst11121498.

Wang, Z., Liu, Q., Liu, H. and Wei, S. (2020). A review of end-point carbon prediction for BOF steelmaking process. *High Temperature Materials and Processes*, 39(1), pp.653–662. doi: https://doi.org/10.1515/htmp-2020-0098.

Watkins, D., Nuruddin, Md., Hosur, M., Tcherbi-Narteh, A. and Jeelani, S. (2015). Extraction and characterization of lignin from different biomass resources. *Journal of Materials Research and Technology*, 4(1), pp.26–32. doi: https://doi.org/10.1016/j.jmrt.2014.10.009.

Worldsteel Association. (2024). *Worldsteel Short Range Outlook April 2024*. [online] Available at: https://worldsteel.org/media/press-releases/2024/worldsteel-short-range-outlook-april-2024/#:~:text=The%20World%20Steel%20Association%20(worldsteel [Accessed 19 Apr. 2024].

www.mst.or.jp. (2024). *MST ∕ [SEM-EDX] Energy Dispersive X-ray Spectroscopy (SEM)*. [online] Available at: https://www.mst.or.jp/Portals/0/en/en_sem-edx.htm [Accessed 3 Sep. 2024]. www.recovery-worldwide.com. (2024). *Slag recycling - recovery*. [online] Available at: https://www.recovery-worldwide.com/en/artikel/slag-recycling-3528047.html [Accessed 3 Sep. 2024].

www.thermofisher.com. (2024). *EDS Analysis ∕ Energy Dispersive Spectroscopy - US*. [online] Available at: https://www.thermofisher.com/my/en/home/materials-science/eds-technology.html [Accessed 3 Sep. 2024].

Yee Cheng Lim, Shih, Y.-J., Tsai, K.-C., Yang, W.-D., Chen, C.-W. and Dong, C.-D. (2020). Recycling Dredged Harbor Sediment to Construction Materials by Sintering with Steel Slag and Waste glass: Characteristics, alkali-silica Reactivity and Metals Stability. *Journal of Environmental Management*, 270, pp.110869–110869. doi: https://doi.org/10.1016/j.jenvman.2020.110869.

Yildirim, I.Z. and Prezzi, M. (2011). Chemical, Mineralogical, and Morphological Properties of Steel Slag. *Advances in Civil Engineering*, 2011, pp.1–13. doi: https://doi.org/10.1155/2011/463638.

Yu, X., Tao, Z., Song, T.-Y. and Pan, Z. (2016). Performance of concrete made with steel slag and waste glass. *Construction and Building Materials*, 114, pp.737–746. doi: https://doi.org/10.1016/j.conbuildmat.2016.03.217.